UPMC HILLMAN CANCER CENTER ACADEMY

FRIDAY, AUGUST 4, 2023

ABSTRACT BOOK

UPMC | HILLMAN CANCER CENTER

University of Pittsburgh

Welcome

Thank you for joining us today to honor our hard-working scholars and laboratories from the Hillman Academy! We strive to provide cutting-edge research and career preparatory experiences to a diverse group of highly motivated high school students who are interested in pursuing higher education and careers in STEM fields. In this hands-on summer program, scholars are placed in laboratories directed by dedicated faculty and trainee mentors across the University of Pittsburgh Campus.

Over the course of its history, the Hillman Academy has become an award-winning science, technology, engineering, and mathematics (STEM) program that prepares students for successful college careers and beyond. The Academy was initiated in 2009 under the directorship of Michael Lotze, MD, and has grown to the program it is today with generous support from the NIH, Doris Duke Charitable Foundation, Jack Kent Cooke Foundation, UPMC, Hillman Foundation, Ear and Eye Foundation, Beckwith Funds, Stan Marks Foundation, Shadyside Hospital Foundation, Pitt, grateful parents and patients, and the many University faculty, trainees, and staff who give selflessly of their time.

Please join us in honoring these students and mentors, as well as the hard work they did this summer to complete an authentic research project. We are so glad that you chose to join us today and are pleased that you have given your scholar a chance to work with our talented faculty, students, and fellows!

Hillman Academy Staff

Program Director: David Boone

Associate Director: Joseph Ayoob

Project Manager: Steven Jones

Site Directors

Cancer Biology (CB): Dr. Deborah Galson

Computer Science, Biology and Biomedical Informatics (CoSBBI): Dr. David Boone

Computational Biology (CompBio): Dr. Joseph C. Ayoob and Dr. David Koes

Immunology and Cancer Immunotherapy (ICI): Dr. Tullia Bruno and Dr. Greg Delgoffe

Ophthalmology (OPT): Dr. Yuanyuan Chen

Surgery: Dr. Steven Evans

Tech Drive X (TDX): Dr. Andrew Duncan, Serafina Lanna and Meagan Makarczyk

Women's Cancer Research Center (WCRC): Dr. Partha Roy and Dr. David Gau

Thank You

This program was made possible with the help of the following people and organizations.

Funding

National Institutes of Health (NIH)

National Cancer Institute Youth Enjoy Science Program

Doris Duke Charitable Foundation (DDCF)

The Beckwith Institute

Hillman Foundation

Shadyside Hospital Foundation

Ear and Eye Foundation

NIH CURE – past

UPMC Center for Engagement and Inclusion – past

Jack Kent Cooke Foundation

Stan Marks Foundation

University of Pittsburgh

UPMC Parking and Security – past

Grateful parents and patients

Partners

Fund for the Advancement of Minority Education (FAME)

Homeless Children's Education Fund (HCEF)

Pittsburgh Public Schools (PPS)

Remake Learning

MPowerhouse

STEM PUSH Network

Precollege STEM Programs at Pitt

The Citizen Science Lab

Gene Team

BioZone

Community Engagement Centers

Propel Schools

Pittsburgh Promise

Neighborhood Learning Alliance

NATIONAL CANCER INSTITUTE

DORIS DUKE CHARITABLE FOUNDATION

Hillman Academy Leadership Team

Dr. Robert Ferris
Dr. Chad Ellis
Dr. David Boone
Dr. Devin Dressman
Dr. Christopher Bakkenist
Dr. Joe Ayoob

Site Heads

Dr. Joe Ayoob
Dr. Andrew Duncan
Serafina Lanna
Dr. David Boone
Dr. Steven Evans
Meagan Makarczyk
Dr. Tullia Bruno
Dr. Deborah Galson
Dr. Partha Roy
Dr. Yuanyuan Chen
Dr. David Gau
Dr. Greg Delgoffe
Dr. David Koes

Administration

Beth Baic
Carrie Fogel
Toni Porterfield
Genine Bartolotta
Deborah Galson
Rayleigh Reynolds
Rebecca Bauroth
Emily Hayhurst
Robert Ferris
Michael Becich
Harry Hochheiser
José-Alain Sahel
Jeremy Berg
Steven Jones
Nicole Scheff
Timothy Billiar
Barbara Karnbauer
Madison Seaver
Andrea Brasili
Geeta Kaul
Lawton Snyder
Kathy Brickett
Robert Kornosky
Lola Thompson
Rob Ceccehetti
Vladislav Leskovtec
Gina Toy-Cutler
Yvonne Chao
Alison Lithgow
John Viaropulos
Greg Cooper
Ines Lohse
Justin Wideman
Dianna Fennell
Lisa McIlvried
Darryl Washington
Toren Finkel
Hatice Osmanbeyoglu

Technology

Bill Best
Scot Dunsmore
Keith Durst
Roland Frasher
Ethan Hay
Bryan Krinberg
Mark Schramm

UPMC Hillman Cancer Center Communications Team

Gera Jochum
Anna Daniels

HDS and Interpreters

Jayde Eng
Marcus Springer
Josh Stresing
Michael Nader

Resident Assistants

Ivy Baker
Donise Griffin
Griffin Hurt
Lauren Weaver

Doris Duke Scholars

Om Arora-Jain
Jason Chen
Madeline Douglas
Donise Griffin
Anyssa Oden

Instructors, TAs, and Education Team

Roshni Bhatt
Katherine Davoli
Chase Dermond
Marissa Di
Caroline Larkin
Ines Lohse
Rim Nassar
Devanshi "Dev" Nayak
Dante Poe
Ellen Scott
Tristan "T" White

TECBio REU @ Pitt Mentoring Committee

Erica Herrera Huaman (Chair)
Elijah Blige
Saúl Castillo
S'Khaja Charles
David Fox
Daphne Garcia
Crystal Lee
Neil MacLachlan
Mildred Morales-Paredes
Phi Nguyen

Speakers, Lecturers, and Guests

Kalil Abdullah
Alyssa Aguglia
John Ash
Joe Ayoob
Michael Becich
Rishabh Bhadouriya
David Boone
Ouahiba Boukaabar
Tullia Bruno
Racquel Buj-Gomez
Paul Cantalupo
Luke Carlson
Yuanyuan Chen
Youngbin Cho
Katherine Davoli
Deepinder Dhaliwal
Devin Dressman
Andrew Duncan
Steve Evans
Robert Ferris
Catherine Gage
Yi-Nan Gong
Ashna Gupta
Ritwik Gupta
Ryan Hartmaier
Meaghan Hazelet
Lisa Hong
Juliana Hougland
Dorota Jazwinska
Charles Jonassaint
Christopher Kargl
Alyson Kavalukas
Paul (Kip) Kinchington
Aidan Lakshman
Sanghoon Lee
Brandon Lehrich
Ines Lohse
John Maier
Meagan Makarczyk
Trinidy Manison
Warren McCoy
Danielle Moss
Nolan Mowery
Ben Nacev
Bradley Nindl
Melanie Ongchin
Andrew Peitzman
Kyle Pulvermacher
Gabriel Quinteros
Ana Radovic
Rafael Ramos-jimenez
April Rich
Lily Rosenblum
Cheryl Ruffin
Melanie Scott
Nicole Sekel
David Silver
Elizabeth Steele
Matt Steinhauser
Davin Sweeney
Dakota Tiede
Shikhar Uttam
Larry Vernetti

Speakers, Lecturers, and Guests (cont.)

Andreas Vogt

Michael Wach

Smriti Wagle

Sierra White

Mazen Zenati

Professional Development Seminar Series Speakers

Joe Ayoob

David Boone

Tullia Bruno

Career Center - Alyson W. Kavalukas, Alex Ball, Alyssa Camerota, Sharon Mickens,

Raquel Montalvo Perez & Erin Wheeler

Devin Dressman

Office for Equity, Diversity, & Inclusion - Cheryl Ruffin, and Warren McCoy

Supporting Our Valued Adolescents - Anna Radovic, Charles Jonassaint, Trinidy Manison, Gabriel Quinteros, Smriti Wagle

Surgeon talk - Steven Evans, Melanie Ongchin, and Ramos-jimenez

Offices and Departments

University of Pittsburgh

UPMC Hospital System

UPMC Hillman Cancer Center

UPMC Children's Hospital of Pittsburgh

Pitt School of Medicine

Eye & Ear Foundation of Pittsburgh

UPMC Security Office

UPMC Volunteer office

Disability Resources and Services

Pitt IT/ Technology Help Desk

Panther Central

Department of Biomedical Informatics

Department of Ophthalmology

Computational and Systems Biology

Department of Immunology

Department of Pathology

Department of Surgery

Department of Bioengineering

Magee-Womens Research Institute

McGowan Institute of Regenerative Medicine

Office for Equity, Diversity, & Inclusion

University Counsel

And the many other departments that support this program.

Mentors

Thanks to the hundreds of mentors across campus each of which is recognized on the individual student abstracts and site schedules!

Cancer Biology Site Agenda

August 4, 2022, 8:30 a.m. - 12:30 p.m.
Auditorium in Assembly Building on 5051 Center Ave
https://pitt.zoom.us/j/98728931430 • Meeting ID: 98728931430 • Passcode: 047051

8:30 a.m. **Welcoming Remarks**
CB Site Education Team: *Deborah L. Galson, PhD (CB Site Director), Ines Lohse, PhD & Rim Nassar, PhD*

CB Scholar Research Presentations

8:45 a.m. **#1** **Jason Chen** ***DDCF Undergraduate Intern**
PI: Timothy F. Burns, MD, PhD; Lab Mentor: Vinod Kumar, PhD

9:00 a.m. **#2** **Leviticus McGraw-Sapp**
PI: Timothy F. Burns, MD, PhD; Lab Mentor: Vinod Kumar, PhD

9:15 a.m. **#3** **Nancy Chen**
PI: Xiaosong Wang, MD, PhD; Lab Mentor: Bashir Lawal, PhD

9:30 a.m. **#4** **Franco Alvarez**
PI: Chris Bakkenist, PhD; Lab Mentor: Joseph El-Ghoubaira, MD

9:45 a.m. **#5** **Harry (Sam) Littwin**
PI: Katheryn Demanelis, PhD

10:00 a.m. **#6** **Averi Elsbury**
PI: Patricia L. Opresko, PhD; Lab Mentors: Samantha Sanford, PhD & Ariana Detwiler, MS

10:15 a.m. **#7** **Lorenzo Aguilera**
PI: Elise Fouquerel, PhD; Lab Mentors: Daniela Muoio, PhD & Rim Nassar, PhD

10:30-10:45 a.m. **---------- BREAK ----------**

10:45 a.m. **#8** **Aarav Supraneni**
PI: Nicole Scheff, PhD; Lab Mentors: Lisa McIlvried, PhD & Megan Atherton

11:00 a.m. **#9** **Tian LeGrande**
PI: Nicole Scheff, PhD; Lab Mentors: Lisa McIlvried, PhD & Megan Atherton

11:15 a.m. **#10** **Desiree Amponsah**
PI: Taofeek Owonikoko, MD, PhD; Lab Mentor: John Schmitz, PhD

11:30 a.m. **#11** **Rami Alhallak**
PI: Shou-Jiang Gao, PhD; Lab Mentor: Wen Meng, PhD

11:45 a.m. **#12** **Daniel Guo**
PI: Shou-Jiang Gao, PhD; Lab Mentor: Wen Meng, PhD

12:00 p.m. **#13** **Anthony Kalvi**
PI: Haitao Guo, PhD; Lab Mentor: Ning Sun, PhD

12:15 p.m. **#14** **Jinyi Guo**
PI: Wayne Stallaert, PhD;
Lab Mentor: Janet McLaughlin, MPPM, Dante Poe, Betsy Varghese, Armani Manov, & Tyler Johnston

12:30 p.m. **------ LUNCHEON (Atrium/Crane Shed)------**

2:00 p.m. **ACADEMY-WIDE CLOSING CEREMONY (Auditorium)**

Computational Biology Site Agenda

August 4, 2023, 9:30 a.m.
Murdoch Building (3420 Forbes Ave, Pittsburgh, PA 15213) Floor 8 Room 814
https://pitt.zoom.us/j/93890426600 • Meeting ID: 938 9042 6600 • Passcode: COBRA

Welcome
9:30 a.m. Dr. Joseph Ayoob - CompBio Site Head

9:35 – 11:55 a.m. Research Presentations

9:35 a.m. **Ruth Ayers, Fatimah Bisiriyu, and Caleb Bocianoski**
Mentor, Dr. David Koes

9:55 a.m. **Stephanie Chen**
Mentor, Dr. James Faeder

10:10 a.m. **Anna Delale-O'Connor**
Mentor, Dr. Jishnu Das

10:25 a.m. **Oliver Adams**
Mentor, Dr. Guangyi Zhao

10:40 a.m. **Break**

10:55 a.m. **Gavin Hou**
Mentors, Dr. Zhiwei Feng and Dr. Sean Xie

11:10 a.m. **Henry Gaston**
Mentors, Dr. Zhiwei Feng and Dr. Sean Xie

11:25 a.m. **Neil Porwal**
Mentor, Tyler Lovelace

11:40 a.m. **Ian Lisien**
Mentors, Dr. Lance Davidson and Sommer Anjum

11:55 a.m. **Break**

12:00 p.m. **Lunch – Murdoch Classroom 814**

2:00 p.m. **Closing Ceremony**
Assembly Building, First Floor Auditorium
5051 Centre Ave, Pittsburgh, PA 15213

CoSBBI Site Agenda

August 4, 2023, 8:00 a.m.
The Offices at Baum, Room 407 A/B
https://us02web.zoom.us/j/85754282549?pwd=elordlNjOE43cFNXOEM4M3RhNGRjZz09

8:00 a.m. **Welcoming Remarks —** David Boone, PhD

8:05 a.m. **CoSBBI Scholars Research Presentations – Session 1**

- 8:05 a.m. **Preetam Jukalkar**
  Mentors: Drs. Terence McGuire and Xiang-Qun Xie
- 8:20 a.m. **Chimdi Isiguzo**
  Mentor: Dr. Margaret Rosenzweig
- 8:35 a.m. **Jeremiah Satcho**
  Mentors: Dr. Greg Cooper and Kevin Guo
- 8:50 a.m. **Alex Schafer**
  Mentors: Eddie Perez
- 9:05 a.m. **Jibraan Rahman**
  Mentors: Dr. Spandan Maiti and Yamnesh Agrawal
- 9:20 a.m. **Samantha Fernsebner**
  Mentors: Drs. Daniel Lundberg and Tugba Kucukkal

9:35 a.m. **BREAK**

9:40 a.m. **CoSBBI Scholars Research Presentations – Session 2**

- 9:40 a.m. **Anyssa Oden* Doris Duke Undergraduate**
  Mentors: Dr. Sossena Wood and Lara Abdelmohsen
- 9:55 a.m. **Jose Maldonado**
  Mentors: Dr. Rafael Ceschin, William Reynolds, and Joy Roy
- 10:10 a.m. **Dylan Sun**
  Mentor: Dr. Xinghua Lu
- 10:25 a.m. **Abril Linares Mendoza**
  Mentor: Dr. David Boone
- 10:40 a.m. **Trinidy Manison**
  Mentor: Dr. Ana Radovic and Gabriel Quinteros
- 10:55 a.m. **Adam Ferris**
  Mentors: Dr. In Hee Lee and Yuyang Li

11:10 a.m. **BREAK**

11:15 a.m. **CoSBBI Scholars Research Presentations – Session 3**

- 11:15 a.m. **Mikaela Dassanaike-Perera**
  Mentors: Drs. Murat Akcakaya and Busra Tugce Susam
- 11:30 a.m. **Om Arora-Jain* Doris Duke Undergraduate**
  Mentor: Dr. Xia Jiang and Yijun Zhou
- 11:45 a.m. **Divye Arora-Jain**
  Mentor: Drs. Liang Zhan and Haoteng Tang
- 12:00 a.m. **Malynn Jones**
  Mentor: Dr. Sandra Murray
- 12:15 p.m. **Shaun Fernando**
  Mentor: Dr. Ye Ye and Yuhe Gao

12:30 p.m. **Lunch – Baum 4th floor foyer and 407A/B**

2:00 p.m. **Hillman Academy Closing Ceremony**
Assembly Building – First Floor Auditorium, 5051 Centre Ave

Immunology and Cancer Immunotherapy Site Agenda

August 4, 2023, 9 a.m. to 2 p.m.
West Wing Auditorium
https://pitt.zoom.us/j/91311468741 | Meeting ID: 913 1146 8741

8 – 8:30 a.m.	**Breakfast (optional)**
8:30 – 8:45 a.m.	**Opening Remarks** *Drs. Tullia Bruno and Greg Delgoffe*
8:45 – 9 a.m.	**Lea Omer** *Mentor: Dr. Tina Sumpter*
9 – 9:15 a.m.	**Alessandra Azure** *Mentors: Drs. Greg Delgoffe and Dayana Rivadeneira*
9:15 – 9:30 a.m.	**Carlo Gambotto** *Mentors: Dr. Tullia Bruno and Allie Casey*
9:30 – 9:45 a.m.	**Ryan Krishna** *Mentor: Dr. Alok Joglekar*
9:45 – 10 a.m.	**Parthiv Reddy Bandi** *Mentor: Dr. Alok Joglekar*
10 – 10:15 a.m.	**Short Networking Break**
10:15 – 10:30 a.m.	**Oluwatobiloba Olaore** *Mentors: Dr. Melissa Kane and Bailey Layish*
10:30 – 10:45 a.m.	**Kamili Wiley** *Mentors: Drs. Ali Kohan and Apoorva Narain*
10:45 – 11 a.m.	**Sulwe Kauffmann-Okoko** *Mentors: Drs. Ali Kohan and Apoorva Narain*
11 – 11:15 a.m.	**Audrey Monro-Neely** *Mentors: Drs. Robert Ferris and Lazar Vujanovic*
11:15 – 11:30 a.m.	**Ruby Krotine** *Mentors: Dr. Jason Lohmueller*
11:30 – 11:45 a.m.	**Short Networking Break**
11:45 a.m. – 12 p.m.	**Jermaine Taylor** *Mentors: Drs. Rachel Gottschalk and Morgan Jackson-Strong*
12 – 12:15 p.m.	**Lily Pulkowski** *Mentors: Drs. Dario Vignali, Creg Workman, and Ellen Scott*
12:15 – 12:30 p.m.	**Camilla Zarour** *Mentors: Dr. Abby Overacre*
12:30 – 12:45 p.m.	**Iliyan Nazarali** *Mentor: Dr. Jishnu Das*
12:45 – 1 p.m.	**Arya Mehta** *Mentor: Dr Hassane Zarour*
1 – 1:15 p.m.	**Norra Coen-Pirani** *Mentor: Dr. Hassane Zarour*
1:15 p.m.	**Final remarks, group picture, and grab and go lunch** **Migrate to Assembly Building**
2 p.m.	**Start of Final Ceremony in Assembly Auditorium**

OPT Site Agenda

August 04th, 2023, 9:30 a.m. to 12:30 p.m.
In-person meeting at MHP-PAV 4.204
https://pitt.zoom.us/j/96656638949

Each session will be started by a brief intro of each student by his/her mentor followed by a 10-minute presentation leaving 2 minute Q&A.

9:30 - 9:45 a.m.	**Start the OPT site meeting**
9:45 - 10:00 a.m.	**YES student Jasmine Horton** *Mentor: J. Patrick Mayo*
10:05 - 10:20 a.m.	**YES student Daniel Komlosi** *Mentor: Dr. Robert M. Shanks*
10:25 - 10:40 a.m.	**Jason Ma** *Mentor: Dr. Shaohua Pi*
10:45 - 11:00 a.m.	**Araina Nevels** *Mentor: Dr. John Ash*
11:05 - 11:20 a.m.	**Ismael Aly** *Mentor: Miguel Betegon*
11:25 - 11:40 a.m.	**Sophia Hati** *Mentor: Dr. Yuanyuan Chen*
11:40 - 12:30 p.m.	**Lunch**

Surgery Site Agenda

August 4, 2023
Scaife Hall Room 1104
3550 Terrace Street
Click here to join the meeting | Meeting ID: 254 534 625 438 | Passcode: 28BBaE

10:15 a.m. **Opening Remarks**
Dr. Steven Evans/Dr. Timothy Billiar

Research Presentations

10:30 a.m. **Mohammed Ali Al-Nagash**
Mentor, Dr. Joshua Brown

10:45 a.m. **Michael Ulis**
Mentor, Dr. Joseph Church

11:00 a.m. **Mariah Harris**
Mentor, Dr. Christine Leeper

11:15 a.m. **Lucas Pu**
Mentor, Dr. Rajeev Dhupar

11:30 a.m. **Terrell Wafford**
Mentor, Dr. Udai Kammula

11:45 a.m. **Break**
12 p.m. **Lunch - Scaife Hall Room 1104**

TDX Site Agenda

August 4, 2023
Bridgeside Point II, Room 503, 450 Technology Drive, Pittsburgh, PA 15219
Virtual: https://pitt.zoom.us/j/91589576294

8:30 a.m. **Welcome**
Dr. Andrew Duncan, Serafina Lanna, & Meagan Makarczyk, TDX Site Heads

8:45 a.m. **Oral Presentations** (10 min. presentations + 5 min. questions); introductions by lab mentors

8:45 a.m. **Abigail Bodart**
Lab, Dr. Vaughn Cooper; Mentors, Dr. Abigail Matela & Talia Grossman

9:00 a.m. **Claire Cho**
Lab, Dr. Hang Lin; Mentor, Meagan Makarczyk

9:15 a.m. **Madeline Douglas**
Lab, Dr. George Hussey; Mentors, Dr. William D'Angelo & Daniela Romero

9:30 a.m. **Gavin Drake**
Lab, Dr. Ioannis Zervantonakis; Mentor, Matt Poskus

9:45 a.m. **Vanessa Gonzalez-Rychener**
Lab, Dr. Shiori Sekine; Mentor, Ryan Houston

10:00 a.m. **Sophia Song**
Lab, Dr. Yusuke Sekine; Mentor, Ryan Houston

10:15 a.m. **August Kollar**
Lab, Dr. TK Kozai; Mentor, Kevin Stieger

10:30 a.m. **BREAK**

10:45 a.m. **Lucas Hertzel**
Lab, Dr. Bill Chen; Mentors, Dr. Travis Lear & Aine Boudreau

11:00 a.m. **Tabo Mkandawire**
Lab, Dr. Yuan Liu; Mentors, Dr. Travis Lear & Aine Boudreau

11:15 a.m. **Jade Lee**
Lab, Dr. Justin Weinbaum; Mentor, Ande Marini

11:30 a.m. **Arnav Patel**
Lab, Dr. Jonathan Vande Geest; Mentor, Adam Forrest

11:45 a.m. **Narendra Ray**
Lab, Dr. Amrita Sahu; Mentor, Adam Jasper

12:00 p.m. **Jada Weikel**
Lab, Dr. Andreas Vogt; Mentor, Laura Vollmer

12:15 p.m. **Lauren Weaver**
Lab, Dr. Jay Tan; Mentor, Dr. Bo Lv

12:30 p.m. **Luncheon – Bridgeside Point II, 5th-floor Lunchroom**

2:00 p.m. **Closing Ceremony**
Assembly Building, First Floor Auditorium

WCRC Site Agenda

August 4, 2023
The Assembly, Room B 1610
https://pitt.zoom.us/j/94802917925

10:30 a.m. **Welcome**
Partha Roy & David Gau, PhD

10:35 a.m. **Research Presentations**

10:35 – 10:50 a.m. **Aneri Shethji**
Lab, Dr. Partha Roy; Mentor, Ian Eder

10:50 – 11:05 a.m. **Na'Taeya Johnson**
Lab, Dr. Lan Coffman; Mentor, Geyon Garcia

11:20 – 11:35 a.m. **Joi Anthony-Gray**
Lab, Dr. Katherine Aird; Mentor, Dr. Racquel Buj

11:35 – 11:50 a.m. **Mae Cano**
Lab, Dr. Ron Buckanovich; Mentor, Stacy McGonigal

11:50 – 12:05 a.m. **Addison McLane**
Lab, Dr. Nadine Hempel; Mentor, Dr. Sierra White

12:05 – 12:20 a.m. **Donise Griffin**
Lab, Dr. Adrian Lee, Dr. Steffi Oesterreich; Mentor, Dr. Jagmohan Hooda

12:20 – 12:35 a.m. **Ny'Azia Roberts**
Lab, Dr. Adrian Lee, Dr. Steffi Oesterreich; Mentor, Haley Arbore

12:35 p.m. **12:35 – 1:45 p.m.** **Lunch – B 1610, The Assembly**

Collaborative Authorship in the Manuscript Development of Deep Learning Techniques and the Creation of a Medical Web App User Manual

Scholar: Om Arora-Jain
College: University of Michigan, Ann Arbor, MI

PI: Xia Jiang, PhD
Mentors: Xia Jiang, Yijun Zhou

Site: CoSBBI

Background

During the summer, my collaboration with Dr. Jiang involved two distinct projects. Firstly, I contributed to the composition of a manuscript detailing machine learning hyperparameter meta tuning. Deep feed-forward learning, also known as deep learning, has gained significant traction in the commercialized market but is yet to be explored in-depth clinically. Our objective was to predict late onset breast cancer metastasis (BCM) using a grid search strategy called Single Hyperparameter Grid Seach (SHGS). Secondly, I created a comprehensive user manual for the iMed web application, which allows users to take raw information and manipulate it in a manner that gives results useful in decision making. This can be to train a model, plot ROC curves, or predict an outcome using models and analysis. The goal was to create a user-friendly guide that would enable anyone from professionals to patients to effectively utilize iMed's functionalities.

Methods

To pursue our research objectives, we used a wide range of methodologies. For the machine learning manuscript, extensive literature search was used to gain a knowledge base and add that information onto our results. Authors with agreeing views, disagreeing views, information that corroborated our hypotheses, or totally alternate ideas were discussed and included using a reference management software called Mendeley. I also used online resources such as Lucidchart, enabling me to create a flow chart for readers to visually understand how SHGS works. In terms of the user manual, a docx file with custom style formatting headers and table of contents allows the user to jump to find what they need, in addition to a browser pdf panel highlighting all enclosed information.

Results

The main subsections I focused on for the manuscript detailing machine learning hyperparameter meta tuning were successfully completed. Of the 8 hyperparameters discussed, I focused on the discussion of learning rate, momentum, and decay as well as their relationship to each other and how certain hyperparameters have more of an impact on model performance than others. The user manual was also completed and incorporated into the web application and can be found at http://imed.odpac.net/static/user_manual.pdf.

Title: The MET-TWIST1 pathway regulates the key glycolytic enzyme, Hexokinase 2 in *MET* altered NSCLC

Scholar: Jason Chen

High School/College/City/State: Johns Hopkins University, Baltimore, MD

PI of group/lab: Dr. Timothy Burns, MD, PhD

Mentor(s): Dr. Vinod Kumar, PhD, Laura Stabile, PhD

Site: Cancer Biology

Non-small cell lung cancer (NSCLC) has the highest incidence of brain metastases (BM) with an occurrence rate in almost 40% of patients, yet there are no BM-specific targeted therapies available. MET is a receptor tyrosine kinase that binds with hepatocyte growth factor (HGF) to mediate many cellular processes evolved in tumorigenesis. The HGF/MET pathway is commonly up-regulated in cancer either as a result of MET or HGF protein overexpression, *MET* genomic amplification or *MET* mutations. We have identified a significant enrichment of *MET* amplification in lung adenocarcinoma (LUAD) BM (16%) compared to primary LUAD (3%). We found that *MET* amplified BM had a distinct transcriptional signature reflecting high glycolysis. We further observed increased glycolysis in *MET* amplified and high MET expressing cell lines. Finally, we found that *MET* altered cell lines are more sensitive to glycolytic inhibitors and MET inhibition decreased glycolysis. How the HGF/MET pathway regulates glycolysis is poorly understood. We hypothesized that the HGF/MET pathway increases the expression of key glycolytic enzymes. Therefore, we examined whether MET inhibition decreased the levels of key glycolytic and other metabolic pathway enzymes. MET inhibitor treatment decreased mRNA and protein expression of the key glycolytic enzyme Hexokinase II (HK2). Conversely, HGF was not sufficient to increase HK2 expression in the presence of complete media. Interestingly, in cells with acquired MET TKI resistance, we found that HK2 levels were significantly increased compared to the parental MET TKI sensitive parental cells. Furthermore, we found the transcription factor, TWIST1 which we have shown is a key downstream mediator of the MET pathway, increased HK2 expression even in the presence of a MET inhibitor both on the RNA and protein level. Ongoing experiments are examining whether TWIST1 is a direct transcriptional regulator of HK2 and whether we can effectively target glycolysis in *MET* altered cell lines.

Isolation and Characterization of Lipids from the Extracellular Matrix

Scholar: Madeline M. Douglas
College: Columbia University, New York, NY
Lab: George Hussey
Mentor: Salma O. El-Mossier
Site: Tech Drive-X

Matrix-bound nanovesicles (MBV) have been identified as an integral and functional component of the extracellular matrix (ECM) and play a critical role in wound healing. Several studies have characterized the nucleic acid and protein composition of MBV, however, the role of MBV lipids is largely unexplored. Herein, we evaluate the effect of MBV lipids on cell viability. Previous methods of isolating lipids from tissues have been thoroughly researched, namely through the Folch method. Thus, a derived version of the Folch method was used to evaluate its ability in isolating lipids. Additionally, we evaluated their bioactivity in-vitro using HET1A and OE33 and aimed to understand if the lipids are the bioactive part of the MBV. Our study compared the lipids isolated from both MBV and ECM in terms of solubility, quantity, quality, bioactivity, and purity. The Folch method was successfully used to isolate lipids without contamination of proteins and nucleic acids. The lipids isolated from MBV and ECM showed different concentrations of phospholipids, unsaturated fatty acids, and neutral lipids. At high doses, lipids extracted from MBV from whole ECM were shown to be cytotoxic to cells. Future experiments will evaluate lower concentrations of lipids on cell viability. Additionally, to determine compositional differences between ECM and MBV lipids, lipidomics would be beneficial. Finally, future experiments will be aimed at delineating the role of lipids on cell phenotype and function.

Age-related changes in gene expression and the tumor microenvironment in ER+ breast cancer

Donise Griffin[1], Neil Carleton[2], Michael Gorry[2], Steffi Oesterreich[2], Adrian Lee[2]
[1]Carnegie Mellon University, Pittsburgh, PA, Lee/Oesterreich Lab - [2]Women's Cancer Research Center of Magee Women's Research Institute, UPMC Hillman

Background *Age is one of the strongest risk factors for the development of cancer, with estimates of 1.9 million new cases of cancer diagnosed in a year[1], thus as the average life expectancy continues to increase it is important to study cancers' relationship with aging. ER+ breast cancer (BC) is an age-related disease, with the peak incidence occurring around ages 65-70. Given the changes in hormone biology, including systemic and local estradiol levels, as well as changes to the estrogen receptor itself, studying differentially expressed and methylated genes such as ESR1 allows for further hypothesis generating studies centered around aging. Studying the differences in biological phenotypes between tumors that develop in younger and older women is necessary to establish more effective and less invasive treatment strategies and ways to mitigate overtreatment.[2]*

Methods Schematic of study design: (n = 115 patients, all with ER+ BC – all plasma, tumor tissue, and normal-adjacent tissue was obtained from the Pitt Biospecimen Core (PBC) at Magee Women's Hospital. (n=90) Patients all non-cancerous, – plasma, tumor tissue, and normal-adjacent tissue was obtained from the Komen tissue bank). After prior analysis and experimentations ran, 83 Er+ BC samples and 85 adjacent samples remained. Bulk RNA-sequencing was used to profile the transcriptome of a cohort of human patient tumor and tumor-adjacent samples using the Illumina platform. Following quality control, of the 83 mapped samples, 8 samples were identified as extreme outliers and not included in the analysis or normalization. Mapping produced 57,773 sites and after further filtering of sites for 0, a noise reduction of <3.1 and protein coding genes resulted in 16,422 remaining sites. Quantile normalization from the {processcore} package library was performed on the remaining 75 (ER+) samples using R.version 4.3.0 (2023-04-21). Selection for protein coding genes (ESR1, GREB1, TFF1, CYP19A1, PGR) and key enzymes (HSD17B7 and HSD17B2) that are commonly referenced as having relation to age and ER+ BC was done and mapping of their expressional relations to age was completed using {ggplot2}.

Results Figure 1 displays a higher ESR1, GREB1, TFF1, CYP19A1, and HSD17B7 expression in the elderly age groups compared to the younger cohorts. Whilst there is lower expression of PGR, and HSD17B2 for the elderly age cohorts compared to the young group.

Conclusion Despite elderly patients harboring an inflamed microenvironment, the tumors do not seem to mount an adequate immune response. Elderly patients seem to have higher gene expression levels of ESR1 and estrogen-related genes despite low circulating levels of E2.

Future directions The performance of further statistical tests to examine if the changes seen are statistically significant across the age groups should be done with the data set to strengthen claims. Additional downstream analysis with measured analytes in the tumor microenvironment and this process should be repeated for tumor adjacent samples.

---

[1] "Cancer Facts & Figures 2022." *American Cancer Society*, amp.cancer.org/research/cancer-facts-statistics/all-cancer-facts-figures/cancer-facts-figures-2022.html. Accessed 28 July 2023.

[2] Carleton, Neil, et al. "Personalising Therapy for Early-Stage Oestrogen Receptor-Positive Breast Cancer in Older Women." *The Lancet Healthy Longevity*, vol. 3, no. 1, 2022, https://doi.org/10.1016/s2666-7568(21)00280-4.

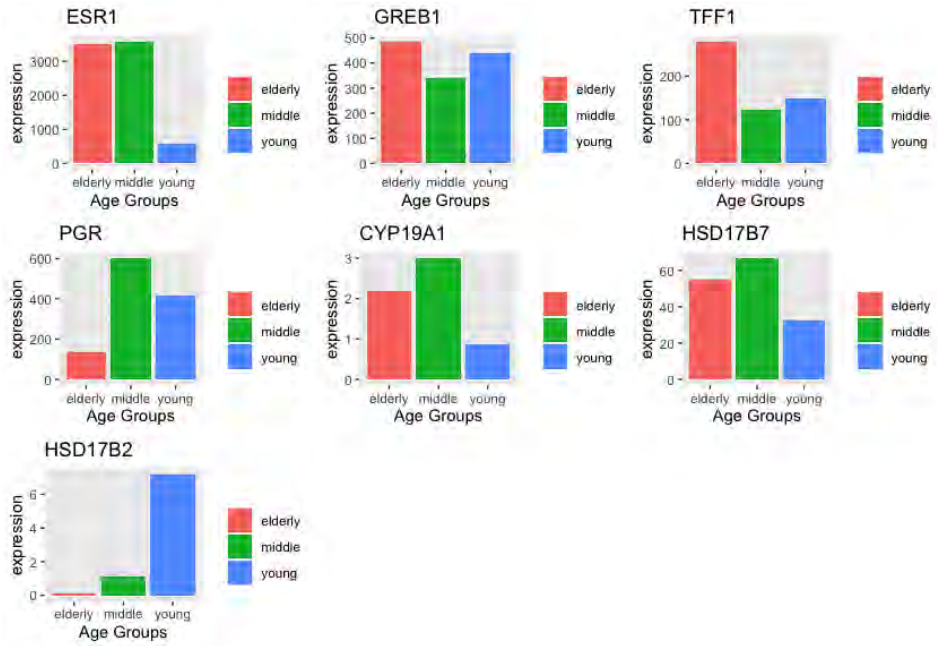

Figure 1: Median expression values of {ESR1, GREB1,TFF1, PGR, CYP19A1,HSD17B7, and HSD17B2} for Elderly (>=70 yo), middle aged (55>69 yo) and young(30<55 yo) patients.

Patient-Specific Computational Modeling of Cerebral Blood Flow in Adults with Sickle Cell Disease

Anyssa R.Oden, High School Diploma[1], Lara Abdelmohsen, BS[1]
[1]Department of Biomedical Engineering, Carnegie Mellon University, Pittsburgh, PA

Abstract (50-75)

Patients with sickle cell disease (SCD) tend to suffer from clinical complications of neurovascular occlusions such as stroke and ischemia. The life expectancy for SCD patients has drastically increased due to the Stroke Prevention Trial in Sickle Cell Anemia (STOP), however research surrounding SCD has not advanced to reflect the age of patients. This study uses MRI images to create 3D models of the cerebral vasculature of patients with SCD and corresponding simulations of blood flow.

Introduction

Sickle Cell Disease (SCD) is an inherited blood disorder that causes sickled red blood cells (RBCs). These RBCs are inflexible, stick together, and are inefficient at carrying oxygen throughout major organs. The brain needs a constant blood flow to maintain normal cognitive function, which is preserved by cerebral autoregulation. However, patients with SCD tend to have vascular instabilities and impairments in cerebral autoregulation due to their blood rheology, which can lead to major complications such as cerebral hemorrhage, ischemic stroke, and impaired cognition [1]. The circle of willis (CoW) is the major vasculature system in the brain in which vascular instability arises for patients with SCD [2]. To understand the altered hemodynamics of SCD, patient-specific modeling of the CoW is important because of differences in geometry that could affect how blood flows. Computational fluid dynamics (CFD) is a useful method for simulating and predicting the effects of the complications that can arise in cerebral vasculature due to vascular instability from varying blood flow [3]. The goal of this study is to create a 3D model of an SCD patient's CoW to use in future simulations of flow in cerebral vasculature to predict disease severity or cascade events for the patients.

Methods

Time of Flight (ToF) images were obtained from a 44-year-old female patient with SCD and a 51-year-old female with no comorbidities in a previous study to visualize cerebral vasculature. The images were gathered from a 7T Siemens Magnetom MRI Scanner, and post-processed using bias correction for clarity of anatomy. SimVascular, an open-source cardiovascular modeling and simulation software was used to create the 3D models [4]. To reconstruct the CoW, centerline paths were created from the MRI images. 2D segmentations were performed using the previous paths as a guide and then a 3D model was reconstructed.

Results

Using the method specified, we successfully produced 3D models for both patients. Figure 1 is the CoW of the control patient, and figure 2 is the CoW of the patient with SCD. Both are color coded to show similarities and differences in anatomy: green is the anterior cerebral artery (ACA), yellow is the internal carotid artery (ICA) that forms into the middle cerebral artery (MCA), orange is the posterior communicating artery (PCA2), red is the basilar artery that branches off into the posterior cerebral arteries (PCA), purple is the superior cerebellar arteries (SCA), and blue is the anterior communicating artery (ACA2). Any vessels without color are patient-specific, meaning these vessels only appear in their respective patient and are not part of the CoW. The patient with SCD has more vessels, especially at bifurcations between arteries or form bifurcations (e.g vessels on left PCA) and an extra ACA2. Additionally, their PCAs look skinnier compared to the control's. On the other hand, the control patient only has two extra PCA2 and 3 other vessels branching from the CoW.

Discussion

Based on comparison between the two anatomies, we can hypothesize that anatomical differences in cerebral vasculature is normal since the branching vessels are different between patients. Based on figure 2, a possible conclusion for the number of extra vessels could be due to vaso-occlusive events throughout the CoW, also evident by the seemingly abnormal curvature of the patient's ACA and PCA. While this patient has no reported strokes, they

could have suffered from a silent cerebral infarct (SCI) which would also explain their CoW's abnormal shapes. It is unclear whether the patient with SCD anatomy is due to vaso-occlusion and angiogenesis as a result or will simply increase risk of complications due to possible alterations in hemodynamics. Further investigation will involve a larger sample of patients from which a pattern could develop and reveal what is (ab)normal variation in patient-specific anatomy, as well as CoW geometry. CFD will be used to understand how geometrically the CoW affects hemodynamics, and vice versa. Patient-specific modeling should continue to be emphasized as it could reveal further complications that a patient may develop or have experienced if not already diagnosed.

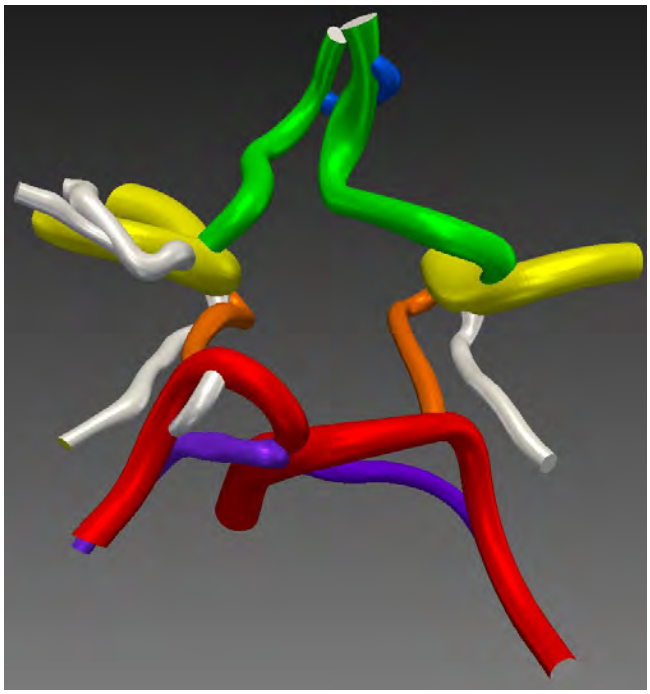

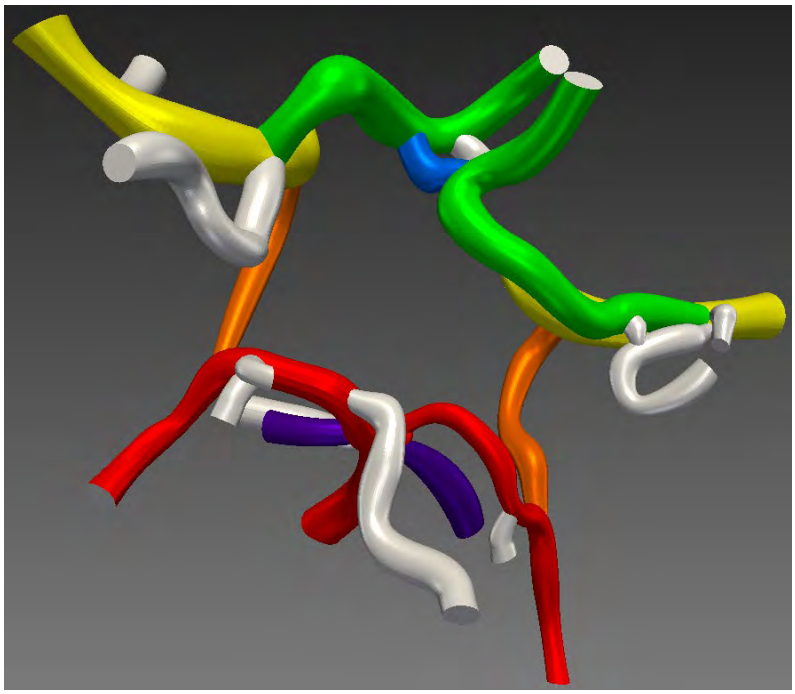

Figure 1 (Left). 3D model of control's CoW, with arteries in color and patient-specific vessels in grey (see results).

Figure 2 (Right). 3D model of patient with SCD's CoW, with arteries in color and patient-specific vessels in grey (see results).

References

1. Stotesbury H., Kawadler J.M., Hales P.W., Saunders D.E., Clark C.A., Kirkham F.J (2019). "Vascular Instability and Neurological Morbidity in Sickle Cell Disease: An Integrative Framework." *Frontiers in Neurology*, 10.
2. Valadi, N., Silva, G. S., Bowman, L. S., Ramsingh, D., Vicari, P., Filho, A. C., Massaro, A. R., Kutlar, A., Nichols, F. T., & Adams, R. J. (2006). "Transcranial Doppler ultrasonography in adults with sickle cell disease." *Neurology*, *67*(4), 572–574. https://doi.org/10.1212/01.wnl.0000230150.39429.8e
3. Devault, K., Gremaud, P. A., Novak, V., Olufsen, M. S., Vernières, G., & Zhao, P. (2008). BLOOD FLOW IN THE CIRCLE OF WILLIS: MODELING AND CALIBRATION. *Multiscale modeling & simulation : a SIAM interdisciplinary journal*, *7*(2), 888–909. https://doi.org/10.1137/07070231X
4. Updegrove, A., Wilson, N.M., Merkow, J., Lan, H., Marsden, A.L., and Shadden S.C(2017). "SimVascular: An Open Source Pipeline for Cardiovascular Simulation," *Annals of Biomedical Engineering,* (45), 525-541. https://doi.org/10.1007/s10439-016-1762-8

RNA-seq data analysis for mechanism of action of p62 targeting small molecular on Multiple Myeloma

Oliver E. Adams, Dr. Guangyi Zhao
South Fayette High School, McDonald, PA; University of Pittsburgh Hillman Cancer Center Academy, Pittsburgh, PA

Abstract: We investigated the efficacy of a new drug lead, Xie25, for treating multiple myeloma by analyzing the reaction of the MM1.S cell line to the drug through bulk RNA-seq. The cells were treated with either 5 or 7.5 micromolar doses of Xie25, and their transcriptome was analyzed at 2, 4, and 8 hours post-treatment. The gene expression data were subjected to Ingenuity Pathway Analysis to identify altered biological pathways. The autophagy pathway and unfolded protein response pathway, along with other stress pathways, were highly upregulated, indicating the drug lead treatment induced severe cell stress.

Introduction: Multiple myeloma is a formidable blood cancer that primarily affects plasma cells, leading to abnormal and destructive growth of mutated plasma cells in the bone marrow. Multiple myeloma is considered incurable due to high rates of relapse and rapid development of drug resistance with autophagy pathway activation. To address these issues, our research focuses on developing a more effective drug for treatment, named Xie25, which uniquely binds to the p62 protein – a critical component in the autophagy pathway. Preliminary data indicates Xie25 aggregates the p62 protein and thus potentially dysregulates the autophagy pathway and leads to cell death. However, the detailed mechanism of action of Xie25 is largely unknown. The objective of the experiment is to understand the detailed mechanism of action that the drug performs to kill the cell.

Methods: To assess the impact of Xie25 on the MM1.S cell line, we treated cells with either 5 or 7.5 micromolar of Xie25 and collected transcriptome data using bulk RNA-seq at 2, 4, and 8 hours post-treatment. The transcriptome data from treatment groups were then compared to an untreated control group and analyzed using Ingenuity Pathway Analysis to learn of the underlying biological processes.

Results: Our analysis revealed significant upregulation of the autophagy pathway and unfolded protein response pathway in the Xie25-treated cells compared to the untreated control in a dosage and time-dependent manner. Additionally, stress indicators, such as the oxidative stress pathway and p38 MAPK signaling pathway, were markedly upregulated, indicating there was considerable cellular stress induced by the drug. The stress signaling pathways were consistently increasing over time. Interestingly, the cell survival signal pathway was increasing initially but began to decline at a later time point.

Discussion: The substantial upregulation of the autophagy pathway and unfolded protein response pathway strongly supports our hypothesis regarding Xie25's mechanism of action. The increased activity of the unfolded protein response pathway indicated that the treatment led to the accumulation of misfolded/unfolded proteins over time. The drug lead might have impaired the autophagy pathway’s capacity to dispose of the misfolded/unfolded protein by aggregating its

critical component, p62. In addition, the aggregated p62 itself may have become a new source of misfold/unfold protein stress. The concurrent upregulation of the autophagy pathway and unfolded protein stress pathway suggests that the drug overwhelms the cell's ability to eliminate misfolded proteins. This is further exemplified by the cell survival signaling pathway starting to decrease at a late time point, while the stress indicators remained constantly increasing. After 4-8 hours, the accumulated stress starts to overwhelm the cell survival signaling pathway, indicating the cell's imminent death. The series of events suggest that the unfolded proteins are the primary cause of cell death but will need to be researched further to certify. The next step of our process will be trying to identify the critical proteins governing the unfolded protein response pathway induced by the drug lead and conducting biological verification.

References: Wagner, E. F., & Nebreda, Á. R. (2009). Signal integration by JNK and p38 MAPK pathways in cancer development. *Nature Reviews Cancer*, *9*(8), 537-549. https://doi.org/10.1038/nrc2694

Role of PARP-2 in DNA Replication Stress

Scholar: Lorenzo Aguilera

High School/College/City/State: Franklin Regional Senior High School, Murrysville, Pennsylvania

PI of group/lab: Elise Fouquerel, Ph.D.

Mentor(s): Daniela Muoio, Ph.D. & Rim Nassar, Ph.D

Site: Cancer Biology

ADP Ribose Transferases (ARTs), including PARP1 and PARP2, are essential enzymes capable of transferring ADP-ribose to specific target proteins, playing crucial roles in DNA repair. In cancer treatment, PARP1 and PARP2 inhibitors are widely used to disrupt their enzymatic activity and trigger a DNA damage response, effectively eliminating cancer cells. Additionally, both PARP1 and PARP2 are involved in the cellular response to DNA replication stress (RS), a condition that arises when replication forks stall, potentially leading to DNA damage and mutagenesis. The precise contribution of PARP2 in this context remains elusive. Some evidence suggests that PARP2 plays a unique role in stabilizing replication forks. To explore this further, a comprehensive analysis was conducted using various HeLa cells in which PARP1 and/or PARP2 genes were depleted. To induce RS, the cells were treated with aphidicolin (APH), a DNA polymerase inhibitor that slows down DNA replication. A combination of techniques, including western blot, immunofluorescence, and metaphase spreads, was employed to assess the impact of APH treatment on RS and DNA double-strand breaks (DSBs) within the cells. Phospho-CHK1, a marker of RS, revealed an increased occurrence of RS in response to increasing concentrations of APH. Notably, the PARP1/2KO cell line exhibited intensified RS, providing compelling evidence for the involvement of both enzymes in RS response. Immunofluorescence analysis allowed visualization of proteins 53BP1 and gH2AX, both indicative of DSBs. Quantification of these proteins indicated that higher APH concentrations triggered more DSBs, and interestingly, the PARP2KO cell line displayed the highest number of breaks. Our findings highlight the unique involvement of PARP2 in the response to DNA RS. Further research is needed to fully understand the underlying mechanisms, which could have implications for targeted cancer therapies. In conclusion, this study provides valuable insights into the role of ADP Ribose Transferases, particularly PARP2, in DNA RS. Understanding these mechanisms enhances our knowledge of DNA repair processes and may offer new avenues for cancer treatment.

N^6-methyladenosine (m^6A) Modification Regulates Kaposi's Sarcoma-associated Herpesvirus (KSHV) Lytic Replication

Scholar: Rami Alhallak

University: University of Pittsburgh

PI of Lab: Dr. Shou-Jiang Gao

Mentor: Wen Meng

Site: Cancer Biology

Background: N^6-methyladenosine (m^6A) is the most prevalent modification on messenger RNAs (mRNAs). Cellular machinery of m^6A consists of "writer" methyltransferases, "reader" m^6A binding proteins, and "eraser" methylases. m^6A modification profoundly influences almost all phases in biogenesis and functions of mRNAs including pre-mRNA splicing, pri-miRNA processing, mRNA export, mRNA stability, translation modulation and mRNA degradation. Recent studies have shown that m^6A modification plays an essential role in both physiological and pathological conditions. Kaposi's sarcoma-associated herpesvirus (KSHV) is the etiological agent of Kaposi's sarcoma (KS), primary effusion lymphoma (PEL), multicentric Castleman's disease (MCD), and KSHV-associated inflammatory cytokine syndrome (KICS). KSHV possesses both latent and lytic replication phases in its life cycle. KSHV transcripts contain abundant m^6A modifications during latent and lytic replication.

Methods: KSHV latently infected iSLK-BAC16-RGB cells were treated with different doses of inhibitors targeting m^6A "eraser" FTO (FB23-2) or ALKBH5 (IOX1, C6, C3) under KSHV latency or lytic. Microscopy was used to quantify the number of GFP-positive cells, which reflected that state of KSHV lytic replication.

Results: FTO or ALKBH5 methylases inhibitors did not induce any GFP-positive cells in untreated KSHV latent cells over time. Treatment with sodium butyrate (NaB) induced KSHV lytic replication based on the increase of GFP-positive cells. However, FTO or ALKBH5 inhibitors reduced the number of GFP-positive cells in NaB treated cells. The highest concentration of inhibitors used in experiments caused minimal cell toxicity.

Conclusion: Neither FTO inhibitor nor ALKBH5 inhibitor was sufficient to induce KSHV lytic reactivation from latency. FTO and ALKBH5 inhibition reduced KSHV lytic replication. Taken together, inhibitors of m^6A eraser proteins could be used as potential therapeutic drugs for KSHV lytic replication.

Relationship Between Social Determinants of Health and Undertriage in Trauma Patients

Mohammed Ali Al-Nagash

PI: Dr. Joshua Brown, MD, MSc

Mentors: Dr. David Silver, MD, MPH; Dr. Joshua Brown, MD, MSc

Site: Surgery

Introduction

Undertriage occurs when a severely injured patient is brought by paramedics to a hospital that is not a trauma center. Patients may not receive necessary care, which increases the risk of death after injury. Social determinants of health (SDOH) are the conditions that people live in, such as their education, economics, social and communal context, and healthcare access. Worse SDOH have been associated with poorer outcomes in trauma patients. Our objective is to evaluate if SDOH are associated with undertriage, which may mediate worse outcomes in disadvantaged communities.

Methods

We defined undertriage as anyone who met emergency medical services (EMS) criteria for a level I/II trauma center but not transported to one by EMS. We used the social deprivation index (SDI; 0-100 scale) to measure SDOH with higher values indicating more disadvantaged communities. Patient-level logistic regression determined the association between undertriage and SDOH controlling for demographics, vital signs, injury severity, mechanism, and EMS transport time and distance. The rate of undertriage was calculated across Pennsylvania at the zip-code level and linear regression evaluated the association with SDI.

Results

166,632 patients were included with a 28.1% undertriage rate overall. Undertriaged patients were clinically similar to appropriately triaged patients; however, they had longer transport times, distances, and were more likely to be transported by ground ambulance. Every 5-point increase in the SDI was associated with a 0.7% increase in the odds of undertriage (aOR 1.007; 95%CI 1.001-1.013, p=0.025). At the zip-code level, the undertriage rate increased 0.2 patients/1000 population for every 5-point increase in the SDI (coeff 0.190; 95%CI 0.082–0.298, p=0.001), with significant variation across Pennsylvania.

Conclusion

There is an association between SDOH and undertriage. This data can inform targeted educational strategies for paramedics in high-undertriage areas. Further studies in different types of trauma systems can help further elucidate this relationship.

ATR kinase and thymidylate synthase inhibitors as a novel therapeutic for induced deoxyuridine contamination in cancer cell genomic DNA and cell death

Scholar: Franco Alvarez

High School/College/City/State: Greensburg Central Catholic, Greensburg, PA

PI of group/lab: Christopher Bakkenist, PhD

Mentor(s): Joseph El-Ghoubaira, MD

Site: Cancer Biology

Background: Traditional cancer therapeutics are effective in inducing DNA damage that combats cancer's ability to survive. These treatments work faster in cancer than normal cells due to the cancer's characteristic high replication speed. For effectiveness, these treatments may require a high dosage that is also lethal to normal cells. ATR kinase inhibitors (ATRi) can alternatively work to prevent a cell with damaged DNA from entering arrest and repairing before replication, and downstream cause a buildup of deoxyuridine in genomic DNA, which can be toxic. However, the introduction of thymidylate synthase (TS) will rescue damaged DNA from deoxyuridine contamination. A potential for combined doses of an ATR kinase inhibitor and thymidylate synthase inhibitor may induce deoxyuridine toxicity at levels adequate for cancer cell death.

Methods: Murine colorectal carcinoma cell line CT26 and murine melanoma cell line B16 were plated into 96 well plates (respectively) and treated with increasing dosages of AZD6738 (ATRi) and Pemetrexed (TS inhibitor), one along the x-axis and the other on the y-axis. Control is a combined DMSO dosage, representing no treatment. CellTiter-Glo® assay and BioTek Synergy LX multimode reader provided quantitative luminescence data representing cell viability after treatment. Combenefit compiled data to create figures.

Results: Several drug combination screenings show a significant decrease in cell viability when treated with ATRi and TS inhibitor when compared to the control in analyzed results. While all results show synergistic reactions, effective drug dosages are not consistent across cell lines.

Conclusion: AZD and Pemetrexed prevented G1 cell arrest, promoting deoxyuridine contamination and retaining toxicity, combining to create an effective synergy in reducing cell viability in varying cancer cell lines *in vitro*. Varying levels of synergy across cell lines suggests that custom dosages are required to achieve synergistic reactions.

Future Directions: Testing a larger quantity of cell lines is an immediate interest, followed by transitioning to drug combination screenings *in vivo*, to observe the effects within the complex organism.

Novel System to Ensure Coinfection of AAVs Used In Retinal Gene Therapy

Scholar: Ismael Aly

High School: Brighton College Abu Dhabi, Abu Dhabi, United Arab Emirates

Mentor: Miguel Betegon, PhD

Site: Ophthalmology

Gene therapy using adeno-associated viruses (AAVs) is an exciting and developing path towards the curing of many inherited retinal disorders, where they can be used as non-pathogenic vectors to deliver therapeutic genes to affected cells in the retina. Also, AAVs are unable to integrate the payload gene into the cell's genome and are engineered to be replication incompetent, meaning they do not continue to replicate after the initial infection. For certain retinal diseases, such as Usher syndrome and Stardgardt disease, the 4.7 kb carrying capacity of an AAV is not large enough to deliver the required gene for the therapy. Long genes must be split into two halves that are packaged into two separate AAVs. However, this is inefficient as co-infection occurs with low probability, and single infection leads to the expression of truncated protein products. We are developing a system to physically tether two AAVs together by engineering the virus' capsid through the addition of a tag that can spontaneously and covalently link to a specially designed linker protein. This allows two AAVs to be linked and ensures they infect simultaneously to always deliver both halves of the gene. This approach will greatly increase the efficiency of full gene expression and reduce the formation of truncated protein products, enabling therapies where delivery of a large gene is necessary. We have expressed and purified the linker protein through fast protein liquid chromotography, and we have cloned 6 different AAV capsid vectors containing the linking tags in different positions. We will then test these AAVs together with the linker protein to determine the most efficient linking conditions.

Evaluating Drug Combinations with Alisertib, an Aurora A Kinase Inhibitor, for the Treatment of Small Cell Lung Cancer

Scholar: Desiree Amponsah

High School/College/City/State: Western School of Technology, Baltimore, Maryland

PI of group/lab: Taofeek Owonikoko, M.D. PhD

Mentor(s): John Schmitz, PhD

Site: Cancer Biology

Small cell lung cancer (SCLC) is an aggressive neuroendocrine tumor characterized by rapid disease progression and poor patient survival. Key transcription factors implicated as drivers of unique biological phenotypes of SCLC include ASCL1, NEUROD1, YAP1, and POU2F3. Strategies to exploit these phenotypes for innovative precision medicine approaches will be impactful. Alisertib is a selective inhibitor of Aurora A kinase which is part of a family of mitotic serine/threonine kinases that play critical roles during mitosis and meiosis to maintain cell proliferation. It has demonstrated activity against SCLC tumors in early clinical trials. As single drug treatments are rarely effective due to the heterogeneity of cancer, we hypothesized that combining alisertib with standard SCLC drug treatments (paclitaxel, irinotecan (SN38), temozolomide, and lurbinectedin that will enhance inhibition of SCLC cell proliferation. We utilized cell proliferation assays and immunoblot analysis to evaluate the effect of alisertib alone and in combinations on DMS114 cell line (YAP1 subtype). After determination of the IC50 of alisertib and four standard drugs, the agents were added to DMS114 cells using non-constant drug ratios. Possible drug synergies were calculated using CompuSyn. Combination index values (CI) greater than, equal to, or lower than 1 represent antagonistic, additive, or synergistic interactions. Combinations of alisertib and paclitaxel had synergy across most drug concentrations while alisertib and SN38 combinations only demonstrated synergy within a narrower range of concentrations. We further interrogated the specific mechanism for which alisertib induced DMS114 cell death. Alisertib was added to cells and allowed to incubate for 24 and 72 hours prior to immunoblot analysis. We observed increase phosphorylation of histone H3 (a marker of G2/M cell cycle block) after 24 h. PARP cleavage was not observed suggesting DMS114 cells were not undergoing apoptosis following alisertib treatment. Future studies will investigate the specific cell death pathway as well as evaluate the drug combinations in other SCLC cell line subtypes.

Suppression of p16 cause dysregulation of the circadian rhythm

Scholar: Joi Anthony-Gray

School: University of Pittsburgh

Lab: Katherine Aird, PhD

Mentor: Raquel Buj Gomez, PhD

Site: Women's Cancer Research center

Background: The circadian rhythm is the 24-hour internal clock in our body that regulates cycles of alertness and sleepiness by responding to light changes in our environment. Recent studies suggest that patient response to immunotherapies may be controlled by circadian rhythms. Interestingly, unpublished data from the laboratory demonstrated that loss of the tumor suppressor and cell cycle regulator p16 drives a pro-tumorigenic metabolic reprogramming leading to immunotherapy resistance. Because circadian rhythms are intimately linked to internal cycles such as the cell cycle and metabolism, we hypothesized that an altered circadian rhythm in tumors with suppression of p16 might be in part responsible for the low immunotherapy response in these patients.

Methods: I used one very well-known clinically relevant alteration of the cell cycle driving tumorigenesis: suppression of p16 in melanoma cells derived in mice (YUMM5.2). These plated cells are all at a different stage in the circadian rhythm and in order to see patterns we need to synchronize them. Using Dexamethasone (Dex), a corticosteroid widely used for this purpose, the cells need to be treated for 30 mins and then left in regular media for 24 hrs. Since there is no data published about what dosage of Dex to use to achieve my goal, two treatments, one with 100nM and another with 1uM was used and I will be looking at which concentration triggers an effect on the cells. After RNA is isolated, cDNA is retrotranscribed and the expression of circadian genes is assessed by qPCR.

Results: p16 suppression in YUMM5.2 cells was confirmed by western blotting. While there was an effect in both the 100nM and 1uM concertation of dexamethasone used to synchronize the cells, I found that the 1uM result showed more of a significant distinction. I also showed that suppression of p16 directly affects the expression of the circadian rhythm genes *in vitro*, however the two shRNAs hairpins used to suppress the expression of p16 have opposite effects, suggesting that off target effects might be occurring.

Conclusion: my experiments shows that 1uM of dexamethasone is ideal for the synchronization of the circadian rhythm core genes in YUMM5.2 cells. Additionally, I found that suppression of p16 affects the expression of circadian rhythm genes in Dex-synchronized cells. Future experiments using multiple other shRNAs hairpins will determine the exact pattern of expression of these genes.

Deep Learning for Adult Self-Report Score Prediction via Brain Networks

Divye Arora-Jain[1], Haoteng Tang, Ph.D.[2], Liang Zhan, Ph.D.[2]
[1]Montour High School, McKees Rocks, PA; [2]Electrical and Computer Engineering, University of Pittsburgh, Pittsburgh, PA

Abstract

MRI-derived Brain networks have been broadly utilized to understand and analyze clinical phenotypes, such as human behaviors. We propose a hierarchical graph learning framework to embed the brain network data based on the network community structure, where the network features are yielded for human behavior predictions. Our proposed framework is evaluated on Human Connectome Project (HCP) dataset including 1000 *young health subjects, and the prediction Mean Absolute Errors (MAEs) are reported in this abstract.*

Introduction

Traditional graph-theoretical methods aim to extract topological features (e.g., centrality) from brain networks and utilized these features to predict different clinical phenotypes [1, 2]. These methods only characterize brain networks from one or a few perspectives, which results in information loss and sub-optimal prediction results. However, deep geometric learning techniques (e.g., graph neural networks (GNN)) can directly embed the topological structures and node attributes of whole brain networks, which will efficiently yield comprehensive network representations. Meanwhile, the propagation mechanism of GNN, though it facilitates the network node embedding, may not capture the intrinsic hierarchical structures that existed in brain networks [3]. To tackle this issue, we propose a community-based hierarchical graph neural network to embed the brain networks for human behavior prediction.

Methods

As shown in Figure 1, our proposed hierarchical brain network learning framework consists of a stacked graph convolution block to perform the network node embedding, a community-based network pooling block to downscale the brain network, and a Multilayer Perception (MLP) block for the behavior score prediction. The graph convolution block consists of a stack of graph convolution neural (GCN) layers. The pooling block includes the following step: (1) Compute the centroid node probability matrix to find M community center nodes, (2) Assign each network node to the closest community, (3) Aggregate features of community members to the corresponding center node, (4) Downscale the brain network based on the partitioned communities. We utilize the MSE loss to minimize the difference between the model prediction $\hat{y}$ and the ground-truth y (such as $L_{pred} = \ell_{MSE}(\hat{y}, y)$).

Results

Our experimental data was downloaded from the publicly available Human Connectome Project dataset [4] (HCP). The details of these four ASR scores can be found at the HCP official website (https://wiki.humanconnectome.org). The regression mean absolute errors (MAEs) are presented in Figure 2. The MAEs on WITD, ATTN, INTR, and EXTN are 6.30, 5.37, 5.21, and 9.11, respectively.

Discussion

The proposed community-based pooling block is flexible that can be inserted into any deep graph learning framework for network classification or regression tasks. The whole proposed framework is flexible for different brain network prediction tasks. The prediction results on 4 different ASR scores are promising.

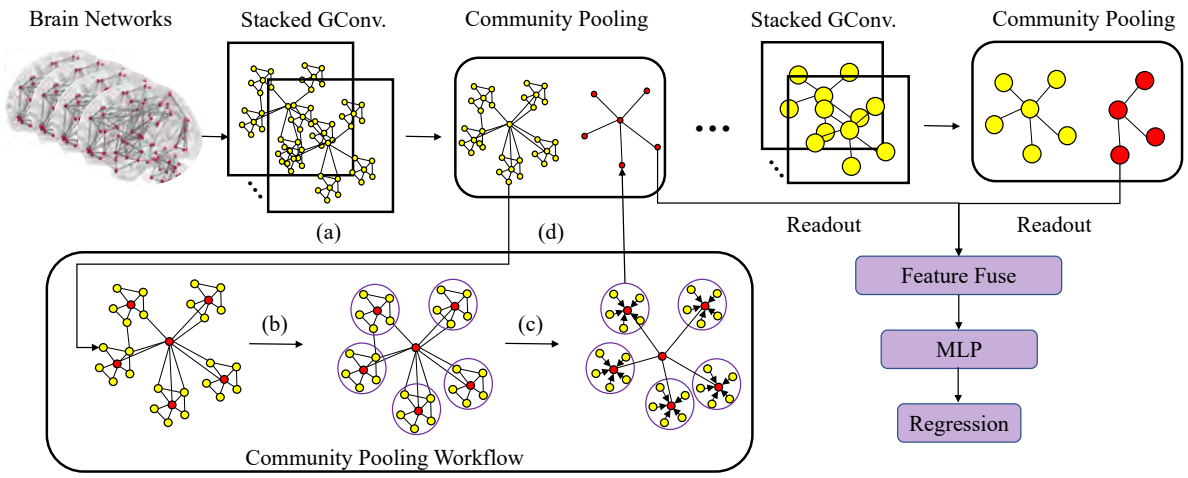

Figure 1: Diagram of the proposed hierarchical brain network learning framework

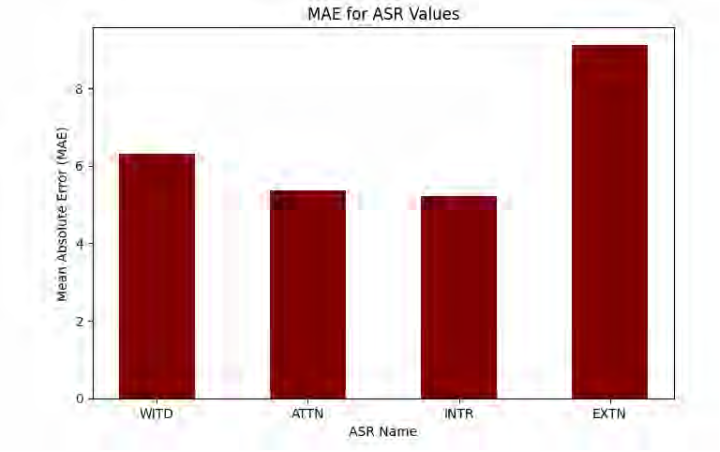

Figure 2: The mean absolute errors of ASR predictions.

References

1. Mohanty R, Sethares WA, Nair VA, Prabhakaran V. Rethinking measures of functional connectivity via feature extraction. Scientific reports. 2020;10(1):1-17.
2. Korthauer LE, Zhan L, Ajilore O, Leow A, Driscoll I. Disrupted topology of the resting state structural connectome in middle-aged APOE ε4 carriers. Neuroimage. 2018;178:295-305.
3. Ying R, You J, Morris C, Ren X, Hamilton WL, Leskovec J. Hierarchical graph representation learning with differentiable pooling. In: NeurIPS; 2018. p. 4805-15.
4. Van Essen DC, Smith SM, Barch DM, Behrens TE, Yacoub E, Ugurbil K, et al. The WU-Minn human connectome project: an overview. Neuroimage. 2013;80:62-79.

Structural Modeling of Cytochrome P450 4F11

Ruth Ayers, Fatimah Bisiryu, Caleb Bocianoski, Dr. David Koes

Pittsburgh Science and Technology Academy, Pittsburgh, PA; The Neighborhood Academy, Pittsburgh, PA; Elizabeth Forward High School, Elizabeth, PA; University of Pittsburgh Department of Computational and Systems Biology, Pittsburgh, PA

Abstract: An ensemble of possible models of enzyme Cytochrome P450 4F11(CYP4F11), which does not have an experimentally resolved structure, were generated using the artificial intelligence Alphafold, Now, molecular docking program Gnina is being used to predict where and how the substrates arachidonic acid, HETE016, and erythromycin may bind to CYP4F11.

Introduction: Emerging research indicates that enzyme Cytochrome P450 4F11's metabolism of various fatty acids may be linked to lung cancer proliferation and growth. The inhibition of CYP4F11 may be useful to treat cancer, but to develop inhibitors of a protein its structure must be resolved. As of now, CYP4F11's structure has not been experimentally resolved, but computational methods can create a relatively accurate prediction of what CYP4F11's structure may be.

Methods: We constructed structural models of the Cytochrome 4F11 protein (CYP4F11) bound to the three different substrates: erythromycin, arachidonic acid, and HET0016. To do this, we first used a website called Uniprot that allowed us to look at the amino acid sequence for the CYP4F11 protein. We then downloaded the sequence and used a program called protein blast that allowed us to compare the amino-acid sequences of other structures and find ones that were the most similar to that of the CYP4F11 protein. After identifying these similar structures we used Pymol which is a molecular visualization system that allowed us to compare these similar protein structures to the CYP4F11 enzyme three-dimensionally. The next thing we did was use Alphafold which is a fairly new artificial intelligence program developed by DeepMind that allows its users to generate 3D predictions of protein structures. We then used the Alphafold program to generate an ensemble of structures of the CYPF411 enzyme. Lastly, we used Pymol to visualize each of the generated structures aligned with the substrates Erythromycin, Arachidonic Acid, and HET0016 to see which generated structure of CYP4F11 aligns best with the substrates.

Results: We have created a diverse ensemble of possible CYP4F11 configurations, complete with a heme, and a root mean square fluctuation comparison of their differences from a similar protein, CYP4B1. To finalize these models, we must make a prediction of where each possible substrate will lie. We are currently using Gnina, a molecular docking program, to give each prediction in our ensemble a prediction for how each substrate may bind.

Discussion: These models could serve as a baseline for further study into CYP4F11 and its metabolism of fatty acids. Further diversification and curation of CYP4F11 models is in progress. Eventually, these models could be replaced by experimentally resolved crystal structures of CYP4F11.

Citrate Transporter's (Slc25a1) Role in Mediating Metabolic Alterations in Exhausted $CD8^+$ T Cells

Scholar: Alessandra Azure

High School/City/State: Newport High School, Bellevue, WA

PI of group/lab: Greg Delgoffe, PhD

Mentor: Kellie Spahr

Site: Immunology and Cancer Immunotherapy (ICI)

Background: T cell exhaustion is a hypofunctional cell state driven by chronic TCR activation in cancer. Preventing T cell exhaustion would improve the anti-tumor immune response. Exhausted T cells lose mitochondrial function and accumulate large lipid droplets, suggesting that their metabolic insufficiency results in alternative glucose utilization. We sought to investigate the connection between lipid accumulation and exhaustion. Citrate transporter, Slc25a1, is a protein that carries citrate, derived from the TCA cycle in the mitochondria, to the cytosol. Citrate transport is an important link between mitochondrial metabolism and *de novo* fatty acid synthesis (FAS).

Methods: $CD8^+$ T cells from C57Blk/6 mice were activated for 24-hours *in vitro* using αCD3/αCD28 dynabeads. Using CRISPR-Cas9, we knocked out the citrate transporter (SLC25A1) in these primary murine $CD8^+$ T cells. The cells were expanded *in vitro* with or without chronic TCR stimulation for 6 days. Cell samples taken on each day of the assay were assessed for citrate transporter protein expression over time using a Western Blot. We analyzed the metabolic efficiency of SLC25A1 KO cells using a Seahorse XF Analyzer.

Results: Acutely stimulated cells upregulated expression of Slc25a1 upon activation, but protein expression largely decreased by day 5. Chronically stimulated cells highly expressed Slc25a1 for all 6 days of the assay. KO cells had a higher basal Oxygen Consumption Rate (OCR) than control cells.

Conclusion: These data indicate that chronically stimulated T cells have an increased capacity to transport citrate to the cytosol where it feeds *de novo* FAS. The increased basal OCR of SLC25A1 KO cells shows that abolishing citrate transport increases mitochondrial metabolism. Taken together, our results suggest that citrate transport contributes to the exhaustion phenotype of lipid accumulation. Future steps include evaluating the effects of knocking out SLC25A1 in $CD8^+$ T cells on the development of exhaustion *in vivo*.

The Effects of Glycerol on the Shape, Size, and Quantity of the Biofilm of the Bacteria P. flu

Scholar: Abigail Bodart
High School: Trinity High School, Washington, PA
Lab: Dr. Vaughn Cooper
Mentor: Abigail Matela
Site: Tech Drive X

Background: As a protective covering of bacteria, biofilm can be anywhere that bacteria is. This can have both positive and negative effects on the environment around it. For example, it can promote plant growth and gut health; however, biofilm can also be the plaque on your teeth or the reason certain diseases are so difficult to remove due to its tolerance to antibiotics and slow growing rates. Therefore, it is essential to experiment on model bacterium such as *P. flu* and learn how to activate and kill the biofilm around it, giving doctors the opportunity to stop more diseases regarding biofilm. Researchers in my lab have recognized that an increased amount of glycerol can make the matrix grow substantially larger than smaller amounts of this media. With this, I hypothesized that the experimental groups with 10.0% and 5.0% QB will have significantly more growth than the 2.5% QB because there is more glycerol to stress the bacteria; therefore, the biofilm will have a larger circumference.

Methods: To stress the colonies even further, a bead transfer took place as colonies of the bacteria *Pseudomonas fluorescens* were chosen, inoculated into test tubes with the two beads and 2mL of designated percentage of QB, and incubated until the next day. For the next three days, the bottom bead from the tube from the previous day would be transferred into a new tube with another bead and 2mL of designated QB. On the final day of the experiment, the bacteria that attached to the bead from the previous day was plated and grew over the weekend.

Results: After analyzing the *P. flu* plates and counting the grown colonies on each, I found that 2.5% QB did have the least amount of mutants as well as colonies within the study, and 5.0% QB had the most of both. With this, I also tested the amount of biofilm in each, and the mutants containing the most biofilm were the tiny mutants, and smooth mutants had the least amount of growing biofilm.

Conclusion: This experiment proves that my hypothesis was correct to an extent. Overall, 2.5% QB had the least amount of bacteria and the least amount of diversity among mutants; however, the 10.0% QB didn't produce significantly more bacteria nor mutants as the 5.0%, demonstrating that 5.0% glycerol is the most effective group to use to grow the bacteria *Pseudomonas fluorescens* as well as multiple other bacterium.

The Function of EGFL6 in Ovarian Cancer Cell Biology, Tumor Initiation, and Therapy

Mae Cano, Dr. Ronald Buckanovich MD, Stacey McGonigal

Mt. Lebanon High School, Pittsburgh, Pennsylvania; University of Pittsburgh Hillman Cancer Center Academy, Pittsburgh, Pennsylvania

Abstract: High grade serous ovarian cancer (OvCa) is typically treated with surgery and chemotherapy. Unfortunately, OvCa has a low survival rate. As such new therapeutic targets are needed, and one is EGFL6. EGFL6 is a protein that is secreted by OvCa cells and drives cancer cell metatasis and proliferation. The goals of this project were to evaluate (i) the role of EGFL6 in tumor initiation and (ii) the ability of a new human-anti-EGFL6 antibody to neutralize EGFL6.

Methods: To evaluate the role of EGFL6 in tumor initiation we used an ex-vivo organoid model. Fallopian tube epithelial cells (FTE—the source of high grade serous cancer) from (i) wild type mice, (ii) mice over-expressing EGFL6 (iEGFL6), (iii) mice carrying tumor driving mutations (BPRN – BRCA1, p53, Retinoblastoma) in the FTE, and (iv) mice carrying BPRN driver mutations in the FTE and overexpress EGFL6 (BPRN-E). FTE cells were grown as organoids ex-vivo and the size and number of the organoids grown from each treatment was evaluated. To evaluate a novel anti-EGFL6 antibodies abililty to neutralize EGFL6 function, the cancer cell line SKOV3 was collected and treated with EGFL6 in the presence of control or EGFL6-neutralizing antibodies. Western blotting was then performed to evaluate the impact of EGFL6 on downstream activation of pERK (phosphorylated ERK).

Results: FTE organoids were successfully generated from all mice. WT and iEGFL6 organoids showed a similar pattern of growth over the two weeks of analysis. As expected, BPRN organoids grew larger and faster than WT mice. Interestingly, the BPRN-E mice which express EGFL6, grew much larger and faster than the BPRN mice. Finally, in an attempt to develop therapies targeting EGFL6, we screened a panel of novel human anti-EGFL6 antibodies and found several that could potentially reduce EGFL6 mediated signal transduction/ERK phosphorylation in vitro.

Discussion: These results suggest that the expression of EGFL6 in evolving tumors significantly increase the rate of growth. However, these results have the caveat that BPRN-E mice were somewhat older than BPRN mice. As such, these experiments will need to be reproduced with age-matched mice. Given the fact that EGFL6 is a secreted protein that appears to be import for cancer initiation and growth, it could be therapeutically targeted with neutralizing antibody therapy. Our initial screen of a new panel human anti-EGFL6 antibodies identified several that could potentially neutralize EGFL6 mediated pERK activation in cancer cells. As pERK is a critical driver of cancer cell proliferation, these antibodies could play an important role in cancer therapy. However, significantly more work will be needed to validate these antibodies.

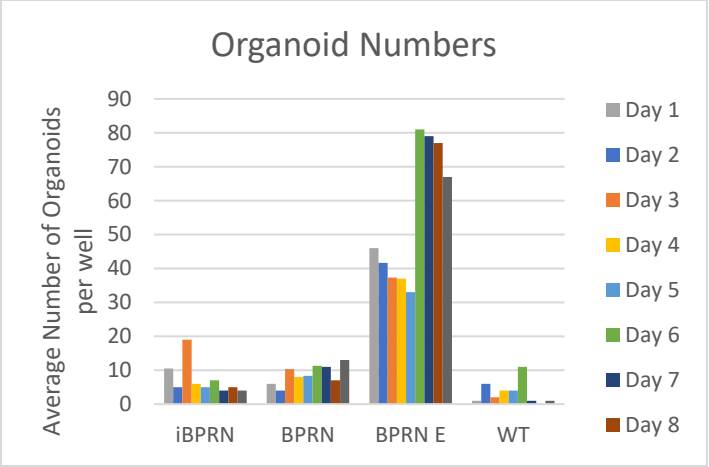

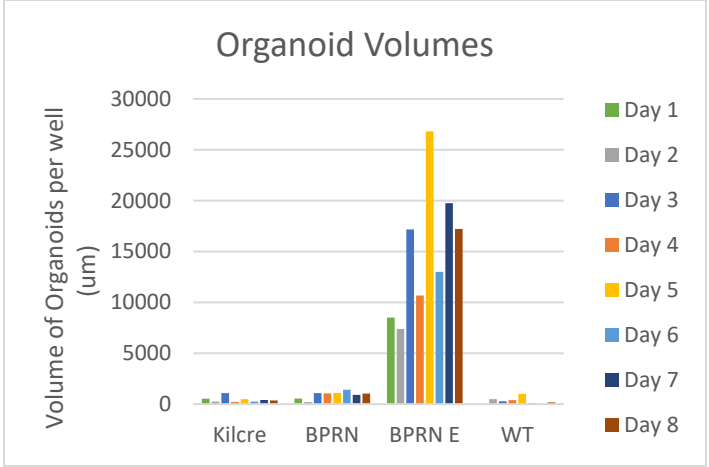

Figure 1: Number of Organoids on Average for Each Treatment

Figure 2: Average Volume Organoids Take Up for Each Treatment

Figure 3: Results of Western Blotting for pERK and Key to Each Column

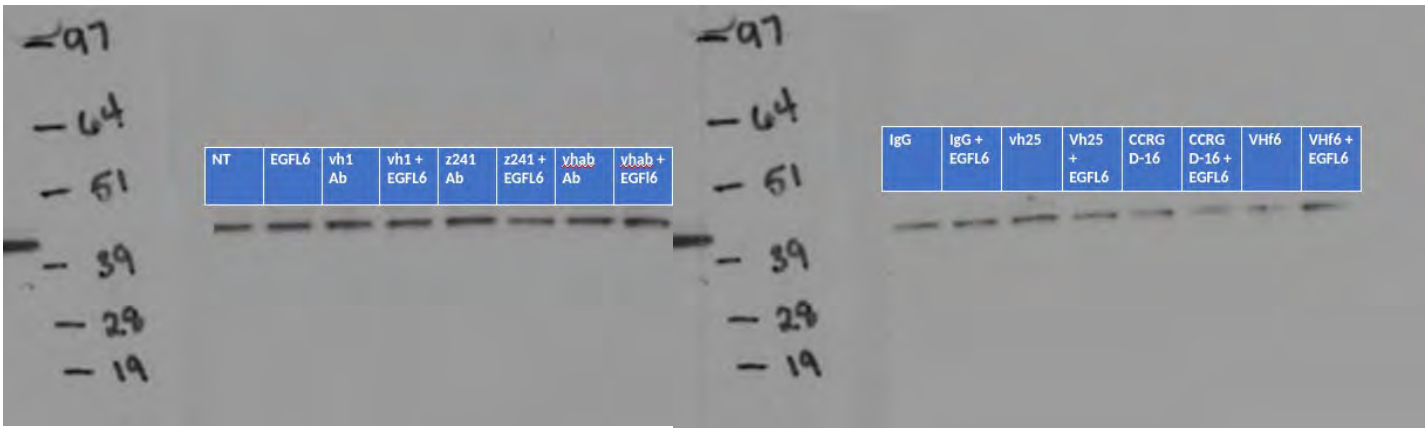

References

1. H. Tang, A.P. Fayomi, S. Bai, N. Gupta, S. Cascio, D. Yang, R.J. Buckanovich, “Generation and characterization of humanized affinity-matured EGFL6 antibodies for ovarian cancer therapy,” Gynecologic Oncology 171 (2023), 49-58.

Title: Landscape Analysis of Kinase Signature for Decoding Immunotherapy Resistance and Therapeutic Evaluation of EPHA3 Inhibitors in HGSC Ovarian Cancer

Scholar: Nancy Chen

High School/College/City/State: Yale University, New Haven, CT

PI of group/lab: Dr. Xiaosong Wang, MD, PhD

Mentor(s): Dr. Bashir Lawal, PhD

Site: Cancer Biology

In this study, we conducted two distinct projects with separate focuses: one aimed to identify kinases that may be important predictors of immunotherapy response and another to investigate the therapeutic efficacy of a known kinase inhibitor in high-grade serous carcinoma (HGSC) ovarian cancer.

One of the major drawbacks of immunotherapy is that only a limited number of patients are responsive while the majority of patients are non-responsive with stable, progressive, or hyper-progressive prognosis. Hence, an unmet clinical need remains to identify biomarkers that can aid in effectively stratifying patients for immunotherapy. We conducted a landscaped analysis and identified a kinase-based signature, known as the Kinase of Immunotherapy Resistant Signature (KIREST), as a predictor of immunotherapy resistance and patient prognosis in multiple immunotherapy trials. KIREST is associated with immunosuppressive tumor phenotypes. Through a subsequent integrative dataset analysis, we identified potential kinase pathways linked to resistant predictions. In conclusion, we have identified an important predictor of immunotherapy resistance which will aid patient stratification for future trials.

HGSC is the most prevalent form of ovarian cancer, accounting for 75% of all epithelial ovarian carcinomas. Its aggressive nature and poor prognosis make it the most lethal ovarian cancer. Studies have implicated Ephrin tyrosine kinase A3 (EPHA3) as a driver of cancer initiation, progression, and metastasis. Recent studies have demonstrated that the kinase EPHA3 inhibitors can effectively reduce the migratory and invasive capacities of cancerous cells. However, the therapeutic efficacy of EPHA3 inhibitors in HGSC ovarian cancer has yet to be investigated. This study employs the use of colony formation and cell viability assays to evaluate the therapeutic potential of EPHA3 kinase inhibitors against HGSC.

Future directions include conducting further i*n vitro* and *in vivo* studies, as well as validating our preclinical findings by translating them to clinical cohorts.

Exploring ChatGPT's Potential: Analyzing Biochemical Kinetics Using Computational Models

Stephanie Chen, James R. Faeder, PhD, North Allegheny Intermediate High School, Pittsburgh PA; University of Pittsburgh Hillman Cancer Center Academy, Pittsburgh PA

Abstract

This project aims to determine if large language models, namely ChatGPT, are capable of generating a code that can be provided to softwares such as BioNetGen, a software tool designed for modeling biochemical kinetics. The code written is validated using a software known as VSCode. ChatGPT was provided the syntax rules of BioNetGen and then asked to generate a sample code. The results showed that ChatGPT could generate workable code if provided an example; ChatGPT was unable to generate a code when given the syntax rule alone.

Introduction

ChatGPT is a large language model developed by openAI. It is designed to understand and generate human-like text based on the input it receives. ChatGPT has been trained on vast amounts of diverse text data from the internet. The language model can generate statistically and contextually significant responses, but it lacks human understanding and processing. ChatGPT generates responses that are appropriate based on patterns learned during its training. The goal of our research is to assess the ability of ChatGPT (v.3.5) to generate a working code based on models of biochemical kinetics. Biochemical kinetics, also known as enzyme kinetics, is a subfield of biochemistry that studies how quickly chemical processes occur within living organisms. It focuses on comprehending through which biological components, such as enzymes and proteins, go through chemical changes and how different circumstances affect these reactions.

Methods

ChatGPT was provided the syntax rules of BioNetGen and then was asked to generate a BioNetGen Language (BNGL) code for testing. BioNetGen is a software tool and language used for modeling and simulating biochemical systems and reactions. It is designed to help in the study of complex biological processes. The code was tested in a source code editor known as Visual Studio Code (VSCode). If the generated code doesn't run, ChatGPT is provided the error, as well as a method of correcting the error. The language model attempts to correct the errors, and the revised code is ran through VSCode. This process repeats for every trial that fails. It is worth noting that GPT was asked to analyze a functional example code, prior to being asked to generate new material. It was tested whether ChatGPT could produce a similar functional code to the provided material.

Results

ChatGPT was able to generate code similar to the example that it was given; this code was functional and was able to run in VSCode. However, ChatGPT was unable to produce a code that could run when asked to generate code solely based on the given syntax rules.

Discussion

ChatGPT is not reliable in terms of generating a BNGL code when only the syntax rule is given. However, ChatGPT is reliable in terms of creating functional code when provided with an example to analyze beforehand. Future directions include determining what the limit of ChatGPT's capabilities are, and figuring out what ChatGPT needs to be trained on in order to succesfully produce functional codes.

Aging-Related Osteoarthritis: Uncovering the Genetic Pathways

Scholar: Claire Cho

High School/City/State: North Allegheny Senior High School, Pittsburgh, Pennsylvania

PI of group/lab: Dr. Hang Lin, PhD

Mentor(s): Meagan Makarcyzk, PhD Candidate

Site: Tech Drive X

Background: Osteoarthritis is the most common form of arthritis, occurring when the protective cartilage between bones wears down. As the cartilage wears down, bone begins to rub on bone, causing drastic amounts of pain. One of the most significant risk factors is aging, and with the lengthening life expectancy resulting in a rapidly growing elderly population, osteoarthritis is becoming more prevalent; symptoms tend to accumulate slowly rather than suddenly. Usually, cartilage does not have its own blood vessels or neurons, however, a person affected by OA will experience blood vessels and neurons beginning to grow into the cartilage, inflaming the synovium, contributing to the osteoarthritis-induced pain. As the disorder has no cure, we attempted to fully understand the correlation between aging and osteoarthritis by studying expression of certain genes, specifically in the knee.

Methods: Multipotent mesenchymal stem cells can differentiate into various types of cells, among those being chondrocytes. Chondrocytes are cartilage cells, highly expressing the gene GATA-4. By way of gel electrophoresis, the GATA-4 concentration was tested alongside a housekeeping gene, GAPDH. Safranin O staining was used, in order to detect the presence of cartilage. Simultaneously, to compare the levels of GATA-4 in young and old donors, IHC (immunohistochemistry) staining was also utilized.

Results: The western blot showed a thicker darker band, which signifies more expression of that protein. A type of staining, Safranin O staining, distinctly detected cartilage cells by staining for the extracellular matrix, or the GAGs (glycosaminoglycans). Another type of staining, IHC staining, clearly expressed the differences in GATA-4 concentration between young and old donors.

Conclusion: The study supports that protein expression, specifically GATA-4, correlates with the progression of osteoarthritis in aged individuals. Aged individuals tend to have chondrocytes with a degraded extracellular matrix, shown by the staining of the GAGs in Safranin O staining.

Title: Neoantigen discovery in melanoma patients treated with neoadjuvant CMP-001 and nivolumab

Scholar: Nora Coen-Pirani

High School/College/City/State: Winchester Thurston School, Pittsburgh, PA

PI of group/lab: Hassane Zarour, MD, PhD

Mentor(s): (name or names of who directly guided your research. If it was the PI, place hers or his name here as well, even if already mentioned): Florent Amatore, MD, PhD

Site: Immunology and Cancer Immunotherapy

Background: Neoadjuvant intratumoral TLR9 agonists (CMP-001) and anti-PD-1 provide durable clinical responses in patients with high-risk resectable melanoma. Response is associated with broad immune activation, especially with increased activity of $CD8^+$ cells in the tumor microenvironment and in the blood. Therefore, treatment efficacy may be driven by the immune response against tumor neoantigens. Neoantigens are peptides derived from mutations presented by HLAs and targeted by antitumor $CD8^+$ cells. Vaccination against neoantigens is an interesting therapeutic approach for selectively enhancing T-cell mediated tumor killing.

Objective: To evaluate the binding capacity of mutation-associated neoantigens derived from tumors of patients treated with CMP-001/anti-PD-1.

Methods: Based on RNA sequencing data of the baseline tumor in a HLA-A2 responder patient, 91 mutant peptides of 9-11mer in length were identified and synthetized, along with their corresponding wild-type(WT) peptide. We performed a T2 Cell-Based HLA-A2 Peptide Binding Assay on 5 mutant peptides and their corresponding WT sequences. The peptides were added to T2 cell cultures at a concentration of 10ug/ml. T2 cells were incubated for 24h at 37°C, then labeled using a PE-conjugated anti-HLA-A2 antibody and analyzed by flow cytometry. The peptide binding ability was calculated using the formula $(MFI_{peptide} - MFI_{DMSO})/MFI_{DMSO} \times 100\%)$. We used MELAN-$A_{27-35}$ and MAGE-$A3_{146-160}$ as respectively positive and negative controls.

Results: All the mutant peptides had a higher binding capacity than the negative control. Mutated peptides had a significantly higher binding capacity than their corresponding WT (Wilconxon matched-pairs signed rank test, $p = 0.04$). Peptides #36 and #43 had the most important difference in MFI ratio with their corresponding WT (respectively 352 versus 0 and 280 versus 0).

Conclusion: Peptides #36 and #43 are good candidates for further evaluation of their immunogenicity and characterization of the CD8 cells that recognize them specifically. Other peptides will be similarly screened and the best ones proposed as targets for cancer vaccines.

Usage of EEG-Based BCI System for Emotion Regulation in Autism Spectrum Disorder

Mikaela Dassanaike-Perera, Murat Akcakaya, PhD, Busra Tugce Susam, Richard Gall

North Allegheny High School, Pittsburgh, PA; University of Pittsburgh Hillman Cancer Center Academy, Pittsburgh, PA

Abstract

Autism spectrum disorder (ASD) is a neurodevelopmental disorder often accompanied by impaired emotion regulation (ER) [1]. The Emotional Awareness and Skills Enhancement Program (EASE), which is 16 weeks behavioral intervention technique, was developed to help them to manage their intense negative emotions. Three random forest classifiers were developed, to ascertain whether there is a difference between Control and EASE, before and after EASE treatment [2], based on neural responses.

Introduction

Electroencephalography (EEG) has been a tool used in emotional processing and regulation in individuals with ASD [3]. In this study, we developed an electroencephalography (EEG)-based brain-computer interface (BCI) system to complement the EASE treatment, and we aim to investigate the significance of EASE treatment by using EEG data before and after the EASE treatment via machine learning.

Methods

A total of thirty-nine participants were asked to play an Affective Posner Task card game where subjects were shown two cards (white squares) and asked to pick the card with a star on its back in four different tasks in which participants were given feedback, win, lose, or too slow, based on their response time [3]. In this study, we focused on task 3 which included deception, where 60% of correct responses, or wins, were given regardless of how fast the task was performed, to induce an emotional reaction. During the task, EEG data were collected from each participant. Spectral and temporal features were calculated to differentiate Pre- and Post-Visit data for each EASE and Control group, separately [4-7].

Three random forest classifiers were developed, to ascertain whether there is a difference between for Control and EASE, before and after EASE treatment using the EEG features extracted during task 3. The data was split into two separate datasets for training and testing with a split of 80%-20% to test the classifiers on unseen data. 5-fold cross-validation was performed on the training set to search for the optimal number of trees across all folds. After finding the optimal number of trees, the classifiers are retrained on the entire training set using the optimal number of trees found. The classifiers are then used to classify the test set and compare the ground truth. Accuracy, sensitivity, and specificity are reported to highlight the performance of the models.

Results

The classification results of pre and post visit for the Control group, shown in Table 1, indicate 78.65%, 76.52%, and 80.74% of accuracy, sensitivity, and specificity during the Win condition while the results of the classification of pre and post visit in EASE group, shown in Table 2, shows 88.24%, 85.19%, 91.26%, accuracy, sensitivity, and specificity, respectively during the Win condition. Similarly, the results of the random forest classifier in the EASE group outperform the classifier in the Control group for Lose and Slow conditions.

Discussion

It can be seen from Table 1 and Table 2, the classification of pre- and post-visit for the EASE group outperforms the control group in accuracy, sensitivity, and specificity. This may indicate there is a greater difference between the

neural responses for pre-EASE and post-EASE treatment. Additional experiments are needed to say whether EEG-based BCI systems can complement EASE treatment, which helps them regulate their negative emotions. Furthermore, studies into whether EASE treatment is responsible for the differences in the neural responses and whether they are due to better emotion regulation or another cause.

Control

	Number of Trees	Accuracy	Sensitivity	Specificity
Win	180	78.65%	76.52%	80.74%
Lose	150	89.71%	90.85%	88.61%
Slow	70	77.83%	72.57%	82.91%

Table 1. Accuracy, Sensitivity, and Specificity using the optimal number of trees found from the 5-fold cross-validation for the Control group.

EASE

	Number of Trees	Accuracy	Sensitivity	Specificity
Win	100	88.24%	85.19%	91.67%
Lose	110	90.65%	91.41%	89.83%
Slow	190	87.57%	82.95%	92.13%

Table 2. Accuracy, Sensitivity, and Specificity using the optimal number of trees found from the 5-fold cross-validation for the EASE group.

References

1. C. A. Mazefsky and S. W. White, “Emotion regulation: Concepts & practice in autism spectrum disorder,” Child and adolescent psychiatric clinics of North America, vol. 23, no. 1, 2014.
2. Conner, C. M. et al. Improving emotion regulation ability in autism: the Emotional Awareness and Skills Enhancement (EASE) program. Autism 23, 1273–1287 (2019).
3. S. Eldeeb, B. T. Susam, M. Akcakaya, C. M. Conner, S. W. White, and C. A. Mazefsky, “Trial by trial EEG based BCI for distress versus non distress classification in individuals with ASD,” Sci. Rep., vol. 11, no. 1, pp. 1–13, Dec. 2021.
4. Welch, Peter. "The use of fast Fourier transform for the estimation of power spectra: a method based on time averaging over short, modified periodograms." IEEE Transactions on audio and electroacoustics 15.2 (1967): 70-73.
5. Thiruchselvam, R., Blechert, J., Sheppes, G., Rydstrom, A. & Gross, J. J. The temporal dynamics of emotion regulation: an EEG study of distraction and reappraisal. Biol. Psychol. 87, 84–92 (2011).

   Cuthbert, B. N., Schupp, H. T., Bradley, M. M., Birbaumer, N. & Lang, P. J. Brain potentials in affective picture processing: covariation with autonomic arousal and affective report. Biol. Psychol. 52, 95–111 (2000).
6. Whitehouse, A. J. & Bishop, D. V. Do children with autism ‘switch off’ to speech sounds? An investigation using event-related potentials. Dev. Sci. 11, 516–524 (2008).

B Cell State Change Analysis Using Gene Regulatory Network Construction and *in silico* TF Perturbation

Anna C. Delale-O'Connor, Swapnil Keshari, Dr. Jishnu Das, PhD
Fox Chapel Area High School, Pittsburgh, PA; University of Pittsburgh Hillman Cancer Center Academy, Pittsburgh, PA

Abstract – In this project, a set of single-cell multi-omic data (scRNAseq and scATACseq) from various B cell states was used to construct a gene regulatory network (GRN) with the goal of simulating transcription factor perturbations within B cells. The constructed GRN was then perturbed through *in silico and experimental* transcription factor knockout to confirm how perturbations would impact specific genes and which perturbations would lead to cell state change.

Introduction – GRNs are networks made of genes and the transcription factors which regulate them. These systems control the expression of genes within a cell and, as such, connect to cell identity and cell state. The transcription factors (TFs) which make up part of GRNs are proteins that bind to sites in regulatory sequences of DNA and control how genes are expressed. Attempting to model how genes and transcription factors are connected within cells is important because if progress is made, it will allow for the creation of GRN models that can prioritize the importance of genes in specific perturbations. This in turn could allow for more effective medicine to be created, as it could target the transcription factors that regulate important genes in B cell state changes.

Methods – While models to simulate the impact of perturbing TFs on GRNs have been made, they have issues with scaling to other inputs and require already perturbed data, so a more recent model, CellOracle, was used in this study. Prior to the use of this model, single-cell RNA (scRNAseq) data and single-cell ATAC sequence (scATACseq) data were collected from B cells in naive, activated, pre-GC, and PB cell states. Importantly, both datasets are matched for each cell, providing higher granularity in gene expression and chromatin accessibility. Such sequencing is known as single-cell multiomics data. The scRNAseq data was processed into a form usable by CellOracle, and the scATACseq data was used to construct a model GRN based on the accessibility of chromatin and potential TFs that could bind there. Afterward, the scRNAseq data was used to refine the model GRN, based on which genes were expressed in each cell. This refined GRN was then perturbed, using vector values to simulate the impact of a transcription factor change on the connected genes. Through this simulation, specific TFs and their corresponding perturbations that change B cells between states can be identified. This is done through the vector graphs produced as a result of perturbation and the individual perturbation scores assigned to each part of the GRN.

Results – The preliminary data suggests that the CellOracle model training and the construction of a base GRN from scATACseq data were successful in the context of B-cell states. As well as this, most of the TF perturbation steps functioned effectively, producing degree distribution and centrality ranking graphs for each gene in the network, allowing for the prioritization of genes in the GRN. However, there were inconsistencies in some graphs, particularly in the scRNAseq processing steps. The genes in the base GRN and the genes in the processed scRNAseq data did not align, leading to incorrect graphs, which require further investigation. More work will be necessary to determine which specific TFs impact changes between cell states, including the current process of changing input data and parameters to debug prior steps.

Discussion – Data about the importance of particular TFs can be applied to medicine, in the context of targeting specific TFs or genes to change the function of B cells. In addition, having a base GRN for B cells in their different states allows for further investigation of the roles every TF plays in regulating cell state change, even beyond those identified as most important. With this knowledge, treatments can be made to more effectively target certain TFs and genes in B cells. Additionally, the graphs already produced from current conclusions can allow particular genes to be prioritized, given their centrality and importance to the network.

The usage of 3D printing to create Microfluidic devices

Scholar: Gavin Drake

School: Science and Technology academy, Pittsburgh, Pennsylvania

Lab: Ioannis Zervantonakis

Mentor: Matthew Poskus

Site: Tech Drive X

Background: The study of cancer cells has recently been pushed forward due to the usage of SU-8 which is an epoxy resin that becomes a solid when exposed to UV light and used in microelectronics to create a 3D model with high resolution and thermal resistance. However, the cost is very high as one bottle 500ml (about 16.91 oz) is $500. The cost of SU-8 is why I am trying to recreate the same high resolution 3D molds with far cheaper resins.

Methods: After I have printed out the mold, I then wash it and heat cure it for 2 days after that I can pour PDMS into the mold. The PDMS is a gel like substance that once exposed to heat becomes a solid capable of biocompatibility. Then the PDMS is cut out of the mold and formed into the microfluidic devices, then it is put into the autoclave to clean of any debris from previous steps, after that I use a vacuum sealed plasma chamber to allow for the device to bind to cover glass which will keep liquids inside the device. I then took the device and put it underneath a microscope which allowed me to see and record the surface roughness of the device.

Results: I have in total created 16 3D molds utilizing various kinds of resins, and 54 microfluidic devices. I have seen that a resin called the TR250LV proved to be denser and more heat resistant than all other resins, and that printing the mold on an angle proved to have less surface roughness and a higher resolution.

Conclusion: the usage of 3D printing these microfluidic devices to create a more cost effective and productive solution is something that I believe will advance the future of cancer research.

Investigating how chemotherapeutic thiopurines inhibit telomerase elongation of telomeres

Scholar: Averi Elsbury
Upper St. Clair High School/Pittsburgh/PA
Lab: Patty Opresko
Mentors: Ryan Barnes, Patty Opresko
Site: Cancer Biology

Background:

Telomeres are at the ends of chromosomes; they are a cap holding and protecting the telomeric ends. Telomeres shorten when a cell divides, once the telomeres get too short the cell stops dividing. When telomeres are absent it causes DNA to fray resulting in cell death or growth arrest. But, when a normally silent enzyme called telomerase is present in a cell it can elongate the telomeres, and most cancerous cells turn on telomerase to become immortal. Since telomerase can add nucleotides to the telomeres elongating them. The elongation allows the cancerous cell to rapidly divide and develop into a tumor. A drug called 6-thio-dG (THIO) is a telomerase dependent telomere uncapping agent. THIO is shown to compromise the telomere structure uncapping the telomeres resulting in rapid tumor cell death.

Methods:

HeLa cells with long telomeres (LT) and very short telomeres (VST) were treated with varying concentrations (0.1, 1.0, and 2.5μM) of 6-thio-dG. Colony assays were conducted to determine relative colony formation. IFFISH was conducted to detect colocalization of the DNA damage.

Results:

After running our tests, we found there are significantly less colony formation when THIO was introduced to VST compared to LT. The VST had the least amount of colony formation at the highest dose (2.5μM) of 6-thiodG. Our IF-FISH results reveal that the VST has significantly more telomere induced dysfunctional foci compared to the LT.

Conclusions:

Our results show that when THIO is introduced to telomerase cells, the VST is more sensitive to THIO than the LT. We hypothesize because the VST are dependent on telomerase, since they can’t divide. But the LT don’t dependent on the telomerase since they can divide more. When they cannot divide, they will start to rely on telomerase.

Future directions:

We will determine the impact of 6-thio-dG on non-cancerous cells and telomerase negative cancer cells.

Applying Data-Based Deep Transfer Learning to Enhance Infectious Disease Case Detection

Shaun Fernando[1], Yuhe Gao, M.S.[2], Jason Xiaotian Dou, M.S.[2], John Chenxi Song, M.S.[2], Ye Ye, Ph.D.[2]

[1]North Allegheny High School, Wexford, PA; [2]University of Pittsburgh, Department of Biomedical Informatics, Pittsburgh, PA

Abstract

Infectious disease outbreaks require sharing of electronic medical record data among healthcare systems to facilitate effective responses and mitigate disease spread. However, transfer of data between settings often leads to a performance drop in its applicability. Data-based deep transfer learning (DDTL) offers a promising solution to this, having the ability to take similarities and differences between settings into consideration. This method was compared against baseline models to assess prediction performance in transferability to a new setting.

Introduction

In the course of infectious disease outbreaks, electronic medical record data sharing between healthcare systems is critical for case detection practices. However, utilizing data from one setting yields a performance drop when applied to a new setting due to differences in patient populations and clinical practices[2]. The use of data-based deep transfer learning (DDTL) holds significant potential as it can effectively evaluate the similarities and differences among various settings. A DDTL model was compared against three baseline approaches to assess prediction performance: source and target models, which use source and target setting datasets respectively for training and a combined model, which uses both source and target setting datasets for training.

Methods

Intermountain Health (IH) and University of Pittsburgh Medical Center (UPMC) served as two settings from which data was collected, where IH represented the source setting and UPMC represented the target setting. This data was extracted from clinical reports using Topaz, a natural language processing (NLP) tool, to determine whether 67 respiratory infectious disease symptoms in the form of Unified Medical Language System (UMLS) concepts were mentioned in the reports as being present or absent[2]. This allowed the presence or absence of influenza and Respiratory Syncytial Virus (RSV) to be identified. For each of the diseases, this data was collected over five seasons from 2010 to 2014. The data was preprocessed before being fed into the model, where missing and unimportant data was removed. A DDTL model known as a Domain Adversarial Neural Network (DANN) consisting of a feature extractor, domain classifier, and label predictor[1] (Figure 1) was implemented to transfer source data to the target setting and utilize both source and target data to create a target model to aid in target setting predictions. The Area Under the Receiving Operating Characteristic Curve (AUC) was calculated to measure model classification performance.

Results

The DANN showed consistent improvements during most seasons for influenza detection (Figure 2), but only during one season for RSV detection (Figure 3). In most seasons the baseline models displayed higher AUC values. The highest AUC of the DANN was achieved using data from the 2014 influenza season and the 2010 RSV season.

Discussion

The results illustrate that DDTL is a promising technique but has room for improvement. Overfitting of source data could have caused a decrease in the AUC for target setting predictions. Furthermore, different approaches to transfer learning (e.g., Model-Based Transfer Learning) could be tested as well.

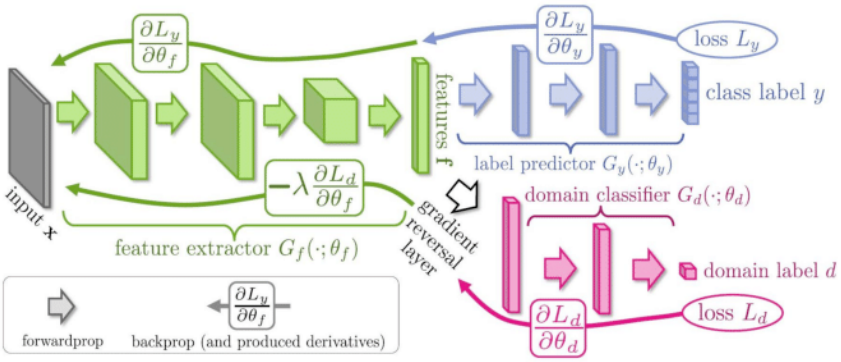

Figure 1. Structure of DANN

(Credit: https://www.researchgate.net/figure/The-domain-adversarial-neural-network-DANN-architecture-18_fig7_323142148)

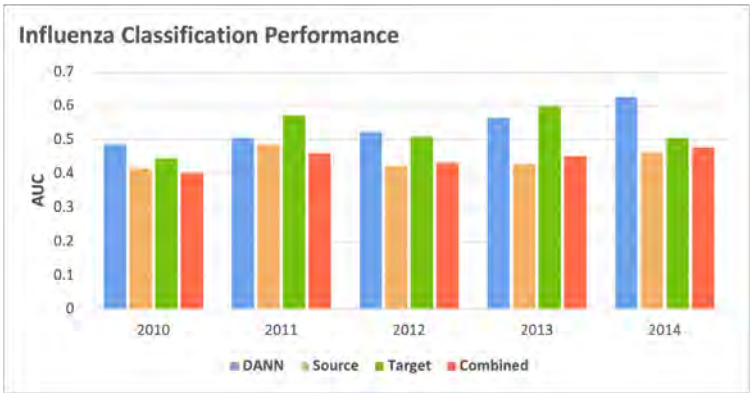

Figure 2. Performance of Influenza Predictions by Models in Target Setting

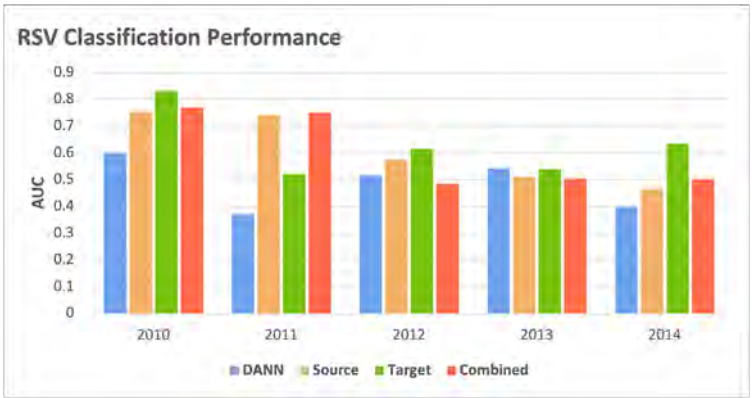

Figure 3. Performance of RSV Predictions by Models in Target Setting

References

1. Ganin Y, Ustinova E, Ajakan H, Germain P, Larochelle H, Laviolette F, Marchand M, Lempitsky V. Domain-adversarial training of neural networks. The journal of machine learning research. 2016 Jan 1;17(1):2096-30.

2. Ye Y, Wagner MM, Cooper GF, Ferraro JP, Su H, Gesteland PH, Haug PJ, Millett NE, Aronis JM, Nowalk AJ, Ruiz VM. A study of the transferability of influenza case detection systems between two large healthcare systems. PloS one. 2017 Apr 5;12(4):e0174970.

Physicochemical and ADMET Pharmacokinetic Properties of Novel Potent Inhibitors of PLK1 in Cancer Therapy

Samantha R. Fernsebner, College Freshman[1]; Dr. Monsurat M. Lawal, Ph.D.[2]; Dr. Daniel Lundberg, Ph.D.[2]; and Dr. Tugba Kucukkal, Ph.D.[2]

[1]University of Connecticut, Storrs, Connecticut; [2]Drug Design Lab, Gallaudet University, Washington, DC.

Abstract
Computational methods remained prominent in the drug discovery pipeline because they are widely acceptable, accessible, economic-friendly, and cost-effective, with improved confidence. This study shows the outcome of physicochemical properties and ADMET screening of newly identified 46 potent molecules inhibiting the polo-box domain (PBD) of polo-like kinase 1 (Plk1). The employed post-analytical approach facilitated a better depiction of the large output from the screening and enabled the most potent molecule selection for subsequent experiments.

Keywords
Computational Drug Design, ADMET, Physicochemical Radar Chart, Anticancer Properties, Plk1 Inhibition.

Introduction
Plk1 inhibitor design and development continued to receive more attention because they can potentially be a more effective and less toxic treatment than traditional cancer therapies[1,2]. The emergence of theoretical approaches and algorithm development have contributed to highly bioactive small molecule identification in pathologic conditions, making *in silico* tools almost indispensable in the drug discovery process. However, mining and trimming the enormous data generated from several computational simulations could pose a challenge in selecting the most promising drug candidates. Therefore, an approach that allows an investigator to streamline the results with relevant information is critical. The present study aims to unveil the physicochemical, solubility, lipophilicity, absorption, distribution, metabolism, excretion, and toxicity (ADMET) properties of the identified Plk1 candidate cancer drugs. These properties are rarely assessable with conventional experiments, whereas in silico approaches enable easy prediction of these concepts.

Methods
The process involved converting the 3D structures of the 46 top hits Plk1 PDB inhibitors into Simplified Molecular Input Line Entry System (SMILES) to facilitate ADMETlab 2.0[3] and SwissADME[4] operations and obtain the values for the various metrics on their interfaces. These 46 molecules were lately identified from a database of 6 million compounds via high-throughput virtual screening by our AtomWise (www.atomwise.com) collaborators as promising Plk1 polo-box domain inhibitors.

Results
Based on the simulation, some drugs show optimal absorption and distribution values mixed with unacceptable outputs of metabolism, excretion, and toxicity or vice versa. More specificity of the structural and ADMET properties would facilitate the assignment of these molecules as more promising drugs. **Figure 1** shows the combined physicochemical properties of these 46 molecules and those with more acceptable values. The formal charge is 0 for all molecules with molecular weights within 143 to 591 g/mol. Only compound 10 failed the Bristol-Myers Squibb (BMS) rule of an undesirable reactive compound, while compounds 20, 40, 41, and 43 have chelating potentials. All 46 compounds have no Pan Assay interference Structure (PAINS) alert. Compound 12 fails the Lipinski rule of 5, compounds 4, 16, 19, 35, 39, and 44 violate the Pfizer druggability rule, while 1, 6, 27, 28, 42, and 43 fail the GoldenTriangle rule. The bioavailability scores are 0.55 and 0.56, except for compounds 6 and 12, with 0.85 and 0.11, respectively. Many of our screened PLK1 inhibitors are PGP–, including 39 and 44, predictably crossing the BBB, while compound 29 is the only outlier (**Figure 2**).

Discussion
A compound with a high propensity to be a PGP substrate/inhibitor might potentially serve as one, leading to lower selectivity for the intended target. Literature review showed that most therapeutic

anticancer drugs never cross the blood-brain barrier (BBB)[5]. Cytochrome P450s are crucial metabolizing proteins with implications in expelling xenobiotics, whereas anticancer molecules often have toxic components required to kill cancer cells. All the compounds showed appreciable metabolism by the CYP isoforms, but a moderate value is necessary to be confident that the molecule does not end up being CYP inhibitor/substrate. Based on standard compounds BI2536, Onvansertib, Volasertib, and Revlimid values, we suggest that a total CYP metabolism probability score not above 4 is sufficient. 25 of the 46 compounds have a probability score of ≥4, denoting their lower CYP affinity and predicted selectivity for the studied protein. More than 30 compounds showed moderate excretion potential with higher half-life ($T_{1/2}$) probability and medium clearance (5–15 mL/min/kg). A total of 31 toxicity metric is available from the ADMETlab screening. Within the acceptable range for these parameters, only compound 28 showed nil toxicity, whereas a subtle level of toxicity is necessary for anticancer molecules. The graphical approach used enabled a better depiction of the outcomes. Overall, the compounds with the most favorable physicochemical and ADMET properties are 1, 18, 26, 30, and 32.

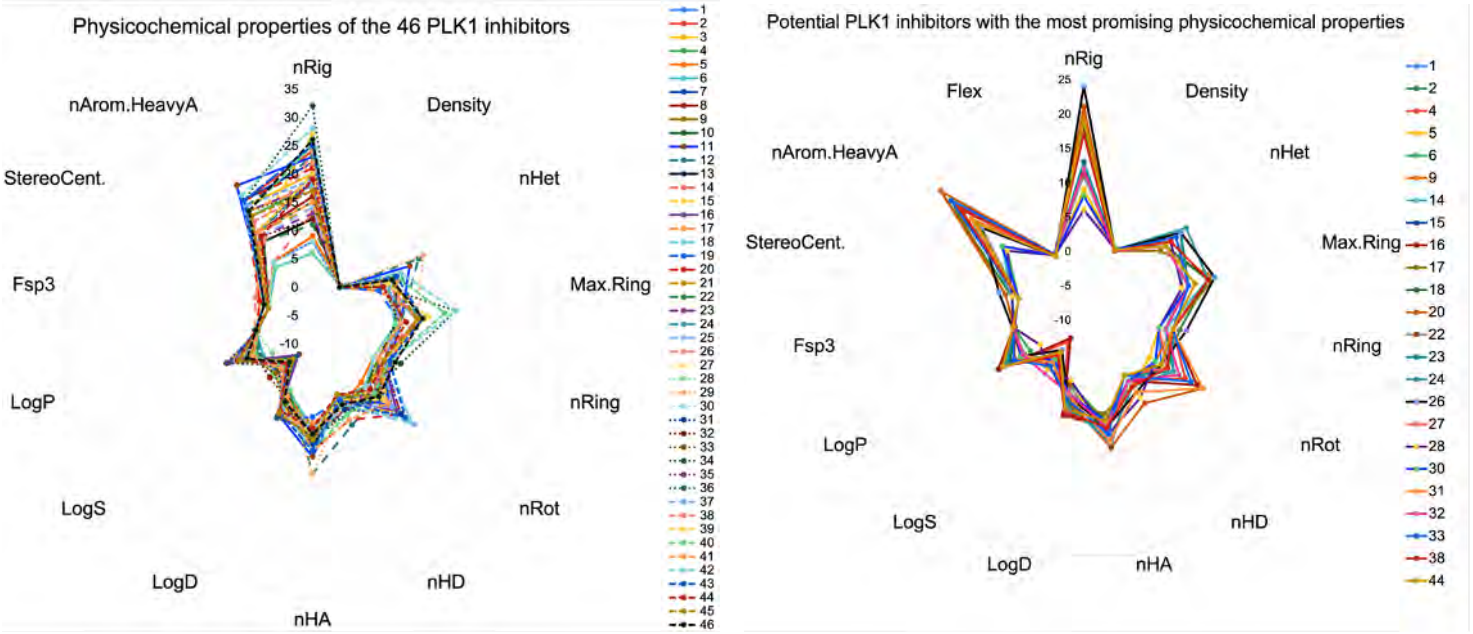

Figure 1: Radar chart of the structural and chemical properties of the 46 potentially active PLK1 inhibitors. All parameters are dimensionless, except the density unit is in g/cm3. nHeavyA = number of heavy atoms, nArom.HeavyA = number of aromatic heavy atoms, nHA = number of hydrogen bond acceptors, nHD = number of hydrogen bond donors, nRot = number of rotatable bonds, nRing = number of rings, Max.Ring = number of atoms in the biggest rings, nHet = the number of heteroatoms, nRig = the number of rigid bonds, Flex. = flexibility (nRot/nRig), StereoCent. = number of stereo centers, LogS = log of aqueous solubility, LogP = lipophilicity measure with octanol/water partition coefficient, and LogD = logP at physiological pH 7.4.

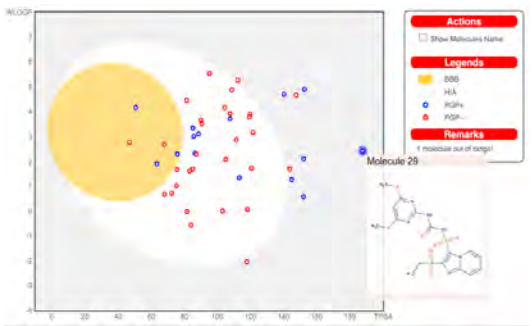

Figure 2: BOILED-Egg output depiction of the absorption and distribution properties of the 46 compounds. HIA = human intestinal absorption.

References

1. Su, S.*et al*. PLK1 inhibition-based combination therapies for cancer management. *Translational Oncology* **16**, 101332 (2022).
2. Wang, B. *et al.* PLK1 inhibition sensitizes breast cancer cells to radiation via suppressing autophagy. *International Journal of Radiation Oncology* Biology* Physics* **110**, 1234–1247 (2021).
3. Xiong, G. *et al.* ADMETlab 2.0: an integrated online platform for accurate and comprehensive predictions of ADMET properties. *Nucleic Acids Research* **49**, W5–W14 (2021).
4. Daina, A. *et al*. SwissADME: a free web tool to evaluate pharmacokinetics, drug-likeness and medicinal chemistry friendliness of small molecules. *Scientific Reports* **7**, 1–13 (2017).
5. Angeli, E., *et al*. How to make anticancer drugs cross the blood-brain barrier to treat brain metastases. *International Journal of Molecular Sciences* **21**, 22 (2019).

Proof of Concept of a Rule-Based, Non-Neural Solution to Fall Detection with Ambient Vision Sensors

Adam Ferris[1], Yuyang Li[2], Dr. In Hee Lee, PhD[3]

Fox Chapel Area High School, Pittsburgh, PA; University of Pittsburgh Hillman Cancer Center Academy, Pittsburgh, PA

Abstract
Improvements in automated human fall detection help minimize emergency response time to potentially dangerous falls. However, existing vision-based detection systems can be inefficient and needlessly complex. We attempt to create a rule-based program which uses Hough Transformation to detect significant rotation of the subject, providing a simplified fall identification process. This approach is advantageous because it does not need to be trained, avoids the inherent design complexity of neural networks, and follows a straightforward, efficient approach to detecting falls.

Introduction
Each year in the US, about 36 million falls by older adults are reported – around 32,000 of which are fatal.[1] The danger of these falls can be reduced, however, by improving detection and response time. Ambient vision systems do so by analyzing a live camera feed, which is fed into a pre-trained convolutional neural network. The model analyzes the video to detect spatiotemporal patterns which might indicate a fall. However, we want to avoid the long training process, computational expense, and overall complexity of a neural network. We first assume that, when someone falls over, their image on the camera rotates by roughly 90°. Following this hypothesis, we propose a traditional/rule-based program, which simplifies the detection process by focusing only on the rotation of the figure in frame to detect falls, saving computational resources.

Methods
Frames are read in from an inexpensive webcam, and the system reads a new frame as soon as it finishes processing the current one. For each frame, we first apply background subtraction to isolate anything moving (i.e. the subject). We blur and threshold the image to make it suitable for processing (see Figure 1 for an example of the convoluted video), and then use OpenCV's HoughLinesP algorithm[2] to efficiently detect the largest line segment in the image. Finally, we use the following rule: if this line deviates from an upright angle by 40° or more for at least 5 seconds, the program detects a fall. We test the system using multiple short testing videos, including both falling and non-falling cases, and recorded both accuracy and processing speed. Figure 2 demonstrates how this system differs from a typical convolutional neural network's approach to fall detection.

Results
According to our tests, the program is about 76% accurate, averaging a processing rate of roughly 23 frames per second. Figure 3 shows the distributions of the correct and incorrect classification across the two types of test videos (correct and incorrect), as well as a confusion matrix based on the testing data.

Discussion
While not perfectly accurate, our program demonstrates the efficacy of optimizing fall detection via traditional programming, since we achieve reasonable accuracy with a low processing time per frame, and avoid the entire process of training a model. By releasing our statistics and source code, we hope others will compare their systems to ours and see how a more traditional, rule-based design can be beneficial in fall detection. Future improvements may include translating the code from Python to C++, which is much more efficient and natively supports OpenCV, and/or using the height/width ratio of the subject's figure to help identify a fall. Additionally, the program is not yet equipped to handle multiple subjects in frame nor significant occlusion (the latter was the cause of both false negatives in testing). However, both of these problems can likely be solved with further development of the program.

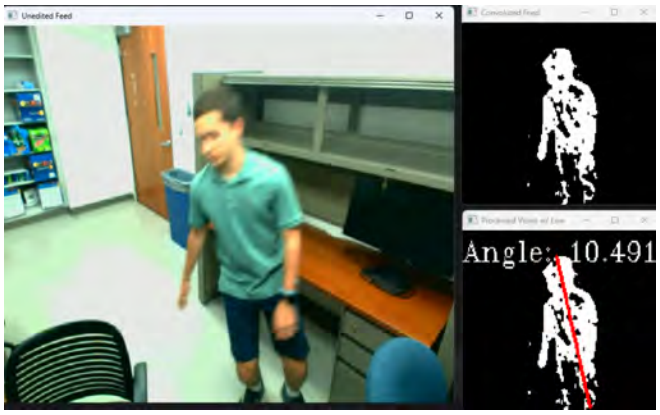

Figure 1 Raw video input (left), convoluted video (top right), and video showing longest line/angle (bottom left).

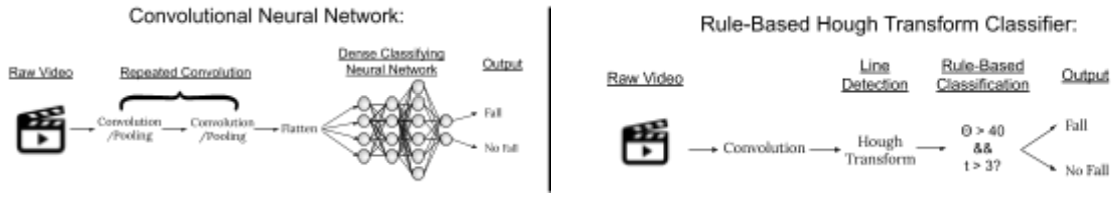

Figure 2 Comparison of typical convolutional neural network vs. our non-neural processing pipeline.

Figure 3 Keyframes of a test video (f0) to demonstrate an example test case (all test videos can be found here).

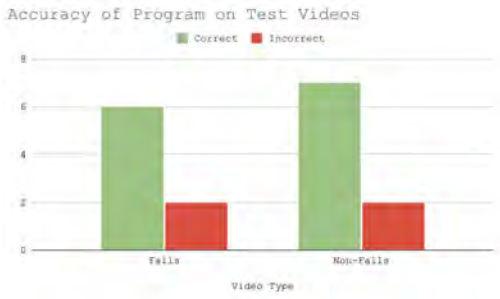

		Actual	
		Fall	No Fall
Predicted	Fall	0.75	0.222
	No Fall	0.25	0.777

Figure 4 Double bar chart and confusion matrix showing results of rule-based program on test videos.

References:
1. CDC. *Keep on Your Feet—Preventing Older Adult Falls*. Centers for Disease Control and Prevention. https://www.cdc.gov/injury/features/older-adult-falls/index.html.

2. OpenCV. *Hough Transform*. OpenCV Documentation. https://docs.opencv.org/3.4/d9/db0/tutorial_hough_lines.html

Investigating the Paracrine Effects of Tumors on B Cell Antibody Production

Scholar: Carlo Gambotto
School: Fox Chapel Area High School, Pittsburgh, PA
Mentors: Dr. Tullia Bruno, Allison Casey
Site: Immunology and Cancer Immunotherapy (ICI)

Background: Understanding how tumors directly influence B cell function, especially antibody production, in cancer is crucial. B cells play a significant role in normal immune responses and their importance in the anti-cancer response is becoming increasingly appreciated. Recent studies have shown that increased B cell infiltration intratumorally correlates to better patient prognosis, however B cell phenotypes and subsequent antibody production can differ by tumor type. This study aimed to investigate how tumors may directly modulate B cell function, particularly in their ability to produce antibodies, as well as affect transcription of key receptors in the activation of B cells. The objectives were accomplished by culturing three different cancer cell lines (HPV+ head and neck cancer, HPV- head and neck cancer, and lung adenocarcinoma) and assessing the impact on antibody production following stimulation of healthy donor B cells with toll-like receptor 9 (TLR9) agonist in the presence of tumor-conditioned media.

Hypothesis: I hypothesized that B cells exposed to the conditioned media from the cancer cell lines would have increased antibody production.

Methods: The experimental process included cell culture, blood processing, and an antibody production assay. Tumor cell cultures were split at a ratio of 1:5 and tumor cell supernatants were collected 3 days after passage. Resulting culture media was sterile filtered before use in the antibody production assay, to ensure conditioned media was cell-free. Peripheral blood mononuclear cells were isolated from healthy donor blood, and bulk B cells were separated using a negative selection bead kit. Total B cells were plated at a density of 50,000 cells/well in a 1:1 ratio of tumor conditioned media to normal culture media for experiment samples, with 10 ug/mL of CPG ODN-2006 (TLR-9 agonist) stimulus to promote antibody production. Samples were cultured for 4 days; supernatants were collected for antibody analysis, and cells were harvested for RNA extraction, and subsequent qPCR analysis of TLR7 and TLR9 mRNA transcription.

Results: The results of this study are anticipated to provide insight on the impact of the tumor on B cells and antibody production, possibly offering insightful information on immune responses associated with cancer. Our qPCR results demonstrated a decrease in transcription of key signaling receptors in B cells, TLR7 and TLR9 in conditioned media samples, relative to control. The ratio TLR7:TLR9 is protective in immune responses, indicating that the B cells may have a dysregulated immune response when the tumor supernatants were present. We expect that antibody response will also be diminished in our supernatants. These data suggest that the media conditioned with tumor supernatants had a negative effect on B cell antibody production. It is possible that different tumor types may cause variations in antibody production due to the unique paracrine effects they exert on B cells. Our results suggest that tumor-conditioned media negatively affected B cell antibody production, but further research would be needed to determine if there are specific differences between the tumor types in terms of their impact on cell function and resulting antibody production. Our findings could provide valuable insights into immune responses associated with cancer and potential therapeutic implications.

Cemiplimab and Teropavimab Redesign using a Computational Protocol for Antibody Engineering

Henry Gaston[1], Tianjian Liang, Dr. Zhiwei Feng, PhD, Dr. Xiang-Qun Xie, PhD

[1]Bethel Park High School, Bethel Park, PA; [2]University of Pittsburgh Hillman Cancer Center Academy, Pittsburgh, PA

Abstract

Antibodies are promising candidates for the treatment of a wide variety of diseases, but current methods for therapeutic antibody engineering are expensive and time-consuming. With current computational capabilities, the entire design process can be carried out with high accuracy *in silico*. In the present work, we examine the capabilities of a computational antibody design protocol[1] with the redesign of two distinct antibodies: cemiplimab and teropavimab.

Introduction

Because of their high affinity and specificity to a wide variety of macromolecules, antibodies have become a popular choice for immunotherapy treatments in various conditions, including cancers, autoimmune diseases, and inflammatory disorders. The continued advancement of antibody therapeutics relies on a more efficient method of engineering these molecules, with current wet lab antibody design methods being too costly and time-consuming for efficient advancement of antibody design. With recent improvements to computational design tools, a fully *in silico* antibody engineering process has become possible. Cemiplimab is an antibody that has been shown to effectively inhibit PD-1, stopping the proliferation of cutaneous squamous cell carcinoma. Teropavimab binds to GP120 and could be an effective treatment for HIV infection. In the present work, we use a computational protocol to improve the effectiveness of these antibodies as treatments.

Methods

We first used IMGT (http://www.imgt.org/) to obtain the amino acid sequence of each antibody. These sequences were then passed through SWISS-MODEL (https://swissmodel.expasy.org/), wherein homology modeling of the antibodies was performed. The known structure information of the antibodies and the antigens was downloaded from the Protein Data Bank (https://www.rcsb.org/). We applied a RosettaRelax protocol to the antigen to make the model closer to its native state, choosing the output model with the most favorable condition. The global docking of the target antibody-antigen complex was performed using ClusPro (https://cluspro.bu.edu/login.php), and local docking was performed using ROSIE SnugDock (https://rosie.graylab.jhu.edu/snug_dock). The interface residues of the complexes were determined with a machine learning model developed by the lab. These complexes were passed through another program based on FlexddG, where the specific point mutations for affinity maturation were determined and carried out.

Results

Several point mutations were made on the cemiplimab antibody, but the validation of these mutations using molecular dynamics simulations has not yet finished. The local docking step of the teropavimab antibody failed multiple times, so we are continuing to obtain better binding information in the global docking step. In the coming weeks, the molecular dynamics simulation should predict the plausibility of the mutations predicted by the protocol.

Discussion

Previous results using a similar protocol show that there is promise for a fully computational approach to the antibody design process. Our results are ongoing, but the proof of principle is promising. The lab is also working to develop other machine learning models for predicting the stability of the antibodies after the mutations are carried out. This step will narrow down the number of molecules passed on to the molecular dynamics simulation validation step.

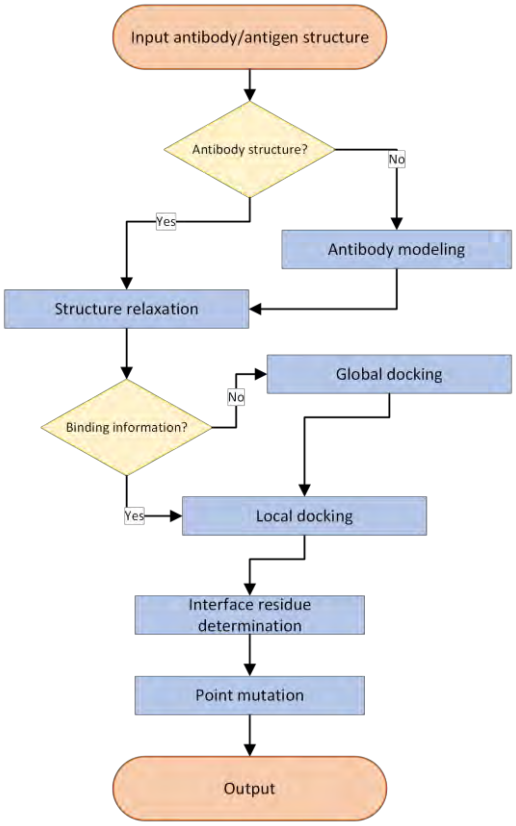

Figure 1. Flowchart displaying the protocol used for the design process.

Residue	Mutation	Score
H52	G	-0.549486992817669
H53	H	-2.718652258564040
H54	R	-0.376537060981645
H57	N	-0.459700663897003
H59	W	-1.448164177845230
L92	W	-1.327981289861600

Table 1. Table containing the residue chain and position, the mutation residue resulting in the lowest score at the specified location (indicating strongest binding affinity), and the ΔG prediction for each mutation.

References

1. Tianjian Liang and others, IsAb: a computational protocol for antibody design, *Briefings in Bioinformatics*, Volume 22, Issue 5, September 2021, bbab143
2. Zhiwei Feng and others, A New Era of Antibody Discovery: An In-depth Review of AI-Driven Approaches, ** *pending publication*

Generation of Reporter Cell Line That Can Visualize Iron Responsive Molecule DELE1

Scholar: Vanessa Gonzalez-Rychener

High School: Winchester Thurston School

Lab: Shiori Sekine, PhD

Mentor: Ryan Houston

Site: Tech Drive X

Mitochondria are organelles associated with the production of ATP, however they also serve various additional functions such as stress signaling. When there is sufficient iron present in a cell (the steady state condition), the mitochondrial protein DELE1 is constantly degraded by the LONP1 protease, which resides in the mitochondrial matrix, soon after mitochondrial import. However, when there is an iron deficiency, the import of DELE1 is arrested and therefore DELE1 cannot be degraded. This causes a stabilization of DELE1 on the mitochondrial surface, activating the HRI enzyme and triggering the cellular stress response. The DELE1-mediated stress response is important for protecting red blood cells from iron-deficiency. Therefore, it is very important to investigate the mechanism of the iron deficiency-induced DELE1 import arrest.

However, this mechanism is still unknown. In order to conduct screenings to identify the upstream regulators, it is necessary to create a reporter cell line in which the stability of DELE1 is visualized. In this study, DELE1 tagged with a fluorescent tag, EYFP, was induced by the Tet-On system which causes the cell to express the DELE1-EYFP only when exposed to doxycycline. By using this system, the expression levels of DELE1-EYFP were evaluated under different conditions (steady state, iron deficiency, and iron supplementation). The results were then visualized using western blots.

DELE1-EYFP was not clearly detected in preliminary experiments; the expression conditions are now being optimized to obtain enough expression to be analyzed. Once optimized, its expression will be examined by microscopy. There is a possibility that since the EYFP tag is relatively large (27 kDa), it may interfere with the import regulation of DELE1 (55 kDa). In that case, we will try using a smaller tag called Spot (1.4 kDa), that is less likely to interfere. DELE1-Spot will be visualized by a recently developed fluorescent dye-conjugated nanobody.

Methyltransferase 3 (METTL3) Regulates Kaposi's Sarcoma-associated Herpesvirus (KSHV) Lytic Replication

Scholar: Daniel Guo

High School/College/City/State: University of Pittsburgh, Pittsburgh, PA

PI of group/lab: Shou-Jiang Gao, PhD

Mentor(s): Wen Meng, PhD

Site: Cancer Biology

KSHV induces multiple malignancies, including Kaposi's sarcoma (KS), primary effusion lymphoma (PEL), multicentric Castleman's disease (MCD), and KSHV-associated inflammatory cytokine syndrome (KICS). There is currently no effective therapy for KSHV infection and its associated malignancies. KSHV has two phases in its life cycle: latency and lytic replication. During latency, the infected cells express minimal viral genes, which facilitate the evasion of the immune system. During lytic replication, KSHV expresses most of its viral genes and produces infectious virions, which facilitates the spread of the virus albeit causing host cell death. N^6-methyladenosine (m^6A) is the most prevalent post-transcriptional RNA modification. The cellular machinery driving m^6A modification includes "writer" methyltransferases, "reader" m^6A binding proteins, and "eraser" demethylases. In this study, a latent KSHV-infected cell, iSLK-RGB-BAC16, were subjected to m^6A writer METTL3 inhibitor STM2457, or METTL3 activators (A: Methyl piperidine-3-carboxylate hydrochloride, B: Tert-butyl 6-methylpiperidine-3-carboxylate, C: Methyl 6-methylpiperidine-3-carboxylate, D: Methyl piperazine-2-carboxylate) in both latent and lytic replication conditions without or with sodium butyrate (NaB) induction, respectively. The KSHV replication states were examined by monitoring the expression of RFP, GFP and BFP proteins, which reflected the expression of viral latent, early lytic and late lytic proteins, respectively. STM2457 treatment increased the number of GFP-positive cells during KSHV lytic replication in a dose-dependent manner. On the other hand, 3 of the 4 METTL3 activators (A, B, D) treatment decreased the number of GFP-positive cells during KSHV lytic replication. Our results indicate that m^6A writer-protein METTL3 likely function to maintain KSHV latency by repressing viral lytic replication.

Investigation of cell decision between therapy-induced senescence and apoptosis in cancer

Scholar: Jinyi(Jinny) Guo

High School: Shady Side Academy, Pittsburgh, PA

Lab: Wayne Stallaert, PhD

Mentor: Dante Poe, Betsy Ann Varghese

Site: Cancer Biology

Background: Cellular senescence, “permanent” cell cycle arrest, theoretically represents a desired outcome for anticancer therapies. However, studies have demonstrated that therapy-induced senescence is reversible, allowing tumor cells to survive and reemerge years after the primary disease eradication. Hence, tumor cell cycle plasticity poses the challenge of therapy resistance and tumor relapse as arrested tumor cells regain proliferative capacity. Understanding the mechanistic pathways whereby tumor cells determine the fate between senescence and cell death under therapeutic stress is critical to developing combination therapies to address therapy-induced dormancy and tumor relapse. In this study, I investigate how ovarian cancer cells choose between senescence and apoptosis in response to therapy-induced DNA damage.

Methods: Ovarian cancer cells OVCAR-8 with biosensors DHB-mVenus and 53BP1-mApple were treated with varying concentrations of chemotherapy drugs cisplatin and olaparib. Live-cell time-lapse imaging of fluorescent biosensors by the THUNDER Imager was used to track single-cell activity over five days. In the follow-up experiment, cells were treated with either a combination of cisplatin and Wee1 inhibitor/Cdk2 inhibitor or cisplatin/Wee1 inhibitor/Cdk2 inhibitor alone. Cell images were captured after five days and segmented using Cellpose for analysis.

Results: OVCAR-8 cells performed apoptosis with high Cdk2 activity under drug treatment, as indicated by high cytoplasmic levels of DHB. Cells treated with Wee1 inhibitor and cisplatin demonstrated increased apoptosis than cells receiving only cisplatin.

Conclusion: Our study shows that tumor cells choose apoptosis in a state of confusion between the chemotherapeutic stress of DNA damage and the inability to shut down Cdk2 activity and halt cell cycle progression. Hence, combination chemotherapy of cisplatin and Wee1 inhibitor is a promising treatment that renders a solution to potential tumor relapse. Future studies will use cells with an additional PCNA biosensor to confirm the finding and distinguish the cell cycle phase in which cells commit to a fate.

Title: Tourniquet Use in a Pediatric Trauma Cohort

Scholar: Mariah Harris

High School/College/City/State:Pittsburgh CAPA 6-12 Shady Side Academy, Pittsburgh, PA

PI of group/lab: Dr. Christine Leeper

Mentor(s): Dr. Christine Leeper, Dr. Erin Feeney

Site: UPMC Department of Surgery

Introduction: There is a lack of research on tourniquet use in pediatric trauma patients. The purpose of this investigation was to better understand the use of tourniquets in children.

Methods: The UPMC Children's Hospital of Pittsburgh trauma database was retrospectively reviewed for patients aged 0-17 who presented with traumatic limb injury and tourniquet (TK) application between 2015-2022. Data recorded included demographics, injury characteristics, and tourniquet use variables (number, location, person applying, proper application and adverse events). Data was summarized using counts, median, and percentages.

Results: In total, 37 children who had a total of 51 tourniquets applied were included. In this cohort, the median (IQR) age was 14 years (10-15), 27/37 (72%) were male, and race was 54% Black, 43% White, and 2% Asian/Pacific Islander. Most (23/37; 62%) had public insurance. The median (IQR) injury severity score was 9 (5-10), mechanism of injury was 70% penetrating versus 30% blunt, and 11% (4/37) were in shock on arrival. Of the 37 children, 27 (73%) required an urgent operation. The in-hospital mortality rate was 0%, and 36/37 (97%) were discharged home. In total, 11/51(22%) tourniquets were applied by bystander/family, 21/51 (41%) by Fire/EMS, 14/51 (32%) by police, and 4/51 (8%) by referring hospital staff. Overall, 30/37 (81%) had properly applied tourniquets. No patient had an adverse complication (kidney injury, amputation, rhabdomyolysis, nerve injury, compartment syndrome) related to application of the TK.

Conclusion: Tourniquet use in this cohort of injured children was feasible and not associated with adverse events. Larger multicenter studies should be performed to provide communities with evidence-based instruction for the safe use of tourniquets in children.

Determining the Subcellular Location of TFEB Degradation During Viral Infection

Scholar: Lucas Hertzel
High School/College/City/State: Bethel Park, Pittsburgh, PA
PI of group/lab: Bill Chen, PhD
Mentors: Aine Boudreau; Travis Lear, PhD
Site: Tech Drive X

Introduction: Lysosomes are key in cellular defense against pathogens and are dysfunctional during viral infection. We have found that the transcription factor responsible for initiating lysosome biogenesis, EB (TFEB), is degraded during viral infection via the ubiquitin-proteasome system (UPS), disrupting lysosomal function and production while increasing viral load. While genetic and pharmacological interventions can prevent TFEB degradation and oppose viral infection, the exact subcellular compartment in which TFEB is degraded remains unclear. We aim to understand the subcellular location(s) where degradation occurs to design a host centric therapeutic process that can augment lysosomal activity to fight viral infection. **Methods:** We created a plasmid library of fluorescent TFEB constructs to measure protein localization using High Content Imaging. These constructs included mutations at key sites to prevent degradation and localization sequences to control trafficking. We expressed these in airway epithelial cells (Beas-2B) and treated cells with UPS inhibitors and coronaviral infection (OC43). Cells were then fixed, counterstained with Hoechst and Phalloidin, and imaged using a fluorescent microscope. We used Cell Profiler to quantify the data to determine TFEB localization via intensity of signal. Additionally, we used immunoblotting to examine protein levels in the nucleus versus the cytoplasm through cyto-nuclear extraction. **Results:** The fluorescent TFEB constructs were successfully expressed in cells and localized based on trafficking signals. When TFEB wild type (WT) was forced into the nucleus, protein signal dropped significantly, while the mutants containing protective motifs saw no such decline. Upon being trafficked to the cytoplasm, both the WT and protected mutants displayed similar protein levels without decline. **Conclusions:** During viral treatment, TFEB, when protected from degradation, persists in the nucleus, while unprotected TFEB levels decrease in the nucleus. Both presented no significant decrease when shuttled to the cytoplasm, indicating the nucleus is the primary site of TFEB degradation during viral infection.

Discovering Eye Movement Patterns by Eye Tracking Videogames

Scholar: Jasmine Horton
Highschool: Winchester Thurston, Pittsburgh, Pennsylvania
Lab: Yuanyuan Chen, Ph.D
Mentors: Dr. Patrick Mayo, Emily Levin
Site: Ophthalmology (OPT)

As humans, we rely on visual processing to interact with our surroundings. Understanding eye movements is crucial because they influence our decision-making, learning, and memory (Miseviciute). This study measures eye movements and how eye movement patterns change as a function of behavioral performance when playing the videogame, Excitebike. We specifically focused on fast and slow eye movements called saccades and pursuits. Saccades are "rapid, ballistic movements of the eyes that abruptly change the point of fixation," whereas smooth pursuit is "slower tracking movements of the eyes designed to keep a moving stimulus on the fovea" (Purves). Our hypothesis is that there's a correlation between a player's eye movements and their Excitebike skill level. We predict that players with quicker lap times, and therefore improved skill, will show noticeable differences in their saccade-smooth pursuit patterns, with these faster lap times corresponding to increased smooth pursuit and reduced saccades towards upcoming obstacles. This result would suggest improved predictive abilities and more consistent eye movement behavior. We had subjects complete ten trials, each consisting of three laps around a predetermined track in Excitebike. We recorded eye movements across all trials using Tobii Glasses 3, a lightweight, nonrestrictive infrared eye tracker. We then processed the data using Matlab to extract the eye speed and position at 10 ms resolution. Based on our current data sets, we have observed a pattern amongst the most efficient trials consisting of saccadic eye movements preceding the player's in-game rider during a turn. As the turn is completed, there's a transition into smooth pursuit eye movement back to the rider. We could use information like this to compare typical eye movements to eye movements in patients with brain diseases, which can cause different movement patterns. Such a simple, noninvasive approach could significantly aid in diagnostic processes of these diseases.

Sources:

Miseviciute, I. (n.d.). Eye tracking – a window to cognitive processes. Tobii. https://www.tobii.com/resource-center/learn-articles/what-eye-tracking-reveals-about-cognitive-processes

Purves D, Augustine GJ, Fitzpatrick D, et al., editors. Neuroscience. 2nd edition. Sunderland (MA): Sinauer Associates; 2001. Types of Eye Movements and Their Functions. Available from: https://www.ncbi.nlm.nih.gov/books/NBK10991/

MD simulations of CB-orthosteric-allosteric ligands to aid the design and validation of allosteric modulators

Guanyu (Gavin) Hou[&,1], Yixuan Hao[1], Terry McGuire[1], Xiang-Qun Xie[*1], and Zhiwei Feng[*1]

[1] Department of Pharmaceutical Sciences and Computational Chemical Genomics Screen (CCGS) Center, Pharmacometrics & System Pharmacology (PSP) PharmacoAnalytics, School of Pharmacy; National Center of Excellence for Computational Drug Abuse Research (CDAR); University of Pittsburgh, Pittsburgh, PA, USA, 15261

Abstract

Cannabinoid receptor sub-types CB1 and CB2 are GPCR receptors that mediate vital signaling pathways in the central nervous system (CNS) and the peripheral immune system. Specifically, CB1 is more abundantly expressed in the CNS, while CB2 is primarily expressed in the peripheral immune system. Targeting CB1 with agonists may cause psychosis and panic, while inhibition of CB1 may cause depression and anxiety. In contrast, targeting CB2 avoids the adverse psychotropic effects. Allosteric modulators (AMs) are an elegant approach to targeting GPCRs and offer many advantages over ligands targeting the orthosteric pocket. While several synthetic CB1 AMs have been reported, limited CB2 synthetic allosteric modulators (AMs) have been reported. Therefore, we used MD simulations and other computational methods to design and validate new CB AMs. MD simulations were conducted on CB1+orthosteric ligand CP55940+allosteric modulator ORG37569 (NAM). The RMSD results show a consistent RMSD of 0.5Å for CP, a RMSD of 1.0Å for CB1, and a fluctuating RMSD of 1-2.5Å for ORG. These results show the stability of the orthosteric compound and allosteric modulator in the protein pocket. The MM/PBSA method was used to calculate the free binding energy of CB1-CP-ORG complex. More MD simulations will need to be conducted to cross-validate the results. A control experiment using only CB1 and CP will also be useful in comparing free binding energy values.

Introduction

GPCR subclass Cannabinoid receptors CB1 and CB2 are potential therapeutic targets for pain, obesity, and other diseases. Compounds targeting CB2 include orthosteric ligands or allosteric modulators (positive and negative). Current CB2 research is limited compared to CB1. Notable compounds include ORG27569 (CB1 NAM) and ZCZ011 (CB1 PAM), along with C2 (first synthetic CB2 PAM) and WIN (CB2 orthosteric ligand).

Molecular dynamics (MD) simulations investigate dynamic interactions between CBs and ligands, aiding in understanding CB1-CB2 differences. Insights from MD simulations can inform the design of allosteric modulators for novel therapeutic strategies targeting CB2.

Methods

Molecular Dynamics (MD) Simulation

Complexes of CB1-CP55940-ORG27569 were used to perform the MD simulations, in which the protein and ligands were extracted from 6kqi pdb file. Each system was put into a 0.15M NaCl solution with a cubic water box. The MD system was conducted using the ff14SB protein forcefield, lipid14 lipid forcefield, TIP3P water model along with the GAFF2 forcefield and AM1-BCC charge model for ligands. After the system was relaxed, the heating-up phase, the equilibrium phase, and the sampling phase were conducted sequentially. CPP trajectory and MM/PBSA Binding Free Energy were used to analyze the results.

Docking of C2 in Site G of CB2

Site G is conserved in CB1 and CB2 as well as in many other GPCRs. CB2 PAM ec-21a (C2) has several binding poses to various binding sites. We docked C2 into site G of CB2 using Sybyl. The energy decomposition and key residues were calculated using MCCS' Jdock function. MCCS can generate nine different energy contribution vectors in total, including Gauss, Gauss1, Gauss2, hydrogen-bonding, hydrophobic, non-steric (hydrogen-bonding and hydrophobic),repulsion, steric (Gauss1, Gauss2, and repulsion), and total energy contribution.

Results

The RMSD results for CB1-CP-ORG show a very interesting jump of ~1Å at ~57ns for NAM ORG27569. This jump is explained by the rotation of ORG during the simulation. Although the binding free energy of -22.7 kcal/mol is very

significant, we are currently cross-validating this result with more MD simulations that have the CB1 PAM ZCZ011 substituted in for the CB1 NAM ORG27569. The RESP model will give a more accurate result. We need to run more MD simulations (up to 500ns) without the AMs as a control for further validation as well. MD simulations for C2 in site G are also crucial in CB2 PAM design. Free energy decomposition of these MD results can significantly add to the selectivity and design of future CB1 and CB2 allosteric modulators.

The binding free energy of complex CB1-CP-ORG was calculated using the MM/PBSA method. The resulting binding free energy score was -22.7 kcal/mol.

Discussion

Molecular Dynamics (MD) simulations and free energy decomposition play a crucial role in the design of cannabinoid (CB) allosteric modulators due to their invaluable contributions to achieving selectivity towards the CB2 receptor. By utilizing free energy decomposition techniques, researchers can identify key residues and interactions that govern the binding of allosteric modulators to CB2. This information allows for the rational design of novel compounds with improved selectivity, targeting specific residues that are unique to the CB2 receptor. Additionally, MD simulations provide dynamic insights into the behavior of these modulators within the receptor's binding pocket, offering a comprehensive understanding of their interactions and stability over time. By validating the results obtained from free energy calculations through MD simulations, researchers can confidently refine their designs and optimize the binding affinity and specificity of CB2 allosteric modulators, ultimately advancing the development of more effective and targeted therapeutic agents.

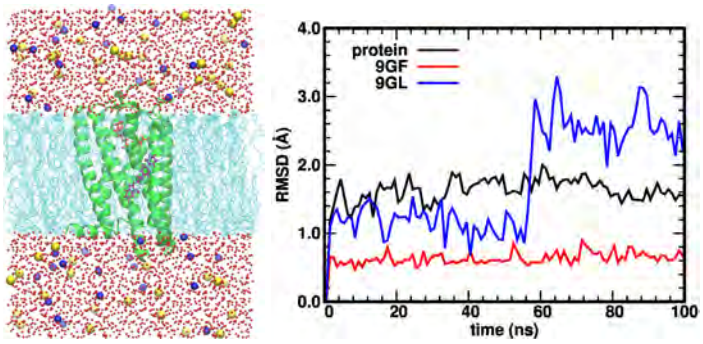

Figure 1. Preparation of MD using CHARMM-GUI. MD settings: P=1atm, T=298K, 100ns total with a timestep of 1fs (.001 ps). RMSD results that show the stability of the respected protein and ligands.

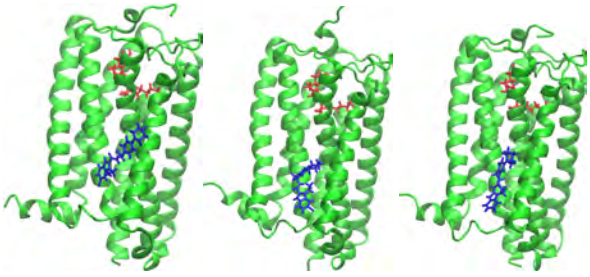

Figure 2. Result of MD simulation with t=0ns frame on the left, t=58ns frame in the middle, and t=100ns frame on the right.

References

1. Yuan J, Jiang C, Wang J, Chen CJ, Hao Y, Zhao G, Feng Z, Xie XQ. In Silico Prediction and Validation of CB2 Allosteric Binding Sites to Aid the Design of Allosteric Modulators. Molecules. 2022 Jan 11;27(2):453. doi: 10.3390/molecules27020453. PMID: 35056767; PMCID: PMC8781014.
2. Cheng, J.; Hao, Y.; Shi, Q.; Hou, G.; Wang, Y.; Wang, Y.; Xiao, W.; Othman, J.; Qi, J.; Wang, Y.; et al. Discovery of Novel Chinese Medicine Compounds Targeting 3CL Protease by Virtual Screening and Molecular Dynamics Simulation. *Molecules* **2023**, *28*, 937. https://doi.org/10.3390/molecules28030937

Title: Stress, and Treatment Tolerance. among Patients with Late-Stage Non-Small Cell Lung Cancer : A Comparison of Race and Neighborhood

Chimdi Isiguzo
Pittsburgh Science and Technology Academy
Margaret Rosenzweig, PhD, FNP-BC,AOCNP,FAAN – Mentor
Ruth Modzelewski, PhD – Mentor
Site – CoSSBI

Background: Racial and economic disparities exist among patients with cancer, for overall survival and treatment tolerance. One mechanism for those disparities may be stress
Aims: This study aims to comprehensively assess, and compare according to race and income, the deep phenotype of lifetime stress and subsequent cancer outcomes among patients diagnosed with late-stage non-small cell lung cancer (NSCLC).
The primary aims are to:
Aim 1: Describe baseline lifetime stress, discrimination, quality of life, allostatic load, and immune markers among patients with late-stage lung cancer, comparing by race and neighborhood deprivation.
Aim 2: Examine symptom distress, financial toxicity, dose modifications, difficulty accessing care, and tumor progression during advanced lung cancer treatment at 3 months, post treatment initiation comparing by race and neighborhood deprivation.
Aim 3: Correlate baseline variables from Aim 1 (discrimination, quality of life, allostatic load, and immune markers) with symptom distress, financial toxicity, and dose modifications.
Methods: Prospective, repeated measures (Baseline, 3 month) cohort design, recruiting late-stage NSCLC patients from 3 sites within the UPMC Cancer Centers.
Instruments: **(Baseline)** Race, - Self Report; Neighborhood Deprivation – Area Deprivation Index (1-10- state, 1-100- national). Valid, reliable measures of lifetime stress (Perceived Stress Scale scores (10-50), Symptoms (PROMIS – scores 29-145); Perceived Discrimination Scale, Daily and Lifetime (daily scores 0-36; lifetime,0-44), allostatic load (derived scores – 0-11, N/Abnormal), and immune markers (Normal/Abnormal),
3 months - Valid and reliable scales of: Symptom Distress (PROMIS – 29-145);Financial Distress (COST - 0-44). Tumor progression (Yes/No) and Treatment modification- Chart Review (Yes/No). reports and clinic notes. Difficulty receiving care – open ended interview, coded and analyzed.
Statistical analysis -descriptive, comparison of means and correlational analysis.
Results: N=29, Female – n=17,58.6%;Black- n=8,27.6%; ADI- Mean-68.3,(National)
Aim 1: Baseline – Significant racial differences – Long term and daily discrimination. Long term (p=.000), (Daily p=.021).
Aim 2: Three months – Significant racial differences – Financial toxicity at 3 months (p=.001).
Aim 3: Significant correlation between Race and AL (p= 0.51); 3-month progression and AL (p=0.22).
Conclusions: Racial disparity exists in the outcomes of patients with late-stage non-small cell lung cancer. These findings may ultimately lead to the development of targeted interventions to reduce treatment disparities and improve overall patient care.

Title: Investigating the non-immune role of IL-33 in High Grade Serous Ovarian Cancer (HGSOC) initiation
Scholar: Na'Taeya Johnson
High School: Uprep Milliones, Pittsburgh Pennsylvania
Lab: Lan Coffman, MD, PhD
Mentor: Geyon L. Garcia
Site: Womens Cancer Research Center (WCRC)

Background: Ovarian cancer, specifically High Grade Serous Ovarian Cancer (HGSOC), is the fifth leading cause of cancer related deaths in women. A woman's risk of being diagnosed with ovarian cancer during her lifetime is 1 in 78. About 19,710 women are affected by ovarian cancer. In 2022, the mortality of HGSOC was ~48% meaning that 1 in 2 women diagnosed with HGSOC will die within 5 years because of their cancer. This is because women are diagnosed in late stages of disease, i.e., after the cancer has already metastasized to other organs. Majority of HGSOC begins in the fallopian tube where abnormal fallopian tube epithelial (FTE) cells start to divide uncontrollably. If not caught early, FTE eventually form a tumor that then easily metastasizes to the ovary and the abdomen. There are currently no early detection or prevention strategies for women who are at risk of being diagnosed with HGSOC other than surgical castration. IL-33 is a novel cytokine of interest for HGSOC given that women with HGSOC have detectable IL-33 in their blood. Stromal cells act as a major source of IL-33 in ovarian tumors, however, the roll biology of IL-33 and FTE remains understudied. IL-33 has been implicated in cancer initiation, progression, and metastasis; therefore, the goal of my work is to determine which pathways IL-33 transcriptionally regulates.

Methods: FTE cells were treated with 0.1ng/mL of recombinant IL-33 for up to 48 hours. I used real-time quantitative reverse transcription PCR (qRT-PCR) to quantify transcriptional changes of genes involved in DNA repair gene, cell survival, apoptosis, and metabolism.

Results: Low dose IL-33 treatment results in subtle transcriptional changes in DNA repair and apoptosis genes.

Conclusion: More work is needed to accurately assess IL-33's effect on FTE gene transcription. Going forward, we will test varying concentrations of IL-33 treatment.

The Life and Times of Annular Gap Junction Vesicles

Malynn Jones
Obama Academy 6-12, Pittsburgh, PA
Dr. Sandra A. Murray, PhD
Site: CoSBBI

Abstract: Gap junction channels allow cells to communicate materials with one another. Channel internalization results in loss of communication and the annular gap junction formation in the cytoplasm. To analyze the fate of annular gap junctions, computer-assisted image analysis with Imaris software was used. Annular junctions are divided, fused with organelles, and recycled to the cell surface. Further investigation will determine if annular gap junctions deliver proteins to other organelles.

Background: Cells communicate with one another by passing materials through cell surface channels, called gap junction channels. These channels are important in regulating cell behavior. They are composed of proteins, connexins, that assemble into hemichannels. Hemichannels from contacting cells pair with one another to form the channels that then cluster into gap junction plaques. Plaque removal from the surface results in annular gap junction formation. Annular gap junctions are degraded by lysosomes; however, it is hypothesized that they have other fates. To accurately track annular gap junction fates, data was collected with a lattice light sheet 3-D microscope which reduced phototoxicity/quenching (a problem with conventional imaging).

Methods: Human adrenal tumor cells (SW-13) transfected to express emerald-green, fluorescent connexin and M-cherryRed membrane marker were used. Light sheet lattice microscope images were collected at the Janelia Research Campus-Virginia and the data was transported to me to analyze with Imaris Software. Changes in annular gap junction size, shape, interactions, and movement were measured.

Results: Four-dimensional rotation allowed us to analyze the images and determine if annular were in contact or overlapping organelles or changed plans rather than being lost from few (problems with typical live cell imaging). We selected the annular to be 0.5. An average annular gap junction size with a diameter was selected for tracking. The average annular gap junction track speed was 0.70 μm/s ±0.34. Annular fused with membrane vehicles divided and flatted out at the cell membrane recycling.

Summary: Annular gap junctions were tracked to determine their fate. They divided, changed shapes, associated with membrane organelles and possibly recycled. The frequency of these events is being determined. Such information will increase our understanding: of gap junction protein turnover; and the role of annular gap junctions in protein delivery to other organelles.

Acknowledgements

Many thanks to:
Dr. Sandra Murray, Dr Anthonya Cooper, Dr. Selma Ferra, Dr. David Boone,
Collin Simon & Simon Watkins -Cell Biology Imaging Center, Dept of Cell Biology, Univ. of Pittsburgh, Sch Medicine

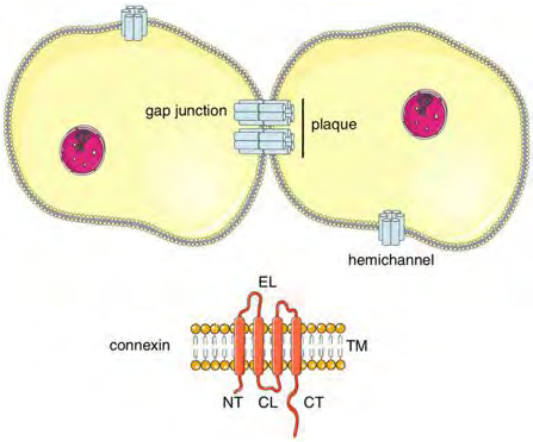

Figure 1: Example of what a gap junction looks like

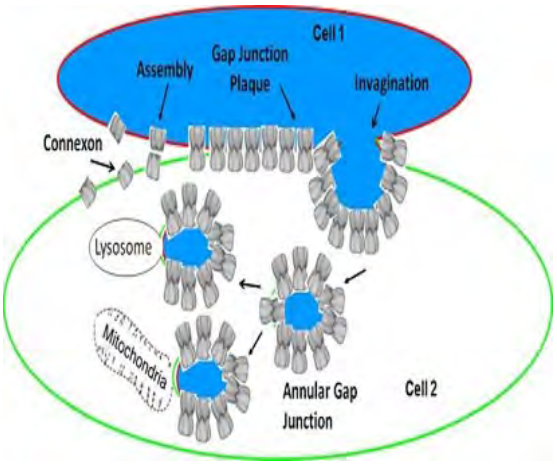

Figure 2: Gap Junction Internalization

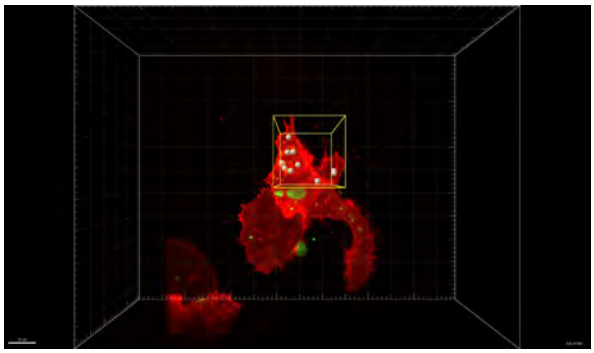

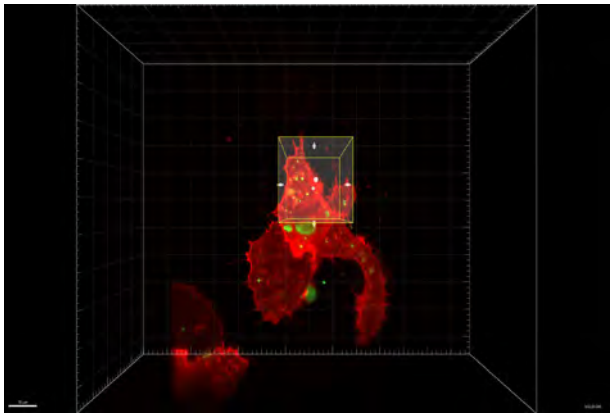

Figure 3 and 4: Image of the cell I had to track on Imaris Software

DeepMT-GAN: Artificially Intelligent Molecular Transformer and Generative Adversarial Network for Cannabinoid CB2 Target-Specific Small-Molecule Sublibraries Generation

Preetam S. Jukalkar[1], Dr. Xiang-Qun Xie, MD, PhD, EMBA[2]
[1]South Fayette High School, McDonald, PA; [2]University of Pittsburgh, Pittsburgh, PA

Abstract *Despite the adoption of high-throughput screening (HTS) and the publication of extensive chemical compound datasets, drug discovery continues to yield low hit rates–ranging from 0-0.01%[1]. This study investigates the efficacy of natural language processing (NLP) algorithms on biological text data and the potential of deep learning methods for generating target-specific small molecule libraries to avoid expensive and time-consuming laboratory testing in the infantile stages of drug discovery.*

Introduction Dug discovery is often compared to "finding a needle in a haystack;" this process is wasteful and findings are largely dependent on luck due to the volatility of compounds, complexity of drug-drug interactions, and the intricate processes that govern the human body. As a result, it takes 18 years on average to discover a drug targeting the central nervous system and receive regulatory approval, with a majority of this time being spent on discovery and clinical trials[2] [Fig 1]. Since clinical trials cannot easily be automated and are necessary to ensure the in vivo safety and efficacy of a drug, this study turns its attention to drug discovery–a field ripe with innovation and at the forefront of computational methods.

Current artificially intelligent (AI) models designed for molecular generation utilize simplified molecular-input line-entry system (SMILES) data and employ lossy encoding [Fig 2A] to convert these text strings into integers–losing information during preprocessing and failing to capture the entire chemical space of potential ligands for a given target [Fig 2B]. Furthermore, these generative models[3] require chemical scaffolds which further limit the novelty and usefulness of generated compounds, limiting the applications of AI in drug discovery with the current landscape of deep learning models. This study aims to alleviate the pitfalls of utilizing AI in pharmacology by introducing techniques that have made groundbreaking contributions in the field of natural language to textual biological data.

Methods The dataset utilized consists of 2723 SMILES for CB2-specific small molecules with reported K_i values under 450 from the publicly available ChEMBL database[4]. Data was collected through the database's Python API, and the distribution of molecules is detailed in. While most models within the context of drug discovery employ one-hot encoding–a lossy form of data storage that can translate text to numbers–this study utilizes a tokenizer developed in [5] to increase interpretability and capture structural information. Once tokenized, the SMILES data was used to train a Transformer model (architecture detailed in [Fig 3A]) to generate embeddings that capture positional data and more accurately describe the original SMILES string as a 2D array of floating point numbers. These embeddings were used to train a Wasserstein Generative Adversarial Network (WGAN) (architecture detailed in [Fig 3B]) which could generate 2D embeddings autonomously that are then decoded through the Transformer into the original tokenized form. The tokenizer can then be used to decode the output and generate a novel SMILES string that theoretically binds to the CB2 receptor. The workflow is detailed in [Fig 3C].

Results The Transformer achieves a sparse categorical cross entropy loss of 0.2119 after training for 100 epochs on tokenized CB2 SMILES. The model is able to represent the original vocabulary (510 words) with dimensions of (128, 510) in a 2D array with shape (128, 32), increasing the efficiency and adaptability of the WGAN model while also curbing overfitting. The WGAN model does not currently achieve satisfactory results, but training is incomplete due to the over three million parameters of the more complex model. On a smaller scale, the WGAN produces promising results with SMILES strings that resemble the input data despite being fed random noise [Fig 4].

Discussion With a sore need for computational methods to hasten the pace of drug discovery, AI and deep learning models hold tremendous potential for the task of receptor-specific molecular generation–particularly in chemically difficult tasks such as that posed by the similarity between CB1 and CB2. Models like that proposed by this study could potentially replace high-throughput screening and the extensive resources HTS requires by screening molecules computationally and testing fewer compounds in a laboratory setting. However, care must be taken to avoid overfitting as an over-reliance on current AI models could lead to naivety in the broader chemical space as the probabilistic nature of artificial intelligence poses challenges in generating completely novel molecules.

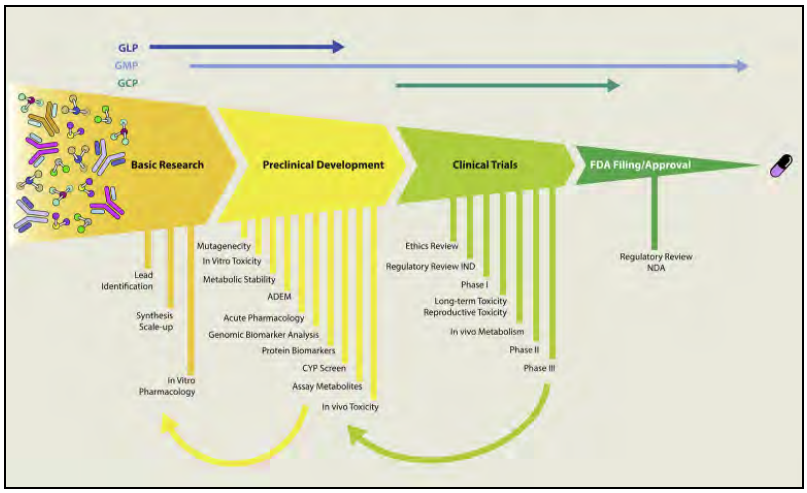

Figure 1. Drug discovery timeline. Beginning with basic research, ligand candidates must first be discovered before preclinical research and clinical trials are conducted, culminating with FDA approval. The process is cyclic and repeats, taking decades to complete [2].

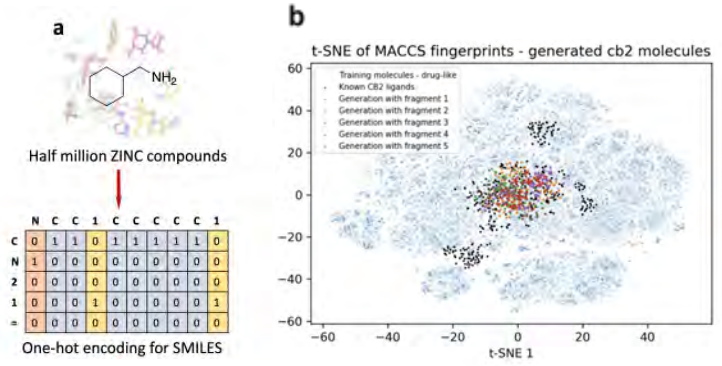

Figure 2.
A) One-Hot Encoding of SMILES strings. Text data is transformed into numerical representation lacking structure.
B) Colored points (generated SMILES) fail to capture entirety of chemical space and do not model all existing ligands (black points) [3].

WGAN Generated SMILES

((ccccccccO()c=ccOc((Oc)cClClCl)NCl
[C@@H]CCCC4[C@@H]CC4
(N=[C@@H]s(=((((([C@@H](ccccccccc==1N1Br[I-]11)
[C@@H]c[N+][O-][C@@H]11cc[O-]
c(c((((c(c((=cc==O)4OO=Occccccc)c)cc)

Figure 4.
SMILES generated by WGAN. While most are not valid, results are promising and display unique chemical features.

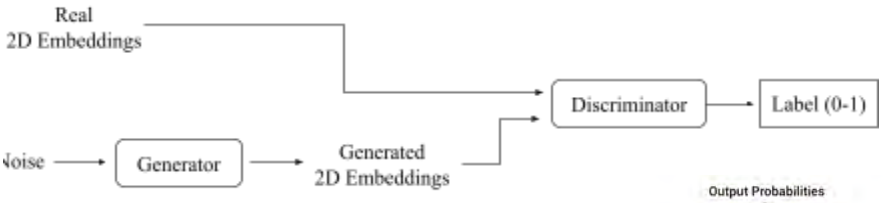

Figure 3.
A) WGAN Model. Classic generator-discriminator set-up to generate 2D embeddings of SMILES strings. Employs Wasserstein loss for stability.

B) Transformer model with attention units. Inputs of tokenized SMILES strings are transformed into 128x32 size embeddings with decoder to expand back up.

MT-GAN uses Transformer to represent SMILES numerically, and GAN to learn generation of novel compounds that follow general pattern of CB2 specific molecules.

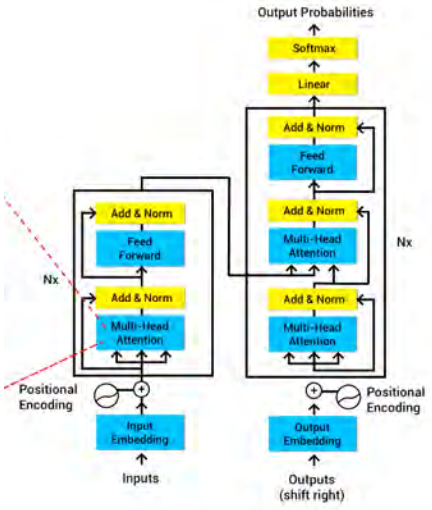

References

1. Schneider, P., Walters, W.P., Plowright, A.T. et al. Rethinking drug design in the artificial intelligence era. Nat Rev Drug Discov 19, 353–364 (2020). https://doi.org/10.1038/s41573-019-0050-3.
2. Mohs RC, Greig NH. Drug discovery and development: Role of basic biological research. Alzheimers Dement (N Y). 2017 Nov 11;3(4):651-657. doi: 10.1016/j.trci.2017.10.005. PMID: 29255791; PMCID: PMC5725284.
3. Bian Y, Xie XQ. Artificial Intelligent Deep Learning Molecular Generative Modeling of Scaffold-Focused and Cannabinoid CB2 Target-Specific Small-Molecule Sublibraries. Cells. 2022 Mar 7;11(5):915. doi: 10.3390/cells11050915. PMID: 35269537; PMCID: PMC8909864.
4. David Mendez and others, ChEMBL: towards direct deposition of bioassay data, Nucleic Acids Research, Volume 47, Issue D1, 08 January 2019, Pages D930–D940, https://doi.org/10.1093/nar/gky1075.
5. Schwaller, Philippe; Probst, Daniel; Vaucher, Alain C.; Nair, Vishnu H; Kreutter, David; Laino, Teodoro; et al. (2019): Mapping the Space of Chemical Reactions using Attention-Based Neural Networks. ChemRxiv. Preprint. https://doi.org/10.26434/chemrxiv.9897365.v3.

Structural Prediction and Functional Validation of Two Zinc-Fingers of Hepatitis B Virus Polymerase

Scholar: Anthony Kalvi

High School/College/City/State: Upper St. Clair High School, Pittsburgh, PA

University of Pittsburgh Greensburg, PA

PI of group/lab: Haitao Guo, PhD

Mentor(s): Ning Sun

Site: Cancer Biology

Hepatitis B virus (HBV) infection affects 300 million people worldwide and is a leading cause of cirrhosis and hepatocellular carcinoma. HBV is a DNA virus that replicates its genome within capsid via reverse transcription of viral pregenomic (pg) RNA by its own polymerase (Pol). The Pol has four consecutive domains: the terminal protein (TP), a spacer (SP), the reverse transcriptase (RT), and the ribonuclease H (RH). Little is known about the structure of HBV Pol due to challenges in purifying full-length proteins for X-ray crystallography or cryo-EM analysis. In collaboration with a structural biologist at NIH, we utilized the AlphaFold program to predict the Pol structure, and identified two putative zinc-finger (ZF) motifs (Cys312-Cys341-His491-His495 and Cys323-Cys327-His468-Cys471) within the SP and RT domains, which are highly conversed among eight HBV genotypes and may play a role in regulating HBV reverse transcription. In this study, three point mutations of Pol (C312A, C323A, and C341A) were generated using the site-directed mutagenesis to disrupt the predicted ZFs. Next, we transfected wildtype and mutated HBV Pol plasmids separately into HepG2 cells along with a Pol-null HBV replicon plasmid. HBV total RNA, encapsidated pgRNA, HBV Pol and core proteins, and capsid DNA were assessed by northern blot, western blot, and Southern blot analyses, respectively. The results demonstrated that the three point mutations abolished pgRNA encapsidation and, consequently, hindered HBV DNA replication, indicating that the putative ZF motifs are crucial for HBV polymerase to mediate pgRNA encapsidation. Future study will be focused on investigating the site-specific and combinational effect of ZF residues on Pol-pgRNA binding, nucleocapsid formation, and reverse transcription, which will shed more light on the structure and function of Pol in HBV life cycle, as well as aid the development of novel antivirals.

Regulation of Tregs' lipid metabolism by APOC3

Scholars: Sulwe Kauffmann-Okoko*, Kamili Wiley*

High School: Winchester Thurston School, Pittsburgh, PA

PI of group: Dr. Alison Kohan

Mentors: Dr. Alison Kohan

Co-mentors: Dr. Apoorva Narain, Dr. Jitendra Kanshana

Site: Immunology and Cancer Immunotherapy (ICI)

Introduction: T-lymphocytes make one half of the immune system, contributing crucially to the host's defense mechanism. The two subtypes of T-lymphocytes CD4 and CD8 cells are primarily pro-inflammatory in nature. The only known/established anti-inflammatory subtype are regulatory T-cells (CD4+ CD25+ FOXP3+). Previous studies in our lab have shown that Tregs accumulate in the small intestine/colon of ApoC3tg (Apoc3 overexpression) and LDLr-/- (LDLr knockout) mice which protects them from colitis.
We hypothesize that in response to ApoC3 chylomicrons, Tregs become highly suppressive as they shift to intracellular lipid catabolic pathways.

Methods: Organs (spleen, liver, colon) and cardiac blood were collected from Apoc3 WT, ApoC3 Tg and ApoC3 k/o mice. Spleen was processed for isolation of CD4+ cells via MojoSort enrichment kit and natural Tregs (nTregs) via FACS. nTregs, liver and colon were then processed for quantitative RT-PCR (qRT-PCR). Plasma isolated from blood was subjected to triglyceride assay (TG assay). Trypan blue staining was performed for cell count.

Results: As expected the ApoC3 Tg mice had significantly higher triglyceride concentration. mRNA analysis interestingly showed increased expression of lipid receptors like LDRr, CD36 in the liver of Tg mice and almost negligible expression in nTregs. SRB1, another major receptor for lipid uptake, has expression levels opposite to CD36. LPL, the enzyme responsible for hydrolysing triglycerides, interestingly though, had increased expression in liver and colon of Tg mice. It was undetected in nTregs.

Conclusion: Tregs in the presence of excess triglycerides (hypertriglyceridemia) become more active by inhibiting their uptake from the extracellular pool. Increased LDLr , SRB1 and LPL expression indicate that clearly. Such Tregs rely more on their intracellular pool of lipids which are skewed towards fatty acid oxidation (FAO).

**equal contribution*

Microglial Responses to Electrode Insertion and Subsequent Low-Frequency Stimulation

Scholar: August Kollar

High School/College/City/State: Mt. Lebanon High School, Mt. Lebanon, PA

PI of group/lab: TK Kozai, PhD.

Mentor(s): Kevin Stieger

Site: TDX

Background: Implanting electrodes into the brain allows for both stimulating and recording the brain's activity. These implants can be used for both studying the electrical signals from the brain as well as controlling and treating specific conditions such as Parkinson's Disease, epilepsy, and depression. However, the electrode's effectiveness deteriorates over time due to natural immune responses in the brain, which cause scarring and inflammation at the site of the implantation. Microglia, a glial cell in the brain, influences this immune response, and therefore a better understanding of the microglia's behavior and response to electrode insertion will support treatments to help improve the longevity of implanted electrodes. Microglia commonly react to their environments using projections from their bodies, called processes, which can either extend or retract to interact with neurons to manage and support them. This study investigates both the potential relationship between the activity of microglia and its distance from the insertion site immediately following the electrode insertion, and the reactions of said microglia to intracortical microstimulation (ICMS) at 10 Hz during the acute phase of the injury (from the insertion of the electrode). We hypothesize that microglia closer to the electrode will conduct less surveillance, or analysis of surroundings, than those further from the electrode site.

Methods: We used a mouse model that expressed green fluorescent protein (GFP) in microglia. Michigan-style electrodes were implanted into the brains of these mice. The brains were analyzed for 1 hour and 40 minutes (20 minutes before ICMS, 1 hour ICMS, and 20 minutes after ICMS) the day of the electrode insertion (~ 1 hour after electrode insertion). The collected data was analyzed using user-drawn lines measuring magnitudes of extension and retraction occurring in processes for each microglia at each time point. These extensions and retractions were summed for each time point to obtain a measure of total surveillance, which we use to assess how much surveillance any microglia does during a specific period. 19 total microglia from 4 animals were analyzed in this study.

Results: Data suggests a positive relationship between the activity of individual microglia and its distance from the electrode insertion site during the acute phase of the injury. Microglia greater than ~250 μm away from the electrode, on average, had 12 to 18 more μm of total process movement than those closer to the electrode. No significant difference in process extension/retraction was identified between baseline and stimulation timepoints.

Conclusion: Our study suggests that microglia near the electrode insertion site are less active than microglia further away in the hours following insertion, which may be a result of microglia near the insertion site interacting with the wound or nearby neurons rather than surveilling their surroundings. More data may support significant differences in behavior between stimulation and baseline timepoints.

Title: Role of two-component regulators in Pseudomonas aeruginosa cytotoxicity to corneal cells

Scholar: Daniel R. Komlosi

High School/College/City/State: Pittsburgh Science and Technology Academy, Pittsburgh, PA

PI of group/lab: Dr. Robert Shanks

Mentor(s): Dr. Robert Shanks, Nicholas Stella, Rachel Calvario, Dhara Patel, and Sonya Mumper

Site: Department of Ophthalmology

Introduction: Pseudomonas aeruginosa is a ubiquitous, gram-negative, bacterial species that can cause disease in plants, animals, and humans. Pseudomonas infections are a serious risk for cystic fibrosis patients and also cause a severe vision threatening infection known as keratitis. P. aeruginosa requires virulence factors, such as toxins to cause infection and how the bacteria turns on expression of these in response to the ocular environment is poorly understood. Two component transcriptional response regulator systems (TCS) are stimulus-response coupling mechanisms that allow organisms to sense environmental stimuli and respond to it through a series of kinase reactions, resulting in a transcriptional response. Pseudomonas aeruginosa rely on these systems to survive and proliferate. In fact, some TCS have been proven to control virulence factors, so understanding how they work could lead to virulence suppression. P. aeruginosa has over 60 TCSs, and the role of most of these in virulence has not been established.

Hypothesis: Two component regulator systems (TCS) regulate pathogenesis to human epithelial cells (HCLE).

Purpose: The goal of this study was to find a TCS mutant strain of Pseudomonas aeruginosa that showed higher and lower virulence levels.

Methods: We compiled an array of distinct TCS mutants of P. aeruginosa onto a 96-well plate to test for virulence. A cytotoxicity assay, repeated for multiple trials, with cellular respiration detection (PrestoBlue), was done to evaluate the virulence of each strain. We used the wild-type strain PA14 as a positive control, and no bacteria (blank) as a negative control. Additionally, wells were stained with crystal violet as a secondary qualitative evaluation of cell virulence/HCLE monolayer status.

Results: Certain TCS mutant strains exhibited slightly increased and majorly decreased levels of cytotoxicity to human cells. Indicating a positive or negative role for the TCS genes in controlling virulence. Certain wells showed a decreased level of virulence, meaning that some change in the genome inhibited its potency.

Conclusion: The data collected support the hypothesis that some TCS are necessary for virulence to corneal epithelial cells. However, more detailed follow-up analysis is warranted.

Investigation of TCR epitope cognate pairs to determine SABR quantitative capabilities

Ryan Krishna, Dr. Sanya Arshad, Dr. Alok Joglekar
University of Connecticut, Storrs, CT; University of Pittsburgh Hillman Cancer Center Academy, Pittsburgh PA

Abstract: In this project, three specific epitopes, OVA-SR SQAVHAAHAEINEAGR, OVA-IA ISQAVHAAHAEINEA, and OVA-IE ISQAVHAAHAEINE with known affinity to OTII TCR were presented to the OTII TCR in a Signaling and Antigen-presenting Bifunctional Receptor (SABR) screen with a library of epitopes in order to determine if SABR screens can produce semi-quantitative results.

Introduction: SABRs allow for the recognition of cognate TCR peptideMHC (p-MHC) pairs. SABRs present antigens in the form of a pMHC complex and induce intracellular signaling via a TCR like signal upon binding with a cognate TCR (Joglekar et al. 2019). The SABR serves as the signaling domain for MHC molecules; when an antigen is successfully recognised by the TCR, the SABR releases a signal that allows for TCR antigen discovery. Studies on the OT II TCR revealed the existence of at least three distinct CD4+ T cell epitopes within OVA323–339 a DO11.10 and OT-II T cells recognize the same C-terminal epitope spanning amino acids 329–337 (Robertson et al. 2000). Determining if the known values match with the values produced by the SABR demonstrate the validity of using SABRs as a technique to measure TCR antigen recognition.

Methods: The first step in the SABR cloning process is a SABR Backbone Digestion which is done by restriction digestion with BSMB (enzyme) followed by a gel extraction. This step gives a plasmid which has a signaling domain and an MHC alpha and beta domain and is encoded with a portion which can be utilized to insert any epitope of interest based on MHC restriction. Epitopes are encoded into oligos and synthesized commercially. The oligos are annealed and ligated into the digested SABR backbone. This is followed by Cloning and Transformation protocols which amplify and clone the plasmids provided in bacterial colonies of Escherichia coli. The colonies are inoculated in LB and grown overnight in a 37 °C shaker incubator. A miniprep using the Zyppy Miniprep kit (Zymo) is done to extract the plasmid DNA from the bacterial culture. The plasmids are sent for Sanger sequencing to check for the correct insert of the epitope. Following this step, lentiviral packaging plasmid vectors are used to package the SABRs and a transfection is done in 293T cells, followed by harvesting lentivirus 48 hours post transfection. The cells of interest (NFAT GFP Jurkat) are transduced with the filtered LV, and G-418 is added to the transduced cells 24 hours later. A transduction check (TD) check is performed on the SABR expressing cells to check functionality of the SABRs, and the efficiency of the previous step. Following the transduction check, a co-incubation assay is performed in which our TCRs are co-incubated with a single SABR. The epitope is potentially recognised when the expression of both Green Fluorescent Protein and CD69 are present in a flow cytometry plot.

Discussion: An important property of a T cell function is the avidity with which its TCR recognizes the epitope. Determining if SABRs can be used for semi-quantitative readout of a TCR- peptide MHC interaction will be an important demonstration. Screens done with OTII TCR against an I-Ab restricted SABR library with analogues of OVA epitope show different enrichment scores (ES) in the screen results. Already published data shows the range of concentrations of the peptides corresponding to the epitopes that we included in the SABR library. Based on our results we suggest that we can use ES in a SABR screen as a direct, semi-quantitative readout of the strength of binding. This data is important for the development of antigen-guided immunotherapies; targeted therapies are able to be produced with higher efficiency due to knowledge about what antigens are recognised most effectively by different TCRs.

Results: Due to the length of time the process takes, the results are unknown as of yet. It is hypothesized that the SABR technique will produce quantifiable values that resemble, or perhaps match the provided values for the OTII TCR. With similar testing for other known TCR epitope cognate pairs, SABR could be proven as a method of quantifiably identifying the level at which different TCRs identify antigens.

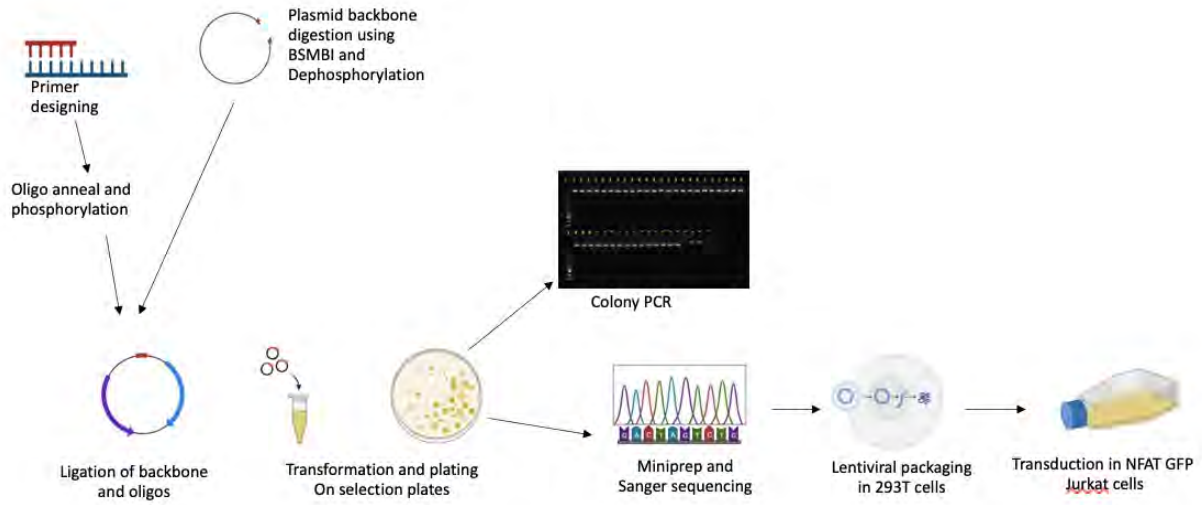

Figure 1. Workflow of SABR Cloning

References

1. Joglekar, A. V., Leonard, M. T., Jeppson, J. D., Swift, M., Li, G., Wong, S., Peng, S., Zaretsky, J. M., Heath, J. R., Ribas, A., Bethune, M. T., & Baltimore, D. (2019). T cell antigen discovery via Signaling and Antigen presenting Bifunctional Receptors. *Nature Methods*, *16*(2), 191–198.
2. Jennifer M. Robertson, Peter E. Jensen, Brian D. Evavold; DO11.10 and OT-II T Cells Recognize a C-Terminal Ovalbumin 323–339 Epitope1. J Immunol 1 May 2000; 164 (9): 4706–4712.

Targeting tumor cells via SNAP SNIPR system

Scholar: Ruby Krotine
Lab: Jason Lohmueller, Ph.D.
Mentor: Avani Parikh
Site: Immunology and Cancer Immunotherapy

Background: Chimeric antigen receptor (CAR) T cells have emerged as a key player in cellular immunotherapy being used to treat various forms of lymphomas, myelomas, and leukemias. A new form of CAR called synthetic notch (synNotch) is designed to bind to specific antigens on cancer cells and release a transcription factor to turn on a therapeutic gene. Our lab previously constructed a universal synNotch receptor that can target various antigens by antibody adaptors. Though this system shows robust activity in a cell line, it showed limited activity in primary human T cells. Recently an improved system of synNotch called SyNthetic Intramembrane Proteolysis Receptor (SNIPR) was reported, and to improve on the universal SNAP system we sought to engineer and test a SNAP-SNIPR system.

Methods: 1) Isothermal assembly cloning was used to add a DNA encoding the SNAP-SNIPR gene into a lentiviral vector backbone. The backbone underwent restriction enzyme digestion and was isolated by gel electrophoresis and gel extraction. 2) Lentivirus was produced via transfection into HEK 293-T cells. 3) Virus was transduced into Jurkat cells using polybrene, and transduction efficiency was measured using flow cytometry.

Results: Cloning of the SNAP-SNIPR construct was successful, as the control bacterial transformation (backbone only) had no colonies while SNAP-SNIPR (backbone and insert) had >100, and the construct was confirmed by DNA sequencing. Production of control SNAP-synNotch lentivirus and transduction of Jurkat cells was successful showing efficient receptor expression.

Conclusion: The SNAP-SNIPR construct was successfully cloned and control viruses and cell lines for the SNAP-synNotch system were generated. As a part of future directions, the new plasmid will be used to generate virus, and activity of SNAP-SNIPR will be compared to SNAP-synNotch.

Exploring the effect of extracellular vesicles effect on matrix metalloproteinases in aortic smooth muscle cells

Scholar: Jade Lee
High School: Westview High School, San Diego, CA
Lab: Justin Weinbaum, PhD
Mentor: Ande Marini
Site: Tech Drive X

Introduction: Abdominal aortic aneurysms (AAAs) are enlargements of the aorta located in the abdomen. The aorta can expand until it ruptures, causing life-threatening internal bleeding. AAA is only treatable by open surgery or endovascular repair, and there is currently no preventive treatment. AAA is caused by the destruction of the extracellular matrix (ECM), a key structural component of the aortic wall. Matrix metalloproteinases (MMPs) have been associated with this destruction, as MMP2 and MMP9 are increased in the walls of AAA and are known for their ability to degrade components of the ECM. We focused on using regenerative signals from adipose-derived mesenchymal stem cells and applying these signals on aortic smooth muscle cells (SMCs). These regenerative signals are carried in extracellular vesicles (EVs) and can help to potentially generate new or prevent degradation of the ECM. We hypothesized that these EVs will decrease the activity of MMP2 and MMP9 in aortic SMCs.

Methods: We compared MMP activity in SMCs with and without EV treatment. The cells were seeded in a fibrin gel construct (3D) or plated on tissue culture plastic (2D), then treated with EVs. The conditioned cell media was collected on Day 3. Expression of MMP2 and MMP9 were measured using gelatin zymography. The four groups analyzed were EV treated SMCs (n=3), control SMCs (n=3), EVs alone (n=1), and non-conditioned media (n=1). Following gel electrophoretic separation, the gel was washed in a 2.5% Triton X-100 solution and then incubated at 37°C in a Ca^{2+} and Zn^{2+} containing buffer for 18 hours. The gel was stained with Coomassie Brilliant Blue, then destained with 15% ethanol and 7.5% acetic acid solution. The gelatinase bands appeared white on a blue background. The bands were then quantified using Fiji software.

Results: SMCs seeded in fibrin gels (3D) did not show any significant differences in MMP activity between those with EV treatment and those without. The SMCs plated on the tissue culture plastic (2D) showed more activity for pro-MMP9, MMP9, and pro-MMP2when treated with EVs than controls (pro-MMP9: 2523 ± 202.0 pixels vs. 1200 ± 493.2 pixels, $p = 0.013$; MMP9: 716.8 ± 28.03 pixels vs. 392.0 ± 140.3 pixels, $p = 0.017$; pro-MMP2: 22720 ± 1919 pixels vs. 16911± 3065 pixels, $p = 0.050$). The EV negative control also had pro-MMP2 activity.

Conclusion: While no significant differences in MMP activity were observed in SMCs seeded in fibrin gels (3D) with or without EV treatment, SMCs plated on tissue culture plastic (2D) showed increased activity of pro-MMP9, MMP9, and pro-MMP2 when treated with EVs. These findings suggest that the fibrin gel could be preventing the EVs from reaching and thus treating the SMCs.

Future Directions: Future studies could explore optimizing the delivery and dosing of EVs to the SMCs in the fibrin gels. Additionally, EVs could be characterized for a better understanding of their regenerative contents.

Title: CGRP & Anti-tumor Immunity: How the sensory neurotransmitter aids in the progression of head and neck cancer.

Scholar: Tian LeGrande

High School/College/City/State: Oakland Catholic High School, 2023 / Carnegie Mellon University, Pittsburgh, PA, 2027

PI of group/lab: Nicole Scheff, Ph.D

Mentor(s): Megan Atherton, Nicole Scheff, Ph.D

Site: Cancer Biology

Background: Head and neck squamous cell carcinoma (HNSCC) patients suffer from severe pain and high recurrence rates. Recurrent HNSCC patients often receive immunotherapy to bolster their anti-tumor immune response; however, response rates remain very low. Calcitonin gene-related peptide (CGRP), a sensory neurotransmitter released during cancer pain, was recently implicated in tumor progression. We hypothesize that CGRP, when released from sensory neurons in the tumor microenvironment, activates tumors cells directly, driving release of immunosuppressive proteins, transforming growth factor beta (TGFβ) and programmed cell death ligand 1 (PD-L1).

Methods: To measure the impact of CGRP release on tumor progression, a capsaicin drinking water assay in an orthotopic oral cancer model was used to stimulate sensory neuronal activation (CGRP release); tumor growth was measured weekly by caliper, and tumor-infiltrating immune cells were quantified by flow cytometry. Mouse oral cancer cell line (MOC2) was treated with 1nM-100nM CGRP and CGRP receptor antagonist (BIBN4096), and gene expression (*Tgfβ, Pd-l1)* was assessed using PCR. Scratch assays measured 1nM-100nM CGRP-induced changes in MOC2 wound healing.

Results: Tumor-bearing mice that received water containing sensory neuron-stimulator, capsaicin, had a 44.6% greater tumor size versus mice that received vehicle water. Additionally, cytometric analysis found a more immunosuppressive tumor microenvironment in the capsaicin mice (e.g. 66.5% decrease in cytotoxic CD8 T cells, 53.5% increase in M2 macrophages). *In vitro*, CGRP treatment in MOC2 cells did not induce significant changes in the relative expression of immunosuppressive genes, *Pd-l1* and *Tgfβ*. Scratch analysis in MOC2 cells found that 1nM CGRP was associated with a 35.3% increase in wound healing ability.

Conclusion: These results show that CGRP release in the oral cavity can increase tumor growth and decrease anti-tumor immunity; however, this effect is unlikely to be caused by direct activation of tumor cells. Future directions will investigate CGRP's impact directly on immune cells.

Differential Gene Expression Analysis on Tumors of Black and White Women with TNBC

Abril Linares Mendoza[1], Dr. David Boone, PhD[2]
[1]Shady Side Academy, Pittsburgh, PA; [2]University of Pittsburgh, Pittsburgh, PA

Abstract *Previous studies demonstrate that Black women are more commonly affected by triple-negative breast cancer (TNBC) than White women. However, it is unclear if there are outcome or gene expression differences based on race within TNBC. Here we show through RNA sequencing analysis of The Cancer Genome Atlas (TCGA) data that there are differences in expression of TNBC tumors based on race. Further, survival analysis suggests Black women with TNBC have lower overall survival than White women with TNBC.*

Introduction In the US, 264,000 women are affected by breast cancer yearly, making it the second most common type of cancer for women[1]. Although progress in understanding and treating different molecular subtypes of breast cancer has been made over the past two decades, therapies are still limited for triple-negative breast cancer, which is the most aggressive subtype[2]. TNBC is defined by the lack of expression of estrogen, progesterone, and HER2 receptors. Prior studies have established that Black women are more likely to get TNBC than White women. Furthermore, Black women with TNBC have lower survival compared to other races. The objective of this study was to determine if there are differences in gene expression between the tumors of White and Black women with TNBC, which could help understand the biology of the tumors and explore possible alternative therapies.

Methods Publicly available RNA sequencing and clinical data from 1247 breast cancer patients within TCGA were downloaded from the XENA browser[3]. R (v.4.3.1) was used for data cleaning and analysis. GGPlot2 was used to create all figures. Survival analysis was performed using the R Survival package. Differential expression analysis was performed with DESeq2 (v.1.40.2) on raw transcript counts of reanalyzed TCGA data between 55 TNBC tumors from Black women and 98 TNBC tumors from White women[3]. A chi-squared test was performed to determine if there was an enrichment of tumor stage based on race. The effect of tumor stage was regressed in the differential expression analysis by using the ~stage + race formula in DESeq2.

Results Survival analysis within the TCGA cohort suggests Black women with TNBC have lower overall survival than White women (Figure 1) with TNBC. The chi-squared test also confirmed that the TNBC tumors from Black women were enriched for higher tumor stage (Figure 2) than White women. However, even when controlling for tumor stage, differential expression analysis of reanalyzed RNAseq data with DESeq2 demonstrates gene expression differences by race (x number of genes upregulated and y number downregulated; FDR<0.001, |FC|>=2, median TPM>=1) as shown in the volcano in Figure 3. However, gene expression alone cannot explain all of the differences as clustering was weak by race but even weaker by tumor stage.

Discussion Here we showed that Black women have worse clinical outcomes than White women even within TNBC. Pathway analyses will be performed on the differentially expressed genes and the highlighted genes in the volcano plot will be examined to provide insight into the biological differences based on race with the hopes of identifying new clinical targets. Additionally, genetic and epigenetic differences within TNBC by race will be examined.

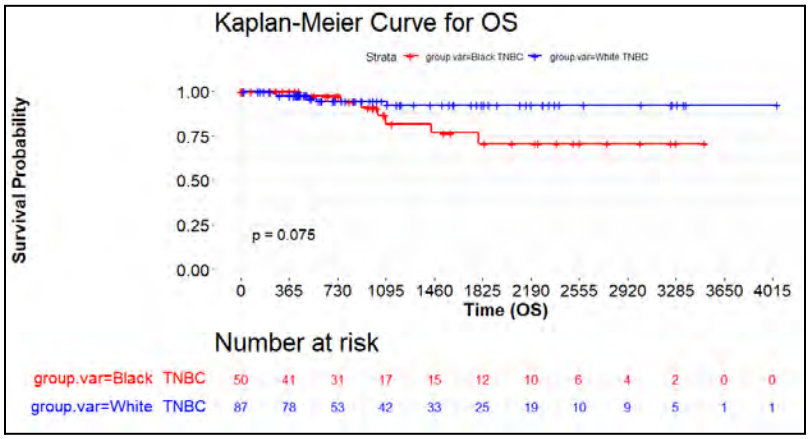

Figure 1. Kaplan-Meier curve for overall survival of TNBC patients of two races.

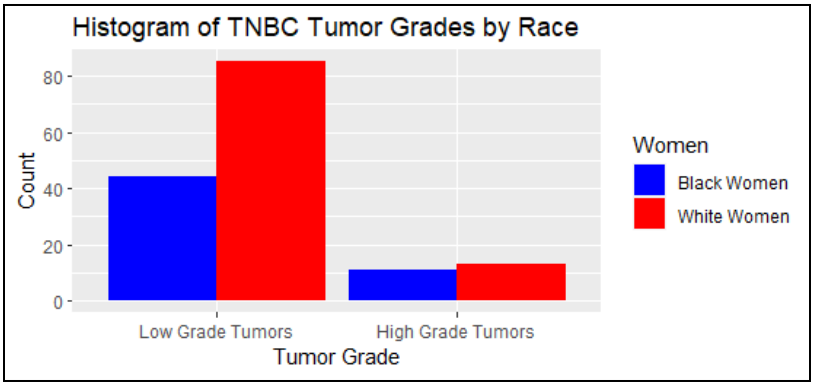

Figure 2. Histogram of the tumor grades for White and Black patients. P-value for the chi-squared test was 0.39.

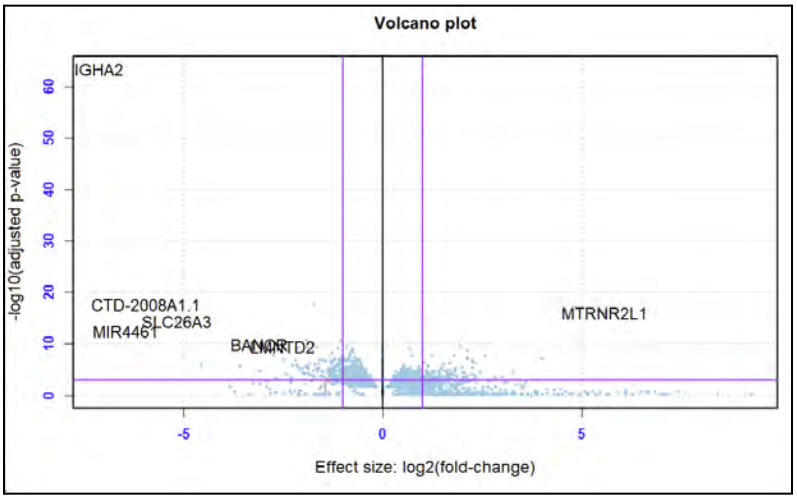

Figure 3. A volcano plot showing significantly differentially expressed genes.

References

1. Centers for Disease Control and Prevention. “Basic Information About Breast Cancer” https://www.cdc.gov/cancer/breast/basic_info/index.htm
2. Siddharth S, Sharma D. Racial Disparity and Triple-Negative Breast Cancer in African-American Women: A Multifaceted Affair between Obesity, Biology, and Socioeconomic Determinants. Cancers (Basel). 2018 Dec 14;10(12):514. doi: 10.3390/cancers10120514. PMID: 30558195; PMCID: PMC6316530.
3. Vivian, J., Rao, A. A., Nothaft, F. A., Ketchum, C., Armstrong, J., Novak, A., … Paten, B. (2017). Toil enables reproducible, open source, big biomedical data analyses. Nature Biotechnology, 35(4), 314–316. http://doi.org/10.1038/nbt.3772

Methods for structure classification in a computational model of the actomyosin cortex

Ian Lisien[1], Sommer Anjum[2], Lance Davidson, PhD[2]

Pittsburgh Science and Technology Academy, Pittsburgh, Pennsylvania, USA[1]; Department of Bioengineering, University of Pittsburgh, Pittsburgh, Pennsylvania, USA[2]

Abstract

In prior research, *in silico* models were employed to investigate the dynamics of the actomyosin cortex[1,2]. We improve upon the efficiency and modularity of an actin-myosin interactions model via an object-oriented approach. A novel technique is developed for the detection, classification, and quantification of cortical structures and their properties within the model. The enhanced efficiency and objective analysis of computational representations of the actomyosin cortex may offer a steadier foundation for future development of multicellular cytoskeletal models.

Introduction

Development of multicellular structures during embryogenesis is controlled in large part by cellular cortices, which allow for cells to generate forces in response to extracellular tension. Cortices are highly dynamic structures consisting primarily of filamentous (actin) and motor (myosin) proteins which interact to produce force. Understanding the complexities of these interactions presents significant challenges due to the emergent nature of cortical force production. To overcome these complexities and gain insights into underlying mechanisms, computational models provide a quantitative and systematic framework for investigating the dynamics of the actin-myosin cortex in parallel with continued experimental data collection. While computational models of actomyosin dynamics have been successfully pursued in the past, reorganization and continued improvement of these models is necessary to allow for additional insights to be drawn on the single cell scale and in future multicellular pursuits. Additionally, while previous studies have demonstrated methods for measurement of cortex force production and subjective identification of the localization of actomyosin structures, the ability to objectively classify and localize cortical structures has not been particularly well developed.

Methods

To improve performance and usability, a previously designed computational model of actomyosin cortex dynamics is rewritten in the Julia programming language and optimized for performance and modularity via a conversion from a primarily matrix-based to a primarily object-oriented data manipulation scheme. Kernel density estimation (KDE) is used to obtain a map of actin filament end / myosin motor densities in the cell which can be used to identify the center points of actomyosin structures. Points in the cell with high myosin density are likely to be centers of asters, where the barbed ends of actin filaments – which bound myosin motors move towards – are grouped to a central point, whereas opposite pointed ends face radially outward (see Figure 2a-b). Points in the cell with notably low barbed end / myosin density are likely to be the centers of rings, in which actin filaments conform to an ellipse in which pointed ends tend towards the center (see Figure 1a-b). Analysis of the mean densities of radially broadcasted slices about these points allows for confirmation of classification and measurement of structure radius.

Results/Discussion

Efforts to improve the performance of the actomyosin model described previously were successful, as the time to execute a 1000 timestep simulation decreased around tenfold (332 seconds to 34 seconds). In addition, analysis of mean radial density about points in the cortex has proved to be an adequate tool in the classification of cortical structures. These components may prove to be quite lucrative in the creation and analysis of future computational models of actin-myosin interactions both at single-cell and multi-cell scales. Results of these future computational studies – in parallel with *in vivo* and *in vitro* experiments – may yield a richer understanding of the complex nature of the cortex in force production and shed light on crucial aspects of embryogenesis.

Figure 1a.

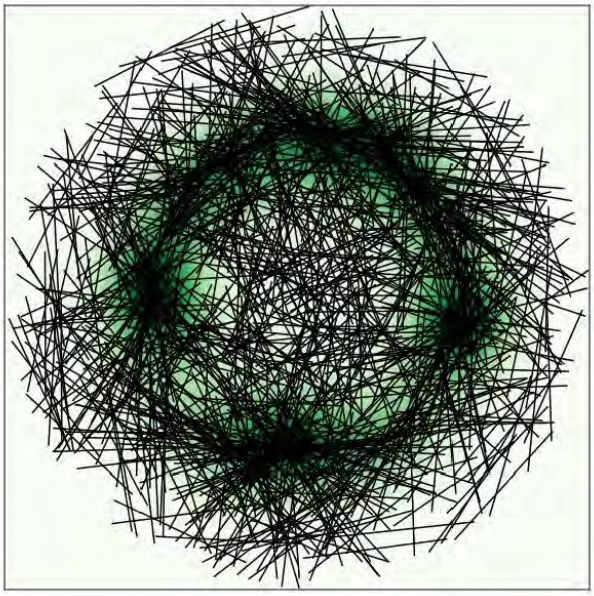

Figure 1b.

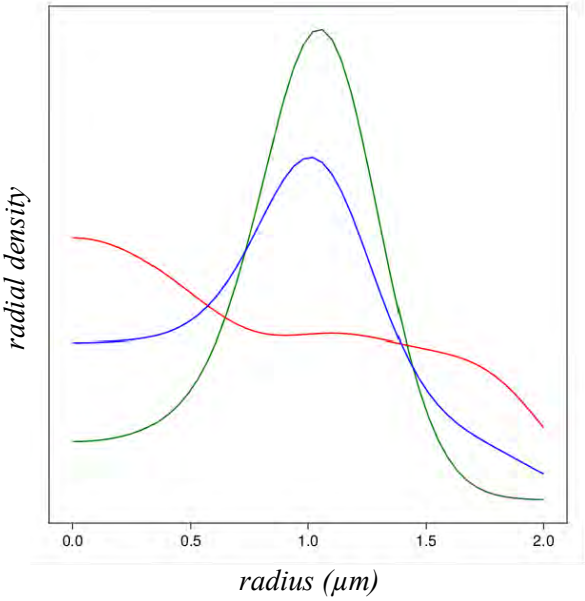

Actomyosin ring. – (a) Projections of actin filaments (black) over a KDE map of myosin concentrations. (b) Mean radial concentration of actin barbed ends (red), actin pointed ends (blue), and myosin (green) about the center of the ring.

Figure 2a.

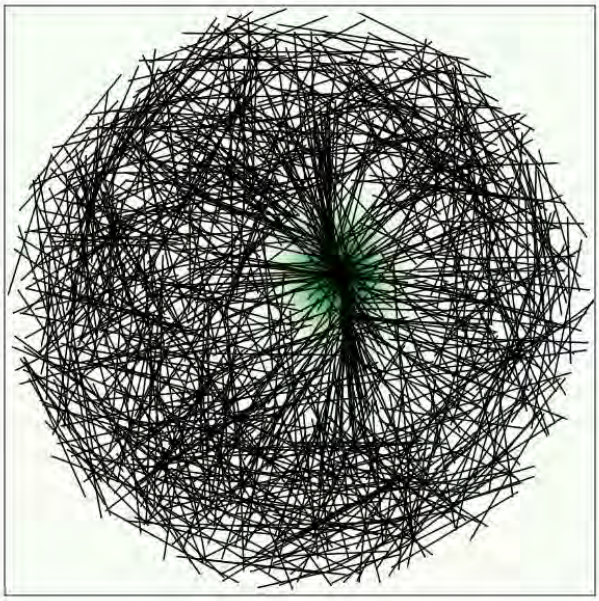

Figure 2b.

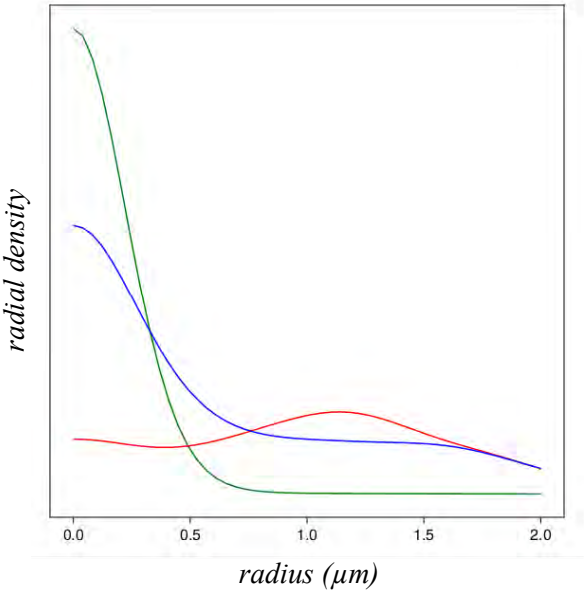

Actomyosin aster. – see Figures 1a. & 1b. for descriptions.

References

1. Chanet, S., Miller, C. J., Vaishnav, E. D., Ermentrout, B., Davidson, L. A., & Martin, A. C. (2017). Actomyosin meshwork mechanosensing enables tissue shape to orient cell force. Nature Communications, 8(1), 15014. https://doi.org/10.1038/ncomms150142. Miller CJ, *et al.*
2. Miller, C. J., Harris, D., Weaver, R., Ermentrout, G. B., & Davidson, L. A. (2018). Emergent mechanics of actomyosin drive punctuated contractions and shape network morphology in the cell cortex. PLOS Computational Biology, 14(9), e1006344. https://doi.org/10.1371/journal.pcbi.1006344

Changes in Colorectal Cancer Diagnosis Before and During the COVID-19 Pandemic in Western Pennsylvania

Scholar: Harry Littwin

High School: Fox Chapel Area High School, Fox Chapel Pennsylvania

PI: Dr. Kathryn Demanelis, PhD

Mentor: Dr. Kathryn Demanelis, PhD

Site: Cancer Biology

Background: The COVID-19 pandemic significantly impacted global healthcare, including colorectal cancer (CRC) screening, diagnosis, and treatment. Previous studies showed disruptions in screenings, leading to delayed diagnoses and poorer outcomes for CRC patients. This analysis aimed to assess the pandemic's impact on CRC diagnosis and time to treatment in Western Pennsylvania

Method: We collected all invasive CRC diagnoses (January 1, 2018-December 31, 2020) from the UPMC Network Cancer Registry. Patient groups in 2020 vs. 2018-2019 were compared using Mann-Whitney U test for continuous variables or Fisher exact for categorical variables. Variables examined included age, gender, stage at diagnosis, time to first treatment, etc. Analyses were performed using RStudio, and joinpoint regression was used to evaluate trends of weekly diagnoses within each year.

Results: There were 828 and 854 diagnoses in 2018 and 2019, respectively. In 2020, 752 cases were diagnosed, 9.2%, and 11.9% lower than in 2018 and 2019, respectively. In 2020, 61.3% of patients diagnosed were over 65 years old compared to 59.6% in 2018-2019 ($p=0.04$), and the percentage of late-stage diagnoses increased to 76.5% from 73.5% in 2018-2019 ($p=0.04$). Joinpoint regression showed no trend in diagnoses by week for 2018 and 2019. In 2020, diagnoses per week decreased by 17% from March to mid-April ($p=0.10$) during the initial lockdown, then increased by 4% per week ($p < 0.001$) from mid-April to the end of September, followed by a 5% decrease per week ($p < 0.001$) from the end of September to December, reflecting the impact of the alpha-wave of the COVID-19 pandemic.

Conclusion: COVID-19 impacted CRC diagnosis in western Pennsylvania in 2020, with fewer cases observed. The pandemic affected the timing of diagnoses and possibly the stage at diagnosis. Future research should include 2021 data, examine racial and socioeconomic disparities, and evaluate changes in cancer screening during the pandemic.

Streamlining the Process of Imaging Multiple Tissue Samples with Visible-light Optical Coherence Tomography

Scholar: Jason Ma

School: North Allegheny Senior High School

Lab: Pi Lab

Mentor: Dr. Shaohua Pi

Site: Ophthalmology (OPT)

Background: Optical Coherence Tomography (OCT) is a technology that can non-invasively provide a high resolution, 3-dimensional image. These images can assist in the diagnosis and management of numerous eye diseases such as glaucoma and age-related macular degeneration. Traditional OCT utilizes light in the near-infrared spectrum, however recent advancements in light-producing technologies have allowed for the development of Visible-light OCT (Vis-OCT). Vis-OCT improves imaging resolution by utilizing light with shorter wavelengths, and allows for unique imaging of tissues that absorb different spectrums of light. The current Vis-OCT system of the Pi Lab lacked an automated system to move a tray of tissue samples and instead required the user to physically move the tray. This was both time-consuming and lacked precision.

Methods: A suitable mini CNC (Computer Numerical Control) Machine was purchased online and assembled. A caliper was used to measure both the dimensions of the tissue sample tray and the distance between screw holes in the CNC Machine. These measurements were used to create a 3D model of a tray that would hold the tissue sample tray and screw into the CNC Machine with the 3D CAD software *SOLIDWORKS*. The model was then printed with a 3D printer and screwed into the CNC Machine. In order to integrate the controller of the CNC Machine with the imaging software of the Vis-OCT system, a separate digital controller was programmed in *LabVIEW*.

Results: The precision of a CNC Machine combined with the customizability of the programmed digital *LabVIEW* controller results in a faster and more precise system to both scan different locations of a single tissue sample, as well as shifting between wells of different tissue samples.

Future Directions: A machine learning algorithm could be developed to automate the imaging of all tissue samples in a tray.

https://www.ncbi.nlm.nih.gov/pmc/articles/PMC5745673/

Exploring the Effects of Congenital Heart Disease on Brain MRI Registration

Jose Maldonado[1] , William Reynolds[2] , Joy Roy[2] , Rafael Ceschin, PhD[2] , Ashok Panigrahy, MD[3], [1]Sewickley Academy, Sewickley, PA; [2]Department of Biomedical Informatics, University of Pittsburgh, Pittsburgh, PA; [3]Department of Radiology, Children's Hospital of Pittsburgh, Pittsburgh, PA

Abstract

Congenital Heart Disease (CHD) patients can have neurocognitive abnormalities. To study differences between CHD and control neurodevelopment, we observed patterns between CHD and control brain MRI registration similarity measures between a fetal and neonatal scan. Our study found patients with CHD have deviations from neurodevelopmental trends. We observed that CHD similarity scores had weaker correlations with fetal age and time duration between the scans than control similarity scores.

Introduction

Congenital Heart Disease (CHD) is a birth defect characterized by structural heart abnormalities, and has been shown to be associated with downstream neurodevelopmental problems[1]. Brain image registration is the process of geometrically aligning one image onto another and is a common step in neuroimaging analyses performed to compare images. The registration correlation ratio measures how similar two images are during the registration process. This study aims to explore how neurodevelopment differs between CHDs and controls by comparing registration performance across fetal and neonatal time points between CHDs and controls. We hypothesize that differences in registration between CHD and control can be indicative of abnormal brain growth.

Methods

To remove non-brain tissue, both fetal and neonatal images were skullstripped. The fetal brains were then linearly registered onto the neonatal image using FSL's FLIRT algorithm[2]. The FLIRT registration's cost function, the correlation ratio, was used as a similarity score to quantify the similarity of the brain between time points. We recorded the subjects and their correlation ratio values, along with their ages at scanning, and the time duration between the two scans. We then analyzed how their age at the time of scanning and the time duration between the two scans correlated with the similarity score using Pearson Correlation Coefficients. Finally, a Mann-Whitney U was performed to examine the differences between the CHD and Control distributions.

Results

69 subjects were included in this study. Two subjects were excluded due to their neonatal age being greater than one year at scan time. Of the remaining 67 subjects, there were 19 CHD and 48 control subjects. According to the Mann-Whitney U, the difference between the CHDs and the controls in relation to their similarity score was not statistically significant. In the controls, the time duration between the two scans had a strong, negative correlation with the similarity score, as the Pearson $r = -0.53$ with a p-value < 0.01. In the CHDs, the time duration between the two scans did not have a statistically significant correlation. In the controls, the fetal gestational age (GA) had a strong, positive correlation with the similarity score, as the Pearson $r = 0.61$ with a p-value < 0.01. In the CHDs, the fetal GA did not have a statistically significant correlation with the similarity score (Fig. 1).

Discussion

For the control group, the similarity measure between the fetal and neonatal scan had a positive correlation to the fetal GA and negative correlation to the time duration between the scans. In contrast, for the CHD group, the similarity measure between the scans did not have statistically significant correlations to the fetal GA and time duration. The fetal brain develops faster than the neonatal brain, which may explain the increased similarity between older fetal brains and their neonatal counterparts in controls. Similarly, there are substantial structural brain changes over time during neurodevelopment which can explain why the similarity decreased across longer time durations within controls. In contrast, the characteristic high variability in neurodevelopment among CHD patients can explain why CHD similarity scores did not have a significant correlation across time[3]. While these results require further validation with more data, they offer a data driven comparison of structural neurodevelopment over time in CHDs and control patients. Future studies will control for variables such as scan time and demographics as these can differ between CHD and controls due to social determinants of health and difficulties in study recruitment.

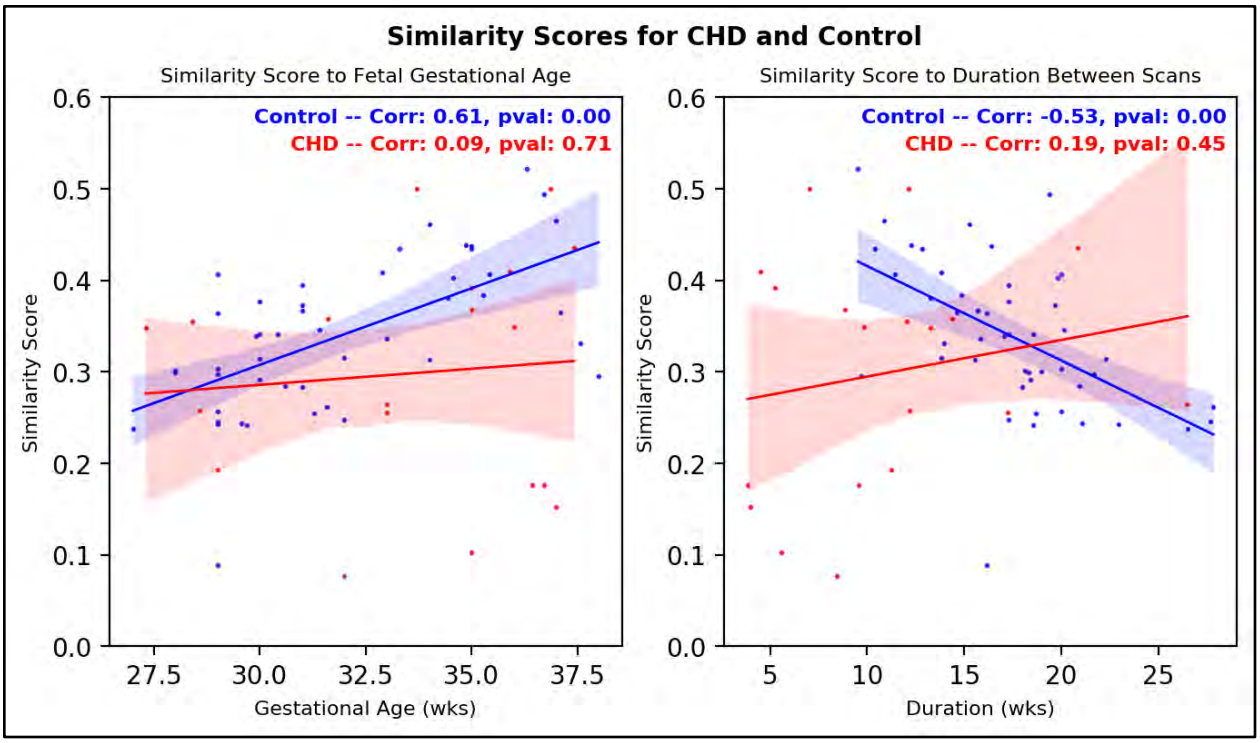

Figure 1. Control patients display a positive correlation between similarity score and fetal gestational age and a negative correlation between similarity score and duration between scans. There were no statistically significant correlations among CHD patients. The shaded region represents the 95% confidence interval. CHD patients show larger confidence intervals than control subjects.

References

1. Panigrahy A, Lee V, Ceschin R, Zuccoli G, Beluk N, Khalifa O, Votava-Smith JK, DeBrunner M, Munoz R, Domnina Y, Morell V, Wearden P, Sanchez De Toledo J, Devine W, Zahid M, Lo CW. Brain Dysplasia Associated with Ciliary Dysfunction in Infants with Congenital Heart Disease. J Pediatr. 2016 Nov;178:141-148.e1. doi: 10.1016/j.jpeds.2016.07.041. Epub 2016 Aug 26. PMID: 27574995; PMCID: PMC5085835.
2. Jenkinson, M., Bannister, P., Brady, J. M. and Smith, S. M. Improved Optimisation for the Robust and Accurate Linear Registration and Motion Correction of Brain Images. NeuroImage, 17(2), 825-841, 2002.
3. Morton PD, Ishibashi N, Jonas RA. Neurodevelopmental Abnormalities and Congenital Heart Disease: Insights Into Altered Brain Maturation. Circ Res. 2017 Mar 17;120(6):960-977. doi: 10.1161/CIRCRESAHA.116.309048. PMID: 28302742; PMCID: PMC5409515.

Title: What the Numbers Say: Depression, Anxiety and Suicide within Adolescents

Scholar: Trinidy Manison

High School/College/City/State: Uprep Milliones

PI of group/lab: Dr. Ana Radovic

Mentor(s): Gabriel Quinteros

Site: CoSBBI

The rate of depression, anxiety, and suicide within adolescents has growing rapidly for years. This study examines the statistics surrounding mental health in kids and implements possible solutions for adolescents struggling with mental illness, such as depression and anxiety, with a main focus on suicidality.

In 2020 suicide was the 2nd leading cause of death for children aged 10-14. That same year also saw a worldwide 28% increase in depressive symptoms and a 25% increase in anxiety likely due to effects of the COVID-19 pandemic. Locally, n Pennsylvania, the teen suicide rate is 8.2 per 100,000, which makes it 36th in the nation and nearly 20% of high school students report serious thoughts of suicide.

SOVA (Supporting Our Valued Adolescents) is a resource provided by the University of Pittsburgh to all adolescents but with a special focus on those from underserved groups (BIPOC, LGBTQ+) that helps prevent mental health problems and also provides support to those already struggling with mental illness. SOVA provides resources such as mental health articles that assist in regulating emotions as well as crisis support to anonymous users. .We distributed SOVA resources across Allegheny County giving 3+ presentations to rooms of 40+ students surrounding mental health and giving advice for better mental tips with the idea that hearing from peers might increase engagement..We found an increase in user activity of SOVA resources within underrepresented youth in Pittsburgh suggesting an increase in exposure to mental health care that we hope will have positive impact on mental health statics in our community.

Targeting Metabolic Pathways in MET-driven Non-small-cell Lung Cancer to Treat Brain Metastases

Scholar: Leviticus McGraw-Sapp
University: The University of Pennsylvania, Philadelphia, Pennsylvania, 19104
Lab: Timothy F. Burns, MD, PhD
Mentor(s): Vinod Kumar, PhD, Laura Stabile, PhD
Site: Cancer Biology

Background: Non-small-cell lung cancer (NSCLC) has the greatest incidence of brain metastases (BM) among all solid tumors with roughly 40% of those diagnosed with NSCLC developing BM during the course of their disease. The development of BM is associated with a poor prognosis and to date, no BM-specific targeted therapies exist. MET is a receptor tyrosine kinase that upon binding to its ligand, hepatocyte growth factor (HGF), controls key signaling pathways responsible for tumorigenesis. We have found that *MET* amplification is significantly enriched in lung adenocarcinoma BM and MET amplified BM have a unique upregulation of glycolysis and oxidative phosphorylation compared to non-*MET* amplified lung adenocarcinoma BM.

Hypothesis: *MET* altered NSCLC will be uniquely sensitive to glycolytic inhibitors and these inhibitors will be effective in MET TKI resistant cell lines.

Methods: Human *MET* altered NSCLC cell lines H596, H1993, and H1993-crizotinib resistant cells were treated with increasing doses of metabolic inhibitors in the absence or presence of a MET TKI. A CellTiter-Glo Luminescent Cell Viability Assay was used to assess the amount of ATP, allowing for a determination of cell viability.

Results: In H596 cells, drugs that inhibited glycolytic enzymes yielded a lower IC50 than those that inhibited downstream and parallel metabolic pathways. In H596 cells, inhibiting glycolytic enzymes in combination with MET was not synergistic. Interestingly, glycolytic inhibitors were effective in a cell line with acquired resistance to MET inhibitors. We are currently testing the ability of these inhibitors to synergize with MET TKIs and determine if MET TKI resistant cell lines are sensitive to other metabolic pathways inhibitors.

Conclusion: MET altered cell lines including those that have acquired resistance to MET inhibitors remain sensitive to glycolytic and other metabolic inhibitors. This may be an effective therapeutic strategy for treating *MET* altered NSCLC with *de novo* or acquired resistance.

Caenorhabditis elegans Drp1 Knockouts stress responses to assess cellular functions

Scholar: Addison McLane

High School: Seneca Valley Senior High School, Harmony, PA

PI: Nadine Hempel, PhD

Mentor: Sierra White, PhD

Site: Women's Cancer Research Center

Background: Mitochondria are an organelle that are responsible for multiple jobs within the cell, including energy production and cell death regulation, and are essential for proper cellular function and survival. Drp1 is a cytosolic protein which facilitates fission of the mitochondria. The shape and size of the mitochondria is linked to its function and regulation, therefore Drp1 is an essential protein. Splice variants of Drp1 exist that localize to different areas within the cell and seem to differently affect fission capacity, which is why different variants of the protein may impact mitochondrial functions. The splice variants that are of interest to my project are those relating to exons 16 and 17. Patients with ovarian cancer containing high levels of Drp1 that lacks exon 16 have a significantly decreased survival rate. The absence of exon 16 decreases fission and enhances proliferation. We would like to further our understanding about what mechanisms the different Drp1 splice variants control. My project will assess different stress effects on *C. elegans* (as model organisms) without Drp1 and investigate how the absence of this protein affects their development.

Methods: cDNA (complimentary DNA) from both groups were run in a gel to verify the knockout gene. Drp1 knockout *C. elegans* and control N2 *C. elegans* were treated with varying stressors, including heat shock in an incubator, cold tolerance in a refrigerator, and sodium azide agar plates. Survival assays were conducted after each experiment to assess the impact on each group by counting the dead vs. live worms, and progeny if applicable.

Results: When exposed to 37°C heat for 2 hours, the Drp1 knockout worms had a much higher mortality rate than the N2 wildtypes. Worms treated with sodium azide for 1 hour prior to heat exposure, however, had a significantly increased survival rate, especially for the Drp1 knockouts. When exposed to 4°C cold for 24 hours, the N2 wildtypes had a nearly complete mortality rate, as opposed to the Drp1 knockouts which had insignificant death.

Conclusion: Drp1 knockout in *C. elegans* differently impacts stress responses. Specific splice variants will be added to the knockout background to determine the impact of the specific splice variants on mitochondrial function.

Title: Analysis of the anti-tumor mechanism of vitamin C.

Scholar: Arya Mehta

High School/College/City/State: North Allegheny Senior High School, Pittsburgh, PA

PI of group/lab: Dr. Zarour

Mentor(s): Dr. Zarour and Dr. Tanegashima

Site: ICI

Abstract: Vitamin C has been proven to exert inhibitory effect on the tumor growth both directly and by modulating immune cells. In this experiment, the direct effect of vitamin C on cancer cells and the effect of vitamin C on immune cells were investigated using mouse cell lines and splenocytes, respectively.

Introduction: It has been reported that tumor growth is inhibited by high-dose administration of vitamin C in mouse models; however, the underlying mechanism of this inhibition remains unclear. Vitamin C has been shown to directly target tumor cells carrying BRAF and KRAS mutations[1)]. Additionally, it has also been reported that high-dose vitamin C stimulate T cells and macrophages, promoting their infiltration into tumors and enhancing the efficacy of anti-PD-1 antibodies[2,3)]. Our study aims to elucidate whether vitamin C attacks cancer cells directly or achieves its effects through the activation of immune cells.

Methods: Mouse cell lines CT26 (colon cancer) and Yummer1.7 (melanoma) were incubated for 48 hours in stepwise dilutions of vitamin C at concentration of 0, $1x10^{-3}$, $1x10^{-2}$, $1x10^{-1}$, and 1 mM. Subsequently, cell apoptosis was evaluated by flow cytometry. Additionally, splenocytes obtained from BALB/c mice, which were treated with either water or high dose vitamin C after inoculation with CT26 tumor cells, were stimulated with PMA/ionomycin and the cytokine-producing capacity of T cells was compared by flow cytometry.

Results: Vitamin C treatment above 10^{-2} mM for 48 hours induced apoptosis in CT26 and Yummer1.7 cells, but not at concentrations of 10^{-1} mM, compared to the vitamin C-naive control group. Analysis of the cytokine-producing capacity of splenocytes is currently underway.

Discussion: Vitamin C has been demonstrated to exhibit selective killing activity against human colorectal cancers carrying KRAS and BRAF mutations through the inhibition of glyceraldehyde 3-phosphate dehydrogenase (GAPDH). The findings in this experiment provide evidence that vitamin C also exerts a killing effect on CT26 murine colorectal cancer cells with KRAS mutations and Yummer1.7 murine melanoma cells with BRAF mutations. Further analysis is currently underway to determine whether high-dose vitamin C administration increases T cell cytotoxic function in the spleen of mice.

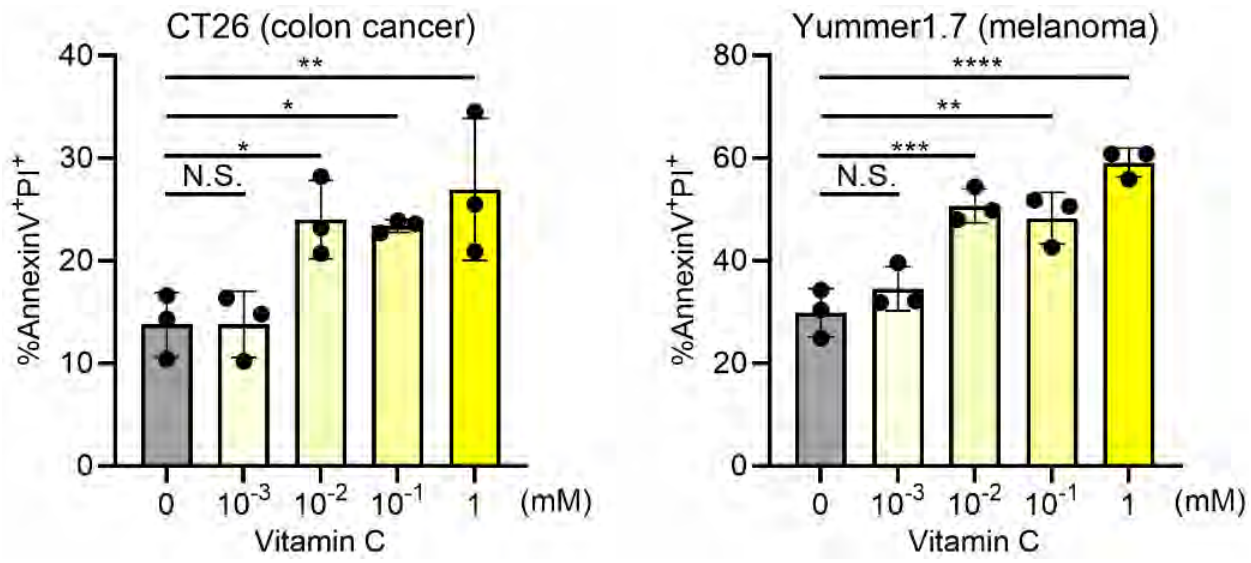

Figure 1. Vitamin C induces tumor cells to apoptosis.

Cell apoptosis assay in the presence of indicated concentration of vitamin C for 48 hours. One-way ANOVA with Dunnett's posttest. *$P < 0.05$, **$P < 0.01$, ***$P < 0.001$, ****$P < 0.0001$, n = 3.

References

1. Yun J, Mullarky E, Lu C, et al. Vitamin C selectively kills KRAS and BRAF mutant colorectal cancer cells by targeting GAPDH. Science. 2015;350(6266):1391-1396.

2. Magrì A, Germano G, Lorenzato A, et al. High-dose vitamin C enhances cancer immunotherapy. Sci Transl Med. 2020;12(532):eaay8707.

3. Luchtel RA, Bhagat T, Pradhan K, et al. High-dose ascorbic acid synergizes with anti-PD1 in a lymphoma mouse model. Proc Natl Acad Sci U S A. 2020;117(3):1666-1677.

Pharmacological Activation of IRE1-XBP1s ER UPR for Host-directed Anti-coronaviral Therapeutic Development

Scholar: Tabo Mkandawire

High School: North Allegheny Senior High School, Wexford, PA

PI of Lab: Yuan Liu, PhD

Mentors: Aine Boudreau; Travis Lear, PhD

Site: Tech Drive X

Viral infection leads to proteotoxic stress and an accumulation of unfolded proteins in the endoplasmic reticulum (ER). One major cellular response is to activate the unfolded protein response (UPR) in the ER, a signaling network that restores ER proteostasis by utilizing three major pathways. One branch, through the inositol-requiring enzyme 1 α (IRE1), produces XBP1s, a transcription factor that activates genes to adapt to the ER folding capacity requirement. To maintain cellular homeostasis, XBP1s levels are expected to increase in response to the early stage of viral infection; however, its protein levels decrease with the progression of infection. This study seeks to characterize the virally induced, time-dependent changes in XBP1s protein level and subcellular localization during infection. Airway epithelial cell lines stably expressing EGFP-tagged XBP1s were infected with the human coronavirus OC43 for 0, 4, 8, 24, 48, or 72 hours. Cells were then subjected to imaging for XBP1s-EGFP or counterstained with phalloidin and Hoechst for High Content Imaging of XBP1s localization. Human wildtype airway epithelial cells BEAS-2B were likewise infected, then analyzed by immunoblotting with anti-XBP1 antibodies to measure endogenous XBP1s protein levels. Additionally, cells were fractionated to analyze the XBP1 signal in cytosolic and nuclear compartments through immunoblotting. Results show that both nuclear XBP1s protein levels and total XBP1s levels decrease during infection. These observations demonstrate that there is a virus-induced dysregulation in XBP1 protein levels and localization during infection. Specifically, the virus may be utilizing this dysfunction to evade the UPR's efforts to maintain cellular proteostasis. Future research efforts will continue to explore the mechanism by which XBP1s protein levels decline and translocate during viral infection. Additionally, the study will investigate the possible role of a small molecule ubiquitin E3 ligase inhibitor that prevents XBP1s protein degradation and a subsequent reduction of viral load in cells.

Title: Unraveling the Impact of CD44 on NK Cell Function in Head and Neck Squamous Cell Carcinoma

Audrey Monro-Neely[1,2,3] , Lazar Vujanovic[1,3] and Robert L. Ferris[1,3]
UPMC Hillman Cancer Center; Pittsburgh PA
Hillman Summer Academy; Pittsburgh, PA
Department of Otolaryngology, University of Pittsburgh; Pittsburgh PA

Natural Killer (NK) cells are effector cells of the innate immunity that are integral players in tumor immunosurveillance. NK cell activation states are intricately regulated by a balance between activating and inhibitory receptors. One potential receptor that may mold NK cell activity is CD44. It has been found to be involved in their development, homing, and functional regulation. CD44 expression was reported to be essential for NK cell differentiation from progenitor cells and for their subsequent maturation and functionality. In the context of immune response regulation, galectin-9 engagement with CD44 was reported to the decrease NK cell activity. Our preliminary studies confirm that galectin-9 suppresses proliferative and cytotoxic potential of NK cells. In the context of head and neck squamous cell carcinoma (HNSCC), CD44 emerges as one of the top differentially enriched genes in tumor-infiltrating versus circulating NK cells. Flow cytometric analyses reveal that CD44 expression is common on NK cells, however that CD44 levels are decreased on tumor-infiltrating versus circulating NK cells. In vitro studies show that CD44 expression is upregulated on NK cells in response to high-dose IL-2 activation, which suggests that CD44 expression may be a marker of NK cell activation. Further research is needed to decipher whether reduced CD44 expression on tumor-infiltrating NK cells correlates with impaired effector functions and if the galectin-9-CD44 interaction contributes to NK cell immunosuppression.

Works Cited

B;, Parkin J;Cohen. “An Overview of the Immune System.” *Lancet (London, England)*, U.S. National Library of Medicine, pubmed.ncbi.nlm.nih.gov/11403834/.

CA;, Sague SL;Tato C;Puré E;Hunter. “The Regulation and Activation of CD44 by Natural Killer (NK) Cells and Its Role in the Production of IFN-Gamma.” *Journal of Interferon & Cytokine Research : the Official Journal of the International Society for Interferon and Cytokine Research*, U.S. National Library of Medicine, pubmed.ncbi.nlm.nih.gov/15153314/.

Delves, Peter J, et al. *Roitts Essential Immunology*. Wiley Blackwell, 2018.

Dong J;Cheng L;Zhao M;Pan X;Feng Z;Wang D; “Tim-3-Expressing Macrophages Are Functionally Suppressed and Expanded in Oral Squamous Cell Carcinoma Due to Virus-Induced Gal-9 Expression.” *Tumour Biology : the Journal of the International Society for Oncodevelopmental Biology and Medicine*, U.S. National Library of Medicine, pubmed.ncbi.nlm.nih.gov/28466780/.

“Home - PMC - NCBI.” *National Center for Biotechnology Information*, U.S. National Library of Medicine, www.ncbi.nlm.nih.gov/pmc/.

I;, Chen DS;Mellman. “Oncology Meets Immunology: the Cancer-Immunity Cycle.” *Immunity*, U.S. National Library of Medicine, pubmed.ncbi.nlm.nih.gov/23890059/.

Wu C;Thalhamer T;Franca RF;Xiao S;Wang C;Hotta C;Zhu C;Hirashima M;Anderson AC;Kuchroo VK; “Galectin-9-CD44 Interaction Enhances Stability and Function of Adaptive Regulatory T Cells.” *Immunity*, U.S. National Library of Medicine, pubmed.ncbi.nlm.nih.gov/25065622/.

Incorporating Coevolutionary Information to PPI encodings for a Natural Language Processing Model used to predict if Protein-Protein Interactions are perturbed by Missense Mutations

Iliyan Nazarali[1], Prabal Chhibbar[2] , Alisa Omelchenko [3], Jane Siwek[4]
[1] Chestatee High School, GA, U.S.; [2,3,4] University of Pittsburgh, PA, U.S.

Abstract

Although protein sequences can be used for natural language processing (NLP) tasks, generating vocabulary for protein-protein interactions is a non-trivial task. We used Grantham score-based metric to encode protein sequences. To improve the NLP Model to better examine whether missense mutation perturb protein-protein interactions, we incorporated coevolution couplings scores along with normalised grantham scores using linear transformation. We used high performance computing to generate robust determiners of the accuracy of the NLP model: AUC curves.

Introduction

In the human body, we have many instances where proteins interact with one another like in a signalling pathway or during protein transport. In this project, we look specifically at an interaction between 2 proteins, also known as protein proteins interaction(PPI). Missense mutations, or a mutation that changes a single nucleotide, sometimes can perturb or disrupt the protein-protein interaction. The location of where the missense mutation occurs is important because disease associated alleles tend to be in the structural interface of the respective protein-protein interactions. In the past, labs have used more complex approaches to determine perturbation such as co-crystal PPI structures and biophysical properties. But, we have developed a way to use natural language processing to create embedding vectors to represent each protein-protein interaction. Protein embeddings have been shown to perform well for prediction tasks in comparison to other prediction methods. So, we can use these embeddings that represent a protein-protein interaction into a prediction model to determine if the interaction has been perturbed or affected.The central aim in this project is to improve the protein-protein encodings by incorporating coupling scores, to the protein-protein encodings. This will add additional evolutionary information between two proteins of which interacting residues have likely co-evolved with one another to improve our model.

Methods

A protein-protein interaction consists of a mutant and interactor sequence. We first began by taking a mutant window and cutting only the middle portion of the mutant window of k-not, the region of interest. We then took the mutant window and slid it across the interactor sequence and atevery alignment of the mutant window and interactor sequence, we calculated the delta grantham score, which is a variable that tells us how evolutionary similar two amino acids are to another as well as obtained coupling score, which is a score of how two protein of interacting residues likely coevolved. We then split the delta grantham score into k-mers and inputted those k-mers into a doc-2 vec natural language processing model, a two layer neural network that can be used for textual analysis. From the model, we generated embeddings which are numeric vector representations of every protein-protein interaction. We input those vectors into a XG boost classifier, tree classifier, which can then determine whether a protein-protein interaction is perturbed by a missense mutation or not. Using the grantham and coupling scores, we were able to perform a linear transformation: lambda * delta grantham (normalised between 0 and 1) + (1-lambda) * coevolutionary score to generate a new score that is likely more specific to how two proteins may have coevolved over time. Hyper Parameterization was utilised in that we ran trials varying different values in order to generate a score of 0.5 or higher. Using the results of 100 trials on 20 PPIs . We generated AUC curves as well.

Results and Conclusion

The current model that incorporates both grantham and coupling scores is where the grantham score is divided by 1000 and the coevolution score is multiplied by 10. This generates an median accuracy AUC score that is equivalent to the AUC score of a permuted data set with the model. A future direction is increased hyper parameterization and model fine tuning to determine if this model can better examine whether missense mutations perturb protein-protein interactions.

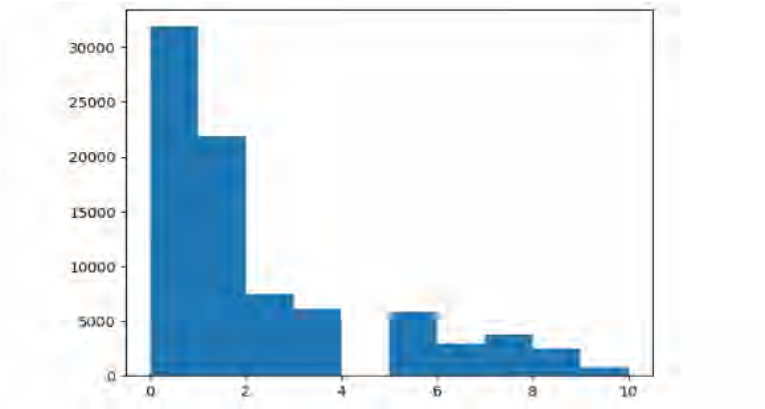

Figure 1: Distribution of total linear transformation score. Total score formula used is lambda * (delta grantham (normalized between 0 and 1) * 100) + (1-lambda) * coevolutionary score What I added was is total divided by 10

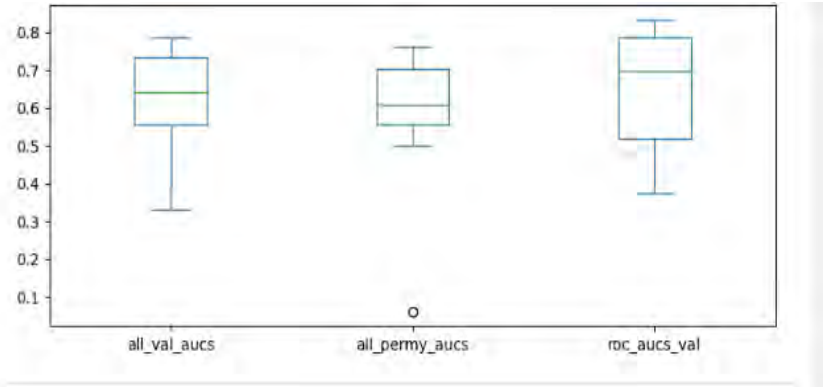

Figure 2: NLP model trained where grantham score divided by 1000

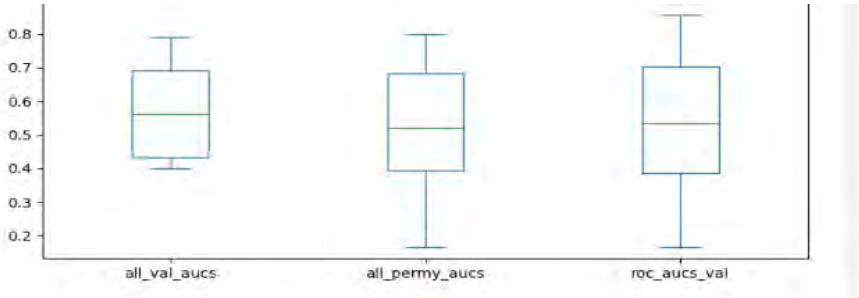

Figure 3: NLP model trained where coevolution score multiplied by 10

References

1. **Saambe seq citation- Li, G., Pahari, S., Murthy, A. K., Liang, S., Fragoza, R., Yu, H., & Alexov, E. (2021). SAAMBE-SEQ: a sequence-based method for predicting mutation effect on protein–protein binding affinity. *Bioinformatics*, *37*(7), 992-999.**
2. **Wang, X., Wei, X., Thijssen, B., Das, J., Lipkin, S. M., & Yu, H. (2012). Three-dimensional reconstruction of protein networks provides insight into human genetic disease. *Nature biotechnology*, *30*(2), 159-164.**
3. Sahni, N., Yi, S., Taipale, M., Bass, J. I. F., Coulombe-Huntington, J., Yang, F., ... & Vidal, M. (2015). Widespread macromolecular interaction perturbations in human genetic disorders. *Cell*, *161*(3), 647-660.
4. ev couplings -- Hopf, T. A., Green, A. G., Schubert, B., Mersmann, S., Schärfe, C. P., Ingraham, J. B., ... & Marks, D. S. (2019). The EVcouplings Python framework for coevolutionary sequence analysis. *Bioinformatics*, *35*(9), 1582-1584.

Investigating the Role of Mitochondrial Dysfunction in

Age-related Macular Degeneration

Scholar: Araina Nevels

High school: Propel Montour High School

Lab: Dr. John Ash

Mentor: Dr. John Ash

Site: OPT (Ophthalmology)

Background: Mitochondrial dysfunction is instrumental in the onset of numerous eye diseases, notably Age-related Macular Degeneration (AMD). A disorder prevalent among individuals aged 50 and above, AMD inflicts damage on the macula, vital for clear central vision. The Retinal Pigment Epithelium (RPE), a significant cell layer for visual function, experiences this impact severely. This study underscores the significance of mitochondrial dysfunction within the RPE as a contributing factor to AMD. As mitochondria balance reactive oxygen species (ROS) and antioxidants—normal byproducts of oxygen metabolism—their function can be compromised under stress conditions such as aging, environmental stressors, or disease, leading to excessive ROS, oxidative stress, and cellular damage. Here we designed a method to explore cellular damage through evaluating mitochondrial health.

Methods: Initially we are using Initially, we employed Human Corneal-Limbal Epithelial (HCLE) cells due to their large size and ease of cultivation. We cultured these cells in 10% FBS Dulbecco#39;s Modified Eagle Medium (DMEM) for 4 days at 37°C and 5% CO2.
Post-treatment with mitochondrial trackers and MitoSOX for 8 hours, the cells were fixed in 4% Paraformaldehyde (PFA) and assessed using a confocal microscope.

Results: We found most cells are green. Few cells exhibit red. The cell with red mitochondria appeared larger or longer, or sometimes manifested as red dots in one spot without revealing a cellular structure.

Conclusion: The majority of cells were healthy under normal conditions. Cells presenting a red coloration are likely undergoing oxidative stress, potentially leading to cell death associated with AMD. The enlarged appearance of these cells suggests possible mitophagy, where cells attempt to recycle dysfunctional mitochondria.

Title: Generating Mx2 Knockout Cell Clones for Studying Nuclear Import

Scholar: Oluwatobiloba Olaore

High School/College/City/State: Pittsburgh CAPA, Pittsburgh, PA

PI of group/lab: Melissa Kane, PhD

Mentor(s): Bailey Layish

Site: Immunology and Cancer Immunotherapy (ICI)

Background: Retroviruses such as human immunodeficiency virus (HIV-1) are a family of RNA viruses that reverse-transcribe their RNA into DNA and then have the unique ability to incorporate that DNA into the host genome. Lentiviruses, like HIV-1, are able to hijack certain nuclear import pathways to infect host cells. Studying nuclear import is important for understanding the mechanism by which these viruses infect cells. The nuclear pore complex (NPC) is located on the nuclear envelope and regulates which proteins enter and exit the nucleus. Mx2 is an interferon-stimulated antiviral protein that localizes to the NPC. Mx2 prevents HIV-1 from entering the nucleus and also blocks certain cellular proteins from entering the nucleus. For this study, we will use CRISPR/Cas9 technology to create knockout Mx2 cell lines and investigate how Mx2 regulates nuclear import and viral infection.

Methods: To generate Mx2 knockout HeLa and HT1080 cell lines, we used CRISPR/Cas9; gRNAs were designed to target the second exon of Mx2, which contains the start codon. Following dsDNA break formation by Cas9, the cells will repair the DNA using non-homologous end joining, resulting in a lack of Mx2 protein expression. To identify Mx2 knockout cell clones, we performed a western blot and probed with antibodies specific for Mx2. We then wanted to determine whether the cells were knockouts at a DNA level. PCR primers were designed to amplify the region where the guides cut to see if one or both guides successfully cut. The resulting bands were cut from an agarose gel, then purified and sequenced.

Results: Following an initial screen, 17 candidates were selected for follow-up. Six HeLa Mx2 knock-out candidates were screened using PCR and a second western, and, unfortunately, all six failed this follow-up screening and were expressing Mx2. Five HeLa Mx1 knock-out candidate clones are in the process of follow-up screening. After being confirmed by both PCR and western blot, one Mx2 knock-out HT1080 cell line, 30T.38, was determined to be a true knockout and its sequence has been verified. Further screening must be done to determine whether any other cell lines were successful knockouts.

Conclusion: We have successfully generated a Mx2 HT1080 knockout cell line and will continue to identify additional clones. These knockouts will eventually be used to help us determine how Mx2 affects nuclear import.

Title: The Exploration of the Activity of Calpain Released through the ABCA1 in Mast Cells

Scholar: Lea Omer

High School: Chartiers Valley High School

PI of Lab: Tina Sumpter PhD

Mentor: Tina Sumpter PhD

Site: Immunology and Cancer Immunotherapy

Mast cells (MCs) are white blood cells found in the connective tissue throughout the body. They release important inflammatory mediators and cytokines to fight foreign invaders. Unfortunately, these cells are also associated with inflammation due to autoimmune responses (allergies). The process of transmembrane transport has been discovered to release the protease calpain through the ABCA1 transporter. Historical laboratory data indicated that the calpain caused vascular leakage in vivo in mice. To confirm that it was the calpain's enzymatic activity causing this, a blue ear experiment was completed. Six mice were injected with Evan's blue dye then the treatments later. After being euthanized, biopsy punches of the ears were taken, and the optical density of the leakage in their ears was measured using a nanodrop machine. The results confirmed that calpain's enzymatic activity caused a significant amount of vascular leakage. To determine what calpain does to mast cells, MCs were isolated from the peritoneal cavities of two mice. The PMCs were grown for 21 days then treatments with varying amounts of calpain were given. Using flow cytometry avidin, CD117, LAMP1, and FCεRI were looked for as markers of degranulation. However, it is important to note that the LAMP1 stain did not work for the control, making this data unreliable. To conclude, calpain causes vascular leakage. It is not known what the calpain does to mast cells directly as it does not appear to cause degranulation.

Differential Expression Analysis of an Osteosarcoma Sequencing Dataset, consisting of differentially expressed gene list

Sara Pahlavan Tafti[1], Dr. Ines Lohse, PhD[2], Dr. Kurt R. Weiss, MD[2],
[1]North Allegheny Senior High School, Wexford, PA; [2]University of Pittsburgh Hillman Cancer Center Academy, Pittsburgh, PA

Abstract

In this project, we utilized an osteosarcoma sequencing dataset to analyze the gene expression in primary and metastatic osteosarcoma samples, aiming to identify potential signs of early detection, and risks for the disease. We used differential expression analysis to find gene expression patterns between the primary and metastatic groups. Key features were fold change and p-values, determining notable alterations. Multiple potential genes were identified, including 6-phosphofructo-2-kinase/fructose-2,6-biphosphatase 4 (PFKFB4) [1]. Further research based on this dataset will explore specific expressions in other osteosarcoma studies.

Introduction

Osteosarcoma is an aggressive bone cancer, and it's crucial to understand its molecular dynamics to determine potential signs of early detection and risks for the disease. Understanding the molecular disparities between primary and metastatic osteosarcoma is influential in interpreting underlying mechanisms of the disease's progression. This study investigates gene expression patterns in primary and metastatic osteosarcoma samples using differential expression analysis. Primary osteosarcoma arises in the bone, and its metastatic spread to distant sites, oftenly the lungs. The results are hoped to distinguish potential drug targets of genes that are associated with signs and risks of primary and metastatic osteosarcoma.

Methods

To obtain results, we focused on key aspects from the method of differential expression analysis. Firstly, gene expression refers to the use of genetic information for a gene's function. Once the gene expression data was obtained, we compared one experimental group vs. a second one (primary vs. metastatic) to find out which genes/transcripts have altered significantly. This is called differential expression analysis [2], in which we focused on the top 10 and bottom 10 genes in the dataset. Additionally, we considered the log2foldchange values derived from the dataset, which compares gene expression between primary and metastatic groups. A positive fold change value indicates increased expression, while a negative value change indicates decreased expression. Lastly, the p-value. When we analyzed the data, the p-value held values ≤ 0.05, indicating the observed difference in the result can be considered as a general rule.

Results

Among the top 10 genes with significant gene expression differences, 4 were previously associated with other cancers, shown in *Table I*. As these genes are in the top 10, their expression increased. In contrast, the bottom 10 genes resulted in limited associations with other cancer types, except for Claudin 18, shown in *Table II.* As these genes are in the bottom 10, their expression decreased. Moreover, all the surfactant genes in the dataset were found in the bottom 10 genes. Surfactant genes are lung-specific genes, which is the site of osteosarcoma metastasis [3].

Discussion

The differential expression analysis of an osteosarcoma sequencing dataset provided valuable insight into gene expression patterns associated with osteosarcoma progression. The top identified genes may hold potential as targets in the prevention of primary osteosarcoma progression, while the bottom genes may be targets in prevention of metastatic osteosarcoma progression. Differential expression analysis within this dataset will be further expanded to focus on gene expression patterns specifically in other osteosarcoma studies.

Table I. Top 10 identified genes

Gene	**Associated Cancer Type**
Thrombospondin 4 (THBS4)	Breast cancer
Matrix Metallopeptidase 9 (MMP9)	None
Cyclin dependent kinase inhibitor 1c (CDKN1C)	Sporadic cancers
Adrenomedullin (ADM)	None
Cellular Communication Network factor 4 (CCN4)	Colon tumors
Megakaryocyte-associated tyrosine kinase (MATK)	None
3-hydroxybutyrate dehydrogenase, type 1 (BDH1)	None
Heat Shock protein family A (HSPA1b)	None
5S Ribosomal Pseudogene 242 (RNA5SP242)	None
6-phosphofructo-2-kinase/fructose-2,6-biphosphatase 4 (PFKFB4)	Supports survival of cancer cells when oxygen is limited

Table II. Bottom 10 identified genes

Gene	Associated Cancer Type
Surfactant Protein D (SFTPD)	None
Solute Carrier family 34 member 2 (SLC34A2)	None
Claudin 18 (CLDN18)	Gastric cancer
Surfactant protein A2 (SFTPA2)	None
Complement component 4 binding protein alpha (C4BPA)	None
Surfactant protein B (SFTPB)	None
Surfactant Protein C (SFTPC)	None
Polymeric mmunoglobulin receptor (PIGR)	None
Surfactant Protein A1 (STFPA1)	None
Secretoglobin family 1A (SCGB1A1)	None

References

1. U.S. National Library of Medicine. (n.d.-j). Pfkfb4 6-phosphofructo-2-kinase/fructose-2,6-biphosphatase 4 [Homo Sapiens (human)] - gene - NCBI. National Center for Biotechnology Information.
2. Comparing experimental conditions: Differential Expression Analysis. Differential gene expression. (n.d.). https://biocorecrg.github.io/CRG_Bioinformatics_for_Biologists/differential_gene_expression.html
3. U.S. National Library of Medicine. (n.d.-h). SFTPD surfactant protein D [homo sapiens (human)] - gene - NCBI. National Center for Biotechnology Information. https://www.ncbi.nlm.nih.gov/gene/6441

Quantifying Subclavian Artery Compliance in Patients with Idiopathic Unilateral Vocal Fold Paralysis (iUVP)

Scholar: Arnav Patel
Mentor: Adam Forrest
Lab PI: Jonathan Vande Geest, Ph.D.
Site: Technology Drive

Background: The left recurrent laryngeal nerve (RLN) bifurcates off the vagus nerve, wraps around the aortic arch, and innervates the vocal folds. Idiopathic unilateral vocal fold paralysis (iUVP) occurs when the RLN is impaired causing vocal fold paralysis causing them to remain open, leaving the airway unprotected. This can lead to issues in swallowing, talking, and breathing. Previous research has shown that iUVP patiends had greater aortic arch compliance compared to individuals without iUVP; the subclavian artery branches off the aortic arch. Our goal is to find and compare the compliance of the subclavian artery using two different methods. The compliance measurements can then be used to draw comparisons between those with and without iUVP.

Methods: Gated MRI images from each patient are taken which synchronize MR data acquisition to the cardiac or respiratory cycles. A maximum intensity projection is compiled across all z-stacks and time. The user selects a region of interest (ROI) that correlates with the subclavian. The ROI is then binarized into 1mm voxels. Areas with the highest volume are kept with the rest being discarded. To gather the centerlines, three binarized, 2D planes are displayed from the top, middle, and bottom. Connecting the center of each of the planes, an estimated centerline is created. The subclavian is eventually 3D modeled over all time points using triangular patches. The diameter is then calculated using two methods. First, the normal vector from the bottom centerpoint and the top center point is caculated. The artery's diameter is found about the vector at the midpoint. Two more regions are selected(∓1mm) to find the diameter. They are ensuingly averaged into one. Second, the volume of the model is calculated, and using the length, the diameter is back calculated. Both diameter outputs along with the pressure pulse are then used to find the compliance of the artery.

Results: Eleven patients were tested without knowing whether they were iUVP positive. The average of the 3 region compliance was 0.0034 1/mmHg, and the average of the compliances from back calculating the volume was .0032 1/mmHg. A match-paired t-test was performed to determine if there was a statistical difference between the two methods of obtaining the compliance. The test yielded a t-statistic of -0.655 and a p-value of 0.5273. Using an alpha value of 0.05, it was determined that there is no statistical difference in compliance computing methods.

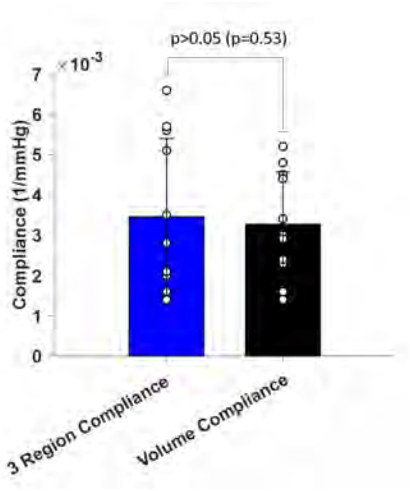

Conclusion: Now that the compliance of each patient has been calculated, the next step will be to unblind the study. Once it is known which patients have iUVP, a test will be run to see if the compliance of the subclavian correlates with iUVP.

Probabilistic Graphical Models Identify Transcriptomic and Clinical Markers of All-Cause Mortality in Moderate to Severe COPD

Name: Neil Porwal

Education: North Allegheny High School, Wexford, Pennsylvania

Mentor: Tyler Lovelace

Site: Computational Biology

Rationale: Chronic obstructive pulmonary disease (COPD) is a prevalent and life-threatening respiratory condition that is the third leading cause of mortality worldwide. While studies have identified clinical markers and biological pathways linked to COPD severity, the causal molecular mechanisms connecting transcriptomic profiles to disease outcomes are inadequately understood.

Question: Can probabilistic graphical models effectively identify transcriptomic and clinical markers associated with mortality in patients with moderate to severe COPD, and can these markers serve as reliable predictors of mortality risk?

Methods: The COPDGene study collected extensive clinical, imaging, and transcriptomic data on COPD patients (n=1037, GOLD stages II-IV). RNA-sequencing data was processed using DESeq2 and normalized with ComBat batch correction. Cell type proportions were estimated by InstaPrism bulk deconvolution. The multi-omic dataset was integrated for modeling. 10-fold cross-validation was implemented, partitioning data into training (90%) and test (10%) sets. Markov blanket graphs were learned on training data using Markov Blanket Graphical Models with stability selection for sparsity. The pcStable algorithm oriented edges via partial correlation, ignoring latent confounders and applying False Discovery Rate control to limit false positives. Elastic net Cox regression selected predictive features from the mortality blanket. Model performance was evaluated by concordance index and deviance on the test set. The pipeline was optimized over MGM algorithms, pcStable rules, and FDR thresholds to maximize prognostic power.

Results/Analysis: The models recovered biomarkers linked to mortality, serving as reliable predictors.

Conclusions: This demonstrates potential for early detection of high-risk patients by screening optimized transcriptomic and clinical markers, indicating precision medicine approaches may enable personalized risk stratification and treatment to improve COPD outcomes.

Body tissues affect lung cancer malignancy and tumor growth

Lucas Pu[1], David Wilson[2], Rajeev Dhupar[3]
[1]North Allegheny Senior High School, Wexford, PA
[2]Department of Medicine, University of Pittsburgh, Pittsburgh, PA
[3]Department of Cardiothoracic Surgery, University of Pittsburgh, Pittsburgh, PA

Abstract: *Identifying factors of lung tumor growth and malignancy can help forecast prognosis and personalize lung cancer screening and treatment. Body composition, which reflects one's long-term habits and lifestyle, may be an important prognostic factor. Correlation and multivariate logistic regression analysis were used to identify significant body composition characteristics. These characteristics can serve as novel biomarkers to facilitate the assessment of indeterminate pulmonary nodules (IPNs) detected in the screening setting.*

Introduction: Low-dose computed tomography (LDCT) lung screening is the only recommended lung cancer screening test. However, its high false-positive rate and the presence of indeterminate pulmonary nodules (IPNs) can lead to unnecessary and potentially harmful follow-up procedures such as PET scans and invasive biopsies. This not only exposes healthy patients to unnecessary radiation but is also worrisome for healthcare providers and anxiety-provoking for patients. As a result, it is desirable to identify new biomarkers that can aid in the evaluation of IPNs. We hypothesize that body tissues, which reflect one's long-term habits and lifestyle, may serve as a biomarker in assessing IPNs and aim to investigate the potential impacts of CT-derived body composition characteristics on lung cancer malignancy and tumor growth.

Methods: A cohort of 159 subjects (75 non-small cell lung cancer subjects) was created, including baseline and follow-up LDCT scans, patient demographics, and clinical information (e.g., tumor malignancy) of each subject. Each subject had undergone multiple LDCT lung cancer screenings and was found to have lung nodules on their baseline CT scans. The nodules identified on each CT scan were segmented, and their doubling time (DT) in days was calculated based on the modified Schwartz formula. Five different body tissues were also segmented, including skeleton muscle (SM), subcutaneous adipose tissue (SAT), visceral adipose tissue (VAT), intramuscular adipose tissue (IMAT), and bone. Their characteristics (e.g., volume and density in the Hounsfield unit) were then computed. The relative change (%) between the baseline and follow-up LDCT scans was also calculated for each body composition and tumor characteristic. Correlation and multivariate logistic regression (LR) analysis were used to identify body composition and tumor characteristics that were significantly associated ($p<0.05$) with VDT, relative tumor growth, and tumor malignancy (i.e., benign or malignant). Multicollinearity was tested, and the variables with a variance inflation factor (VIF) larger than 3.0 were removed. The LR models were evaluated through five-fold cross-validation using the Area Under the Receiver Operating Characteristic (AUC-ROC) curve as the performance metric.

Results: The identified CT-derived body composition features, including IMAT density, SM density, % IMAT volume, % IMAT density, and % SM density, were significantly associated ($p<0.05$) with % tumor growth metrics, but not with DT when analyzing all subjects. However, when analyzing only cancerous subjects, body tissue characteristics, including % SM density and % bone density, were significantly associated with DT. When analyzing only baseline LDCT scans, IMAT density, SM density, % VAT density, % IMAT volume, and % IMAT density were significantly associated with tumor malignancy. Given only baseline LDCT scans, these significant body tissues achieved an AUC of 0.735 (95% confidence interval (CI): 0.657-0.813) in predicting tumor malignancy, and significant tumor characteristics achieved an AUC of 0.780 (95% CI: 0.711-0.850). Combining both significant body tissue and tumor characteristics from only baseline LDCT scans increased the AUC to 0.831 (95% CI: 0.769-0.892). Given both baseline and follow-up LDCT scans, the combination of significant body tissue and tumor characteristics achieved an AUC of 0.968 (95% CI: 0.946-0.991), whereas using only significant tumor characteristics achieved an AUC of 0.963 (95% CI: 0.940-0.987) and using only significant body tissue characteristics achieved an AUC of 0.759 (95% CI: 0.684-0.834).

Discussion: Like tumor characteristics, body tissues are significant contributors to lung cancer malignancy and tumor growth. However, no associations were found between DT and tumor malignancy, indicating that DT may not be a good prognosis factor. When only baseline CT scans are available, body tissue characteristic is a significant predictor of tumor malignancy but is not significant when follow-up CT scans are also available. Further validation on an independent dataset would be beneficial. This is the first study to investigate the impacts of various CT-derived body tissues on tumor malignancy and growth. We believe that CT-derived body tissues can serve as a novel image biomarker to facilitate the assessment of IPNs.

References

1. Wilson, D. O., Ryan, A., Fuhrman, C., Schuchert, M., Shapiro, S., Siegfried, J. M., & Weissfeld, J. (2012). Doubling times and CT screen–detected lung cancers in the Pittsburgh Lung Screening Study. American journal of respiratory and critical care medicine, 185(1), 85–89. https://doi.org/10.1164/rccm.201107-1223OC
2. Aberle, D. R., DeMello, S., Berg, C. D., Black, W. C., Brewer, B., Church, T. R., Clingan, K. L., Duan, F., Fagerstrom, R. M., Gareen, I. F., Gatsonis, C. A., Gierada, D. S., Jain, A., Jones, G. C., Mahon, I., Marcus, P. M., Rathmell, J. M., Sicks, J., & National Lung Screening Trial Research Team (2013). Results of the two incidence screenings in the National Lung Screening Trial. The New England journal of medicine, 369(10), 920–931. https://doi.org/10.1056/NEJMoa1208962
3. Nitsche, L. J., Mukherjee, S., Cheruvu, K., Krabak, C., Rachala, R., Ratnakaram, K., Sharma, P., Singh, M., & Yendamuri, S. (2022). Exploring the Impact of the Obesity Paradox on Lung Cancer and Other Malignancies. Cancers, 14(6), 1440. https://doi.org/10.3390/cancers14061440

Investigating the role of IL-18 during Regulatory T cell fragility induction

Scholar: Lily Pulkowski
High School: Quaker Valley High School, Leetsdale Pennsylvania
Lab: Dario Vignali, PhD
Mentor: Ellen Scott
Site: Immunology and Cancer Immunotherapy

Background: Regulatory T cells are a part of the adaptive immune system and are identified by their master transcription factors Foxp3. Tregs suppress the immune system from fighting self cells, which is known as autoimmunity. It has been shown that depleting the entire body of Tregs will cause the immune system to kill cancer, but it will lead to lethal autoimmunity. Instead of completely depleting Tregs, labs have moved to inducing Treg fragility. In some cases Tregs will start making IFNg (an inflammatory cytokine) and lose their suppressive abilities. Cytokines such as IFNg, Il-12, and IL-18 can induce the production of IFNg driving Tregs fragility. The lab tested anti-CD40, which is known to induce IL-12, on mice to see if their Tregs would become fragile. This experiment showed that Tregs do become fragile after treatment of anti-CD40, but when repeated on mice that could not respond to IL-12 the results were the same. This experiment concluded that anti-CD40 induces a different cytokine, such as Il-18, that produces IFNg.

Methods: Spleens from three Wild Type mice are processed and their cells are plated. The cells are stimulated with 50 ng/mL of IL-12, IL-18, IFNg, and anti-CD40. The cells are incubated at37 C for three days. After three days the cells are collected and spun. After the samples are spun, the soupes are collected for an ELISA and the cell pellets are collected for Flow Cytometry. ELISA is run to quantify the levels of IFNg production. Flow Cytometry is run to determine if the Tregs have become fragile.

Results: The ELISA determined that IL-18 produces the most IFNg . Flow data showed that IFNg production, TBET presentation, and CXCR3 presentation increased with IL-18 stimulation (Tregs start showing fragility markers after IL-18). Nrp1 and Foxp3 markers remain stable through the cytokine stimulation which shows that the Tregs have not lost all function and become unstable.

Conclusion: Our experiment shows that IL-18 increases IFNg production in cells. Therefore it is promising that after treatment of anti-CD40, IL-18 is driving Tregs fragility by producing IFNg. In the future, repeat experiments will be done with sorting of only Tregs.

The Use of Digital Screening to Further Improve Intervention Methods for Aneurysms of the Ascending Aorta

Jibraan Rahman
Canton High School/Drexel University/Plymouth, MI
Dr.Maiti's lab
Dr. Spandan Maiti and Yamnesh Agrawal
CoSBBI

My project is motivated by the urgent need to improve the prevention strategies for Type A Aortic Dissection (TAAD), a highly lethal condition that affects the ascending aorta. Aneurysm of the ascending aorta is a primary risk factor. However, in current clinical practice, aortic aneurysms are typically not operated on until they reach a certain size. The current size for dissecting the aorta comes at over 5.5 centimeters. By the time for dissection, intervention can lead to be too invasive or stressful for the patient. Therefore, better prediction metrics are critical for better intervention in prophylactic aortic resection. This would hereby reduce the risk of TAAD for said patient. Previous work has revealed the importance of aortic biomechanics in predicting dissection risk. However, the unmet need is to evaluate patient-specific aortic biomechanics non-invasively from simple clinical datapoints. Specifically, the variations in biomechanical state of the aorta over the entire cardiac cycle is not well understood.
Towards that goal, my project will focus on constructing aortic geometries, amenable to biomechanical evaluation, from patient-specific 4D CT scans. I will utilize a set of software tools and programs, available at Maiti lab, to construct a series of geometries at different time points over the entire cardiac cycle. The goal was to complete at least one full 4D CT scan using these newly learned software and techniques. I have done some work in isolating the 3D model of the aorta, then using these scans to create a 4D CT scan model. In conclusion, my project endeavors to bridge the gap between clinical data and patient-specific aortic biomechanics, leveraging advanced technologies and cutting-edge research to revolutionize the prevention and intervention strategies for Type A Aortic Dissection. Through these efforts, we aspire to bring about a significant positive impact on patient care and contribute to the advancement of medical knowledge in the field of cardiovascular health.

The Effects of Electrical Stimulation on Young and Old Mouse Hippocampi
By: Narendra Ray, Adam Jasper, Amrita Sahu
Education: Canon McMillan High School, Canonsburg, PA
Site: Tech Drive X

Background:

The cognitive benefits of exercise are well-known[1]. With age, the ability to exercise becomes more difficult, creating the need for alternative forms of skeletal muscle stimulation[2]. Electrical stimulation (e-stim) involves electrical impulses being transmitted to the muscles, often used as a form of therapy or light exercise. The purpose of the study was to test if e-stim therapy in young and old mice led to greater volume and structural integrity in the brains, particularly the hippocampal regions, and if the age of the mice impacted the effects of e-stim. Volume and Quantitative anisotropy were calculated to determine of the structural integrity of the hippocampal sub regions.

Hypothesis:

I hypothesize that the e-stim therapy will lead to an increase in the volume and decrease in the quantitative anisotropy, indicating greater structural integrity, in hippocampus sub regions. The older mice will have a more profound response to the e-stim treatment.

I expect that Hematoxylin and Eosin (H&E) staining will provide qualitative confirmation for my hypothesis.

Methods:

The data was collected through both the use of a cryostat to collect samples of mice brains and the analysis of statistics of brains with DSI Studio. The cryostat data was collected by making fine slices of the brains of either 10 µm, 16 µm, 20 µm, or 30 µm. The samples were kept frozen before going through the H&E staining process which stains for nuclei and various other cellular components. Qualitative analysis of the stained sections was carried out to compare the effects of age, section size, and eosin exposure on integrity of the samples. Ultimately, a protocol was created to inform future H&E staining of brains specifically.

The DSI statistics were acquired with MRI scans of mice brains. A reconstruction effect was run on them, creating a 3d recreation of the entire brain. The hippocampal sub regions (dentate gyrus, CA1, CA3, and adj. entorhinal cortex) were then analyzed for volume and the pathways for quantitative anisotropy in Excel.

Another protocol was drafted to compute region and tract statistics for present and future analyses.

A python script was created to run a Mann-Whitney U Test on the data, testing the difference between the old and young E-stim and control mice. Mann-Whitney U Test functions similarly to a linear regression, but is made for underpowered data sets.

Results/Conclusion:

DSI results awaiting, one last batch of MRI scan files, conclusions to follow.

Histology analysis revealed better image quality and better protein exposure by halving the time spent in eosin during the staining protocol.

Analysis of age and slice thickness to be added.

References:

[1] Mandolesi L, Polverino A, Montuori S, et al. Effects of Physical Exercise on Cognitive Functioning and Wellbeing: Biological and Psychological Benefits. Front Psychol. 2018;9:509. Published 2018 Apr 27. doi:10.3389/fpsyg.2018.00509

[2] Langhammer B, Bergland A, Rydwik E. The Importance of Physical Activity Exercise among Older People. Biomed Res Int. 2018;2018:7856823. Published 2018 Dec 5. doi:10.1155/2018/7856823

Validation of the sequence alteration and affinity towards OT1-TCR in H2Kb bound SIINFEKL variants utilizing Signaling and Antigen-presenting Bifunctional Receptors

Parthiv Reddy Bandi, Venkata Krishna Kanth Makani, Ph.D., Alok Joglekar, Ph.D.
North Allegheny Senior High School, Wexford, PA; University of Pittsburgh Hillman Cancer Center Academy, Pittsburgh, PA

Abstract - *CD8+ T cells play an essential role in the immune system's ability to identify and eliminate tumors. Signaling and Antigen-presenting Bifunctional Receptors (SABR shown in Figure 1) is a powerful method to identify tumor antigens for T cell therapy. SABRs present epitopes to CD8+ T cells and induce an output of GFP and CD69 if they correspond. SABR libraries containing numerous epitopes coincubated with T cells result in a method that is rapid, adaptable, and practical for discovering antigens.*

Introduction - The ability of CD8+ T cells to identify and kill cancer cells is well-established and exploited by immunotherapies. However, finding the antigens of tumor-reactive T cells is difficult and confines immunotherapy. Current methods for TCR antigen discovery are either low-throughput or need prior knowledge of possible antigens. Tasking T cells to target neoantigens derived from tumor proteins can allow the body to fight back against tumors. SABR is a new method that can allow for identification of tumor antigens since there is a CD28 and a CD3ζ signaling output that activates when the cognate epitope and respective TCR match. Generating a SABR library from known or predicted antigens and screening them against TCR of interest allows for the quicker and accurate identification of the highly mutating antigens.

Methods - Upon interaction of the TCR to the epitope presented on SABRs, there is activation of the downstream NFAT signaling pathway containing a GFP reporter gene under the control of the NFAT promoter. Using retroviral vectors, the OT1 TCR was cloned and transduced into mCD8+ Jurkat cells. The SIINFEKL variants (N4, E1, G4, V4, Q4, T4) underwent a series of procedures beginning with their transformation and cloning in E.coli for plasmid production. Subsequently, a maxiprep procedure was employed to isolate and expand the plasmid. Moreover, these plasmids were transfected in HEK293T cells for lentiviral production and virus was used to transduce NFAT-GFP Jurkat cells. The following analysis involved subjecting the H2Kb SIINFEKL variants to a single SABR coincubation assay, allowing for the measurement and examination of the impact resulting from modifications in the amino acid sequence responsible for encoding SABRs.

Results - The success of the OT1 TCR in recognizing and signaling its corresponding antigen was demonstrated by the high transduction efficiency achieved. Additionally, the extraction and purification process of SIINFEKL variant plasmids from the E. coli bacteria was proven to be successful through an analysis conducted on the UV-Visible spectrophotometer. The expanded plasmids were used to transfect and trasduce the Jurkat cells with high transduction efficiency. Further, a single SABR coincubation assay was performed at 1:1 ratio with OT1 TCR in mCD8+ Jurkats and SIINFEKL variants in NFAT-GFP Jurkats. Notably, the positive control, PMA, further validated the ability of SABRs to be succesfully signal through the NFAT-GFP reporter upon activation. As depicted in Figure 2, the SIINFEKL variants exhibited varying percentages of cells displaying CD69 and GFP readout, highlighting their distinct response to the OT1 TCR.

Discussion - SABR technology is capable of efficiently screening thousands of epitopes in a single assay, without the need for prior knowledge of potential antigens or soluble TCRs. SABRs ability to succesfully read out the changes in the amino acid corealting to the alteration in the GFP/CD69+ population indicate the extended application of the system. By utilizing this platform, researchers can

identify both public and private antigens that are reactive toward tumors or pathogens, thereby facilitating the development of new immunotherapies.

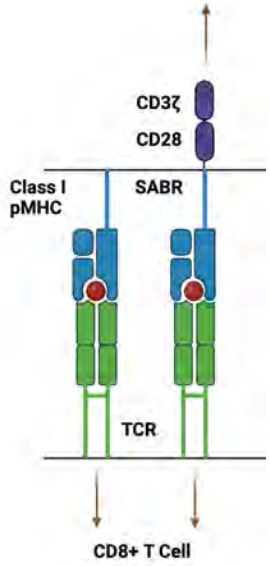

Figure 1: Schema demonstrating the structure of pMHC molecule and SABRs with costimulatory domains.

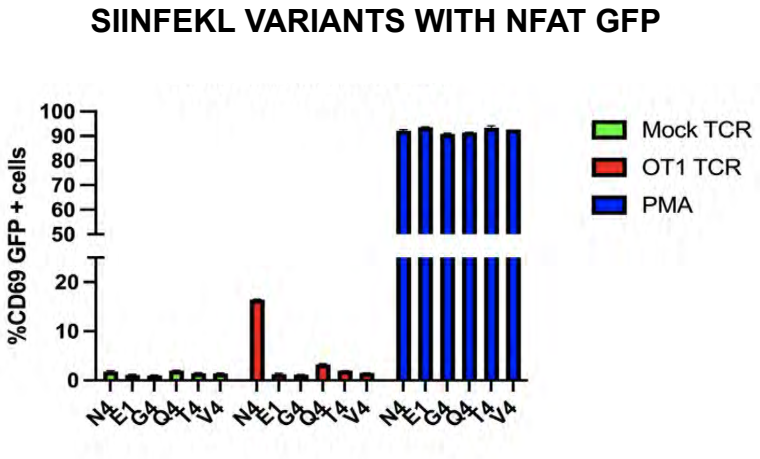

Figure 2: Plot depiciting the single SABR coincubation assay for the OT1 TCR containing mCD8+ Jurkats and SIINFEKL variants in NFAT-GFP Jurkat cells. Flow cytometry analysis of the GFP/CD69+ population clearly indicates the signaling is active only upon cognate epitope-TCR pairs.

References

1. Joglekar AV, Leonard MT, Jeppson JD, Swift M, Li G, Wong S, Peng S, Zaretsky JM, Heath JR, Ribas A, Bethune MT, Baltimore D. T cell antigen discovery via signaling and antigen-presenting bifunctional receptors. Nat Methods. 2019 Feb;16(2):191-198. doi: 10.1038/s41592-018-0304-8. Epub 2019 Jan 28. PMID: 30700902; PMCID: PMC6755906.
2. Alok Joglekar, Michael Leonard, John Jeppson et al. T cell antigen discovery using signaling and antigen presenting bifunctional receptors (SABRs), 13 May 2019, PROTOCOL (Version 1) available at Protocol Exchange [https://doi.org/10.1038/protex.2018.126]

TFAP2B as a biomarker for development and progression of Invasive Lobular Carcinoma

Scholar: Ny'Azia Roberts

High School: Woodland Hills High School

PI of group/lab: Lee/Oesterreich Lab

Mentor(s): Haley Arbore, Jagmohan Hooda, Steffi Oesterreich, Adrian Lee

Site: Women's Cancer Research Center

Background: Invasive lobular carcinoma (ILC) is responsible for 10%-15% of invasive breast cancers, and ILC is the second most common type of breast cancer after no special type breast cancers (NST). ILC is understudied and currently lacks appropriate research models for studying the disease. Currently patients with ILC are receiving the same types of treatment plans as those with NST and are having worse outcomes. Previous data from our lab showed that AP2B is the top differentially methylated (hypomethylated) gene in ILC, leading to an increased expression of AP2B in ILC compared to NST breast cancer. AP2B is a transcription factor protein that regulates genes that control cell division, stimulates cell proliferation, and is involved in tissue development.

Methods: Immunohistochemistry (IHC) staining was performed in the following models: human breast cancer cell lines (MCF7, T47D, MM134, MM453), patient derived organoids (PDOs), mouse xenograft tumors (MM134), and clinical tumor samples (six ILC tumors, six NST tumors). PDOs were generated by our lab from patient tissue samples and then grown in culture. All samples were embedded in FFPE blocks, sectioned, stained, and imaged.

Results: There is increased expression of AP2B in ILC models compared to NST models. Staining showed that the expression of AP2B is heterogeneous across all models studied.

Conclusion: The results of this study showed that increased expression of AP2B is a potential biomarker for development and progression of ILC. Thus, further research is necessary to understand the role that AP2B plays in the development of ILC.

Detecting Changes in Influenza Clinical Presentation Using Causal Machine Learning

Jeremiah Satcho[1], Kevin Bui, BS[2], Ye Ye, PhD[2], Gregory Cooper, MD, PhD[2]
[1]North Allegheny Senior High School, Pittsburgh, PA
[2]Department of Biomedical Informatics, University of Pittsburgh, Pittsburgh, PA

Abstract

Influenza in the population can change from year-to-year both genetically and in terms of clinical presentation. The clinical findings caused by a strain of influenza may signify the virulence of that strain, which in turn may affect population health planning and patient treatment. We applied a computer algorithm to two consecutive years of clinical data to estimate the findings caused by influenza in each year. From one year to the next, there were a substantial number of findings that were shared and that were unique.

Introduction

Biosurveillance is the field of study concerned with the monitoring and detection of diseases in the population, particularly infectious diseases.[1] Biosurveillance research predominantly focuses on the detection of known diseases or of aberrations in signals that are indicative of known diseases, such as patient chief complaints.[2] In contrast, our work is focused on characterizing the clinical presentation of known outbreak diseases, such as the symptoms of influenza. The clinical findings caused by a disease can provide useful insights into the nature of the disease, such as its virulence. We are unaware of any existing research reported in literature on this problem. The problem requires that we estimate the findings that a disease causes during a given period, such as an outbreak season.

Causal discovery is an area of machine learning that is concerned with learning causal relationships from data under assumptions, particularly from observational data, such as electronic medical records.[3] We applied a causal discovery algorithm to data on patients who visited UPMC emergency departments to estimate the clinical findings being caused by influenza during a given year. We then analyzed how much those findings change from one year to the next. *We hypothesize that there will be substantial similarities and differences in findings from one year to the next.* If so, the results will provide initial support that the approach may be clinically useful in disease monitoring.

Methods

We analyzed data on patients seen at the following UPMC emergency departments (EDs) during the periods June 2013 to May 2014 (year 1) and June 2014 to May 2015 (year 2): Children's, Mercy, McKeesport, Presbyterian-Montefiore, and Shadyside. In year 1 a total of 384 influenza cases had either positive laboratory test results or an ICD discharge diagnosis of influenza; in year 2 there were 709 cases. Non-influenza cases were obtained from August of each year, when influenza cases are rare, yielding 21,889 in year 1 and 21,553 in year 2. For each patient case, we applied MetaMapLite[4] to map clinical free-text ED reports into 487 UMLS codes. In each case, we also included 16 discretized lab results and whether the patient had influenza. We used these 487 + 16 variables as patient-case findings. We reduced the findings to the top 300, according to their information gain for predicting the presence of influenza.[5] For computational efficiency, we down sampled the number of negative cases in each year to equal the number of positive cases for the year. We used the Tetrad software[6,7] to apply the PC stable algorithm[8] to the data for each of the two years to learn a causal Bayesian network (CBN) for each year under the assumption of causal sufficiency.[3] We actually learned 100 CBNs for each year, using a Tetrad option that bootstraps the data and reports the frequency that influenza causes each finding, which provides an indication of reliability of the estimates.

Results

Tables 1 and 2 show the clinical findings estimated to be caused by influenza in each year, organized by the bootstrap threshold. The results suggest that from one year to the next influenza has many similar effects, such as fever and myalgia. In contrast, Table 3 shows the clinical findings caused by influenza in year 2 but not in year 1. At a bootstrap frequency of 0.9, the unique clinical findings in year 2 are as follows: back pain, malaise, red throat, and tissue congestion. These findings indicate how influenza has changed from year 1 to year 2.

Discussion

In this study, we found a substantial number of both common and unique findings that were estimated to be caused by influenza between consecutive years. These results support our hypothesis and open the possibility for future applications, once the method is validated. To do so, a larger number of years should be compared. Also, it would be useful for experts to assess prospectively whether the estimated causal relationships are biologically accurate.

Table 1: Findings estimated in year 1 to be caused by influenza at bootstrap thresholds over the range of 0.5 to 1.0.

Features	0.5	0.6	0.7	0.8	0.9	1
Adverse Event Associated with Pain	x	x	x	x	x	x
Discharge status	x	x	x	x	x	x
Fever	x	x	x	x	x	x
Pain	x	x	x	x	x	x
Dry cough	x	x	x	x	x	
Illness (finding)	x	x	x	x	x	
Influenza-like symptoms	x	x	x	x	x	
Myalgia	x	x	x	x	x	
Redness	x	x	x	x	x	
Wheezing	x	x	x	x	x	
Sinus Tachycardia CTCAE 3.0	x	x	x	x		
Hemoptysis	x	x	x			
History of present illness	x	x	x			
Lesion	x	x	x			
Unconscious State	x	x	x			
Hydration status	x	x				
Malaise	x	x				
Meningitis CTCAE	x	x				
Muscle Pain CTCAE 3	x	x				
Recurrent fevers	x	x				
discharge diagnosis	x	x				
3 to 5 days	x					
Earache	x					
Pruritus	x					
Rhinorrhea	x					
Scleral injection	x					

Table 2: Findings estimated in year 2 to be caused by influenza at bootstrap thresholds over the range of 0.5 to 1.0.

Features	0.5	0.6	0.7	0.8	0.9	1
Adverse Event Associated with Pain	x	x	x	x	x	x
Fever	x	x	x	x	x	x
Illness (finding)	x	x	x	x	x	x
Pain	x	x	x	x	x	x
Tissue Congestion	x	x	x	x	x	x
Back Pain	x	x	x	x	x	
Dry cough	x	x	x	x	x	
Malaise	x	x	x	x	x	
Red throat	x	x	x	x	x	
Wheezing	x	x	x	x	x	
Family history	x	x	x	x		
Rhinorrhea	x	x	x	x		
Unconscious State	x	x	x	x		
Earache	x	x	x			
Influenza-like symptoms	x	x	x			
Myalgia	x	x	x			
Immunocompromised Host	x	x				
Low Back Pain	x	x				
Redness	x	x				
Skin Bruise	x	x				
Symptoms	x	x				

Table 3: Findings unique to year 2 at bootstrap thresholds over the range 0.5 to 1.0.

0.5	0.6	0.7	0.8	0.9	1
Back Pain	Back Pain	Back Pain	Back Pain	Back Pain	Illness (finding)
Family history	Earache	Earache	Family history	Malaise	Tissue Congestion
Immunocompromised Host	Family history	Family history	Malaise	Red throat	
Low Back Pain	Immunocompromised Host	Malaise	Red throat	Tissue Congestion	
Red throat	Low Back Pain	Red throat	Rhinorrhea		
Skin Bruise	Low Back Pain	Rhinorrhea	Tissue Congestion		
Symptoms	Red throat	Tissue Congestion	Unconscious State		
Tissue Congestion	Rhinorrhea				
	Skin Bruise				
	Symptoms				

References

1. Wagner MM, Moore AW, Aryel RM, editors. Handbook of Biosurveillance. Elsevier; 2011.
2. Yuan M, Boston-Fisher N, Luo Y, Verma A, Buckeridge DL. A systematic review of aberration detection algorithms used in public health surveillance. Journal of Biomedical Informatics. 2019 Jun 1;94:103181.
3. Glymour C, Zhang K, Spirtes P. Review of causal discovery methods based on graphical models. Frontiers in genetics. 2019 Jun 4;10:524.
4. Demner-Fushman D, Rogers WJ, Aronson AR. MetaMap Lite: An evaluation of a new Java implementation of MetaMap. Journal of the American Medical Informatics Association. 2017 Jul 1;24(4):841-4.
5. Mitchell T. Machine Learning. McGraw Hill, 1997, Section 3.4.1.
6. Ramsey JD, Zhang K, Glymour M, Romero RS, Huang B, Ebert-Uphoff I, Samarasinghe S, Barnes EA, Glymour C. TETRAD—A toolbox for causal discovery. In8th international workshop on climate informatics 2018 Sep (p. 29).
7. Tetrad Manual. https://cmu-phil.github.io/tetrad/manual/
8. Colombo D, Maathuis MH. Order-independent constraint-based causal structure learning. J. Mach. Learn. Res.. 2014 Jan 1;15(1):3741-82.

Designing a Pipeline to Explain Time-Series Predictive Models Trained on Clinical Data with Missing Values

Alex E. Schafer[1,2]; Eddie Perez Claudio, M.S.[3]; Tanupat Boonchalermvichien, MD[3]; Harry Hochheiser, PhD[3]; Christopher M. Horvat, MD, MHA[4]

[1]Taylor Allderdice HS, Pittsburgh, Pennsylvania; [2]University of Pittsburgh Hillman Cancer Center Academy, Pittsburgh, Pennsylvania; [3]University of Pittsburgh, Department of Biomedical Informatics, Pittsburgh, Pennsylvania; [4]Department of Pediatrics, UPMC Children's Hospital of Pittsburgh, University of Pittsburgh School of Medicine, Pittsburgh, Pennsylvania, USA

Abstract

With the increased use of machine learning in hospital environments, we must ensure the model's fairness and trustworthiness. Explainable Artificial Intelligence (XAI) may be a pathway to develop trustworthy models. However, missing values in clinical data influence explanation fidelity, which, combined with the limited availability of model-agnostic time-series XAI methods, is a critical barrier to explaining time-series models. Therefore, we built a pipeline to facilitate assessing and explaining time-series model predictions containing missing values.

Introduction

Predictive models must be fair and trustworthy, especially in clinical settings where lives are at stake [5]. Explainable AI (XAI) enables users and developers to inspect the rationale for a model's prediction. This feature of XAI may allow clinicians to use their knowledge to assess model predictions and increase confidence in these potentially lifesaving systems [4]. However, there are two challenges clinical data present which make usable XAI tools difficult to find. The first challenge is the time-series nature of clinical data, especially Intensive Care Unit (ICU) data. This eliminates many prominent explainer tools, such as SHAP, because they only produce explanations that are based on a single input instance [2]. The second challenge presented is the number of missing values common in clinical data [1]. Most XAI methods are not designed with missing values in mind. This creates a need to either impute the data or alter how XAI methods handle missing values. However, these steps to handle missing values can affect explanation fidelity (accuracy) [1]. Therefore, the immediate goal of this project was to build a model-agnostic pipeline that facilitates generating explanations for time-series model predictions trained on clinical data with missing values. To achieve our goal, we made custom functions for an XAI method called TimeSHAP [2]; and we built a custom GRU-D model [3] based on an implementation openly available in the PyPOTS library [3].

Methods

Dataset: To test our pipeline, we trained our custom GRU-D model on the Physionet Challenge 2012 dataset, which contains time-series data for 12,000 Cardiology ICU patients [3]. The target of the dataset labels patient mortality in the ICU, which we call a Dire Outcome (DO) in the rest of this text. The features (variables) we have access to encompass vitals, physical measurements, and drug dosage. *Changes to the Model and Model Training*: GRU-D is a type of model that can handle time-series datasets that contain missing values by using an internal imputation algorithm that decays the missing values to the mean. To achieve our goal, we made two changes to the PyPots GRU-D model implementation. The first was adding a prediction method for single samples/patients since TimeSHAP requires the model to generate one prediction at a time. The second change was to create a special case where the model would internally substitute NaN values for 0 when it received a single observation for prediction rather than trying to get an average across samples. After training, the predictive model had an AUROC of 0.82, AUPRC of 0.44, F1-Score of 0.45, Precision of 0.32, and a Recall of 0.78. *Changes to the XAI Method:* TimeSHAP is a post-hoc, model-agnostic explainer independent of the predictive model which we used to explain our GRU-D model. However, to use TimeSHAP we must generate a baseline sample. The built-in functions for this method do not accept data with missing values [2][5]. We modified the baseline generating function to ignore missing values in its estimations.

Results

With all our changes, we generated Local and Global explanations for a predictive model trained on clinical data with missing values. For the individual with the highest probability of a dire outcome, we found that the 5 closest events were the most impactful while the most important feature was Albumin, this can be visualized in **Figs. 1.A** and **2.A**. For the individual with the lowest probability of a dire outcome, we found that the 6 closest events were the most impactful to the prediction and the most important feature was white blood cell (WBC) count. This can be visualized in **Figs 1.B** and **2.B**

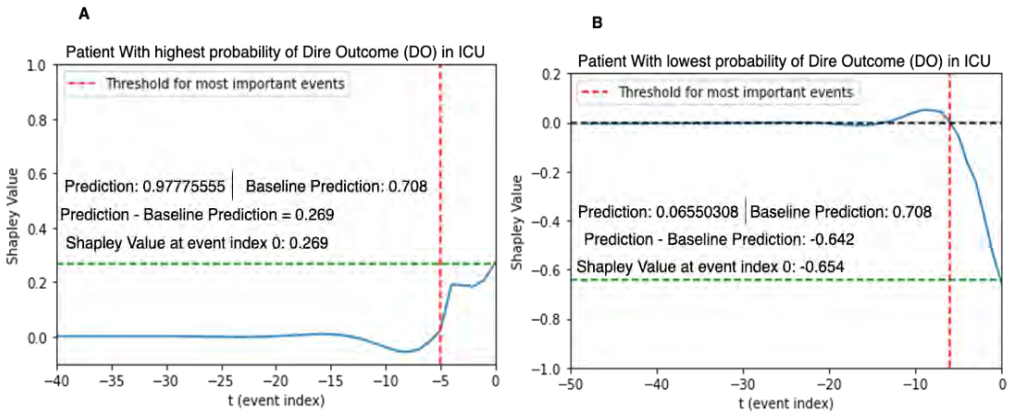

Figure 1. Line plots of the sum of feature Shapley values over time

Discussion

An important limitation to address is the commonality of missing values in medical data. The amount of missing data could impact the quality of the explanation of tools such as TimeSHAP. To handle missing values, there were edits to the TimeSHAP code where NaN values were imputed with zeroes, this could create skewed explanations by TimeSHAP. Another result of note is the slight fidelity error in the sample with the lowest prediction probability. TimeSHAP may have problems calculating explanations when negative values are involved. Future work should study the impact of missing values on our modification of TimeSHAP, and a further look into how TimeSHAP calculates with negative values to understand why an imperfect explanation fidelity may occur.

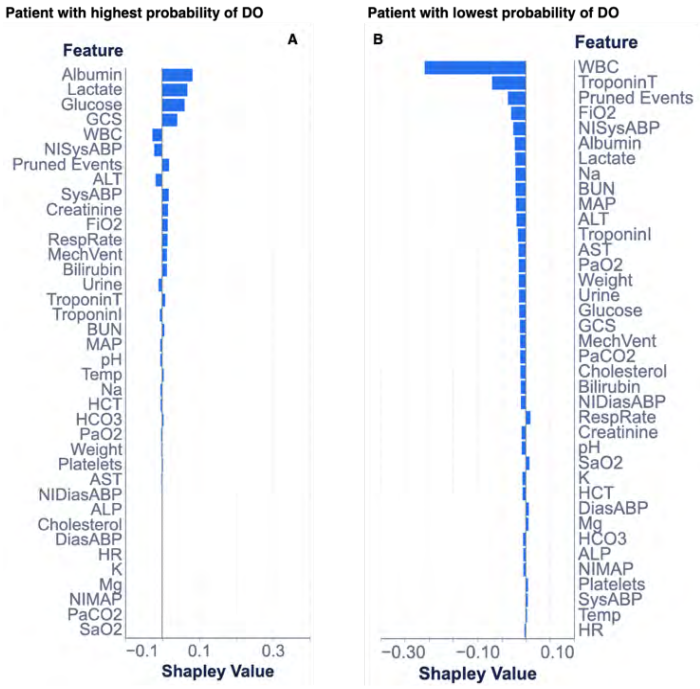

Figure 2. Feature importance values

References

1. Austin PC, White IR, Lee DS, van Buuren S. Missing Data in Clinical Research: A Tutorial on Multiple Imputation. Canadian Journal of Cardiology. 2021 Sep 1;37(9):1322–31.
2. Bento J, Saleiro P, Cruz AF, Figueiredo MAT, Bizarro P. TimeSHAP: Explaining Recurrent Models through Sequence Perturbations. In: Proceedings of the 27th ACM SIGKDD Conference on Knowledge Discovery & Data Mining [Internet]. New York, NY, USA: Association for Computing Machinery; 2021 [cited 2023 Jul 25]. p. 2565–73. (KDD '21). Available from: https://dl.acm.org/doi/10.1145/3447548.3467166
3. Du W. PyPOTS: A Python Toolbox for Data Mining on Partially-Observed Time Series. 2023.
4. Holzinger A, Goebel R, Fong R, Moon T, Müller KR, Samek W. xxAI - Beyond Explainable Artificial Intelligence. In: Holzinger A, Goebel R, Fong R, Moon T, Müller KR, Samek W, editors. xxAI - Beyond Explainable AI: International Workshop, Held in Conjunction with ICML 2020, July 18, 2020, Vienna, Austria, Revised and Extended Papers [Internet]. Cham: Springer International Publishing; 2022 [cited 2023 Jul 28]. p. 3–10. (Lecture Notes in Computer Science). Available from: https://doi.org/10.1007/978-3-031-04083-2_1
5. Theissler A, Spinnato F, Schlegel U, Guidotti R. Explainable AI for Time Series Classification: A Review, Taxonomy and Research Directions. IEEE Access. 2022;10:100700–24.

The role of Profilin-1 in the infiltration of macrophages into the tumor microenvironment in Breast cancer

Scholar: Aneri Shethji
High School/College/City/State: North Allegheny Senior High School, Pittsburgh, PA
PI of group/lab: Dr. Partha Roy
Mentor(s): Ian Eder, Dr. David Gau
Site: Women's Cancer Research Center

Breast cancer is the second leading cause of cancer-related deaths in women in the United States. A promising treatment for breast cancer is immune checkpoint inhibitor, however current response remains low due to an immunosuppressive nature of the tumor microenvironment (TME). One potential regulator that could influence inflammation in the TME is Profilin-1 (Pfn1). Studies have shown Pfn1 expression is reduced in breast cancer cells and increasing its expression suppresses tumor growth and metastasis. The objective of this project was to determine the effect of Pfn1 on the TME. We previously found that Pfn1 upregulation in a human breast cancer cell line increased CCL2 expression, a monocyte chemoattract. Further, we found the secreted factors from Pfn1 overexpressing 231 cells increased monocyte migration. We hypothesized Pfn1 knockdown in tumors would decrease macrophage migration into the tumor microenvironment.

To verify CCL2 upregulation was consistent across cell lines, we performed qPCR on GFP & GFP-Pfn1 transfected 4T1 cells for CCL2 and found no change in CCL2 expression. Additionally, we performed immunohistochemistry (IHC) for F4/80, a macrophage marker, in control and Pfn1 knockdown MDA-231 tumors implanted in mice and found an increase in macrophages upon Pfn1 knockdown. Given the data, we thought there may be an alternative explanation. Vascular Endothelial Growth Factor (VEGF) is a protein that plays a role in angiogenesis and is known to be upregulated upon Pfn1 knockdown. We hypothesized that knockdown of Pfn1 would increase VEGF expression, increasing angiogenesis, thereby increasing macrophage infiltration. IHC for CD31, an endothelial cell marker, indicated that Pfn1 knockdown tumors had significantly more endothelial cells.

In this study, we found knockdown of Pfn1 increases macrophage and endothelial cell presence in the tumor microenvironment potentially through its regulation of VEGF. Further research is necessary to confirm Pfn1's effect on endothelial cells and macrophages is VEGF dependent.

To Reveal the Mechanism of Clusterin Degradation Under Glucose-Deprived Conditions

Scholar: Sophia Song

High School: Upper St. Clair High School, Upper St. Clair Pennsylvania

Lab: Yusuke Sekine, PhD

Mentor: Ryan Houston

Site: TDX

Background: Clusterin is a secreted protein that acts like a chaperon protein that helps protein folding in the extracellular space. One of Clusterin's targets is Aβ, a pathogenic protein for Alzheimer's disease. Clusterin helps the degradation of Aβ and changes of clusterin level in the brain affects progressions of the Alzheimer's disease. For clusterin to properly function, it needs to go through glucose-dependent post-translational modification, glycosylation, in the endoplasmic reticulum. However, patients with Alzheimer's disease have low levels of glucose. Studying the mechanism of clusterin degradation under glucose-deprived conditions might help to develop a new treatment for Alzheimer's Disease. The two main clusterin degradation pathways in the cells are through lysosome and through proteasome. The purpose of this project is to find the specific mechanism of clusterin degradation under glucose-deprived conditions.

Methods: A172 glioblastoma cells were treated with various conditions in 7 groups for 6 hours. Group 1, 3, 5, and 7 were treated with glucose + condition while group 2, 4, 6 were treated with glucose – condition. Group 1 and 2 were control groups. Group 3 and 4 were treated with BafA1, which inhibits the lysosome pathway. Group 5 and 6 were treated with MG132, which inhibits the proteasome pathway. Group 7 was treated with tunicamycin (Tm), which induces deglycosylation. Immunoblotting was used to determine the amount of clusterin in each group and immunocytochemistry was used to determine the locations of clusterin and lysosome.

Results: In Figure 1, group 1 shows a band in the range for pre-spliced clusterin while group 2 has a band in the range for deglycosylated pre-spliced clusterin. Group 3, 4, 5, 6 all show bands that indicate an increase of the amount of clusterin. Group 3 and 5 both have two bands: one around the range of pre-spliced clusterin, the other around the range of spliced clusterin. The pre-spliced clusterin gets cut in half before it gets secreted in the golgi. The spliced clusterin has a weaker signal since some of it already got secreted. The clusterin in group 4 and 6 are mostly in the range of deglycosylated pre-sliced clusterin due to the low glucose levels. Group 4 has a clear band, indicating clusterin gets degraded through lysosome pathway under glucose-deprived condition. In Figure 2, it is shown that the lysosome and clusterin overlap under glucose – condition. Under glucose – condition with BafA1 treatment, the lysosome surrounds clusterin.

Conclusion: The results suggest that when glucose is present, degradation of clusterin, including pre-spliced and spliced clusterin, go through both lysosome and proteasome pathways. Under glucose-deprived conditions, the lysosome pathway is preferential.

Figures:

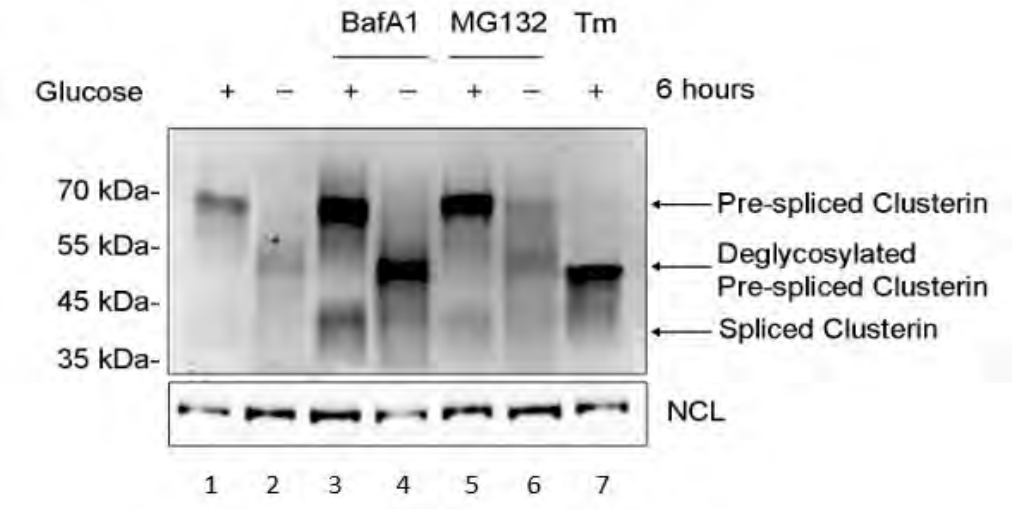

Figure 1. Image from Immunoblotting

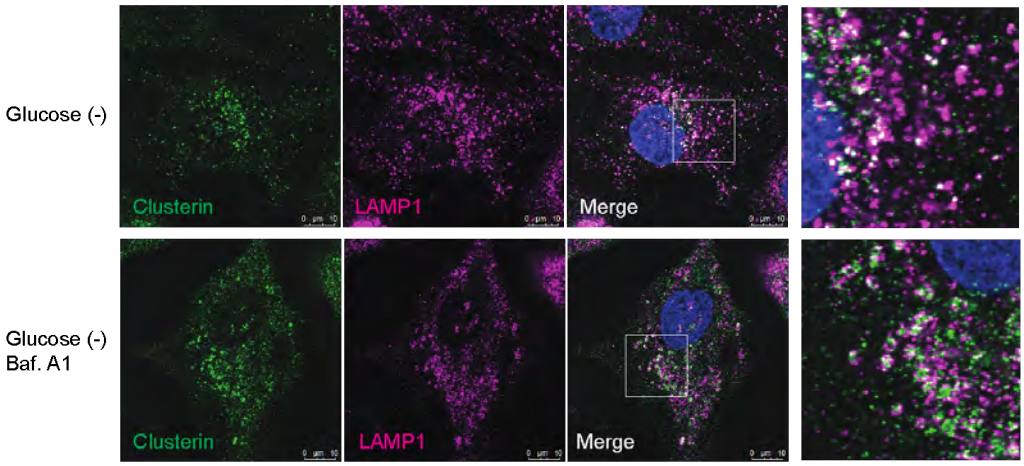

Figure 2. Image from Immunocytochemistry

Investigating Transcriptomic Changes in Early Stage Ovarian Cancer Using Spatial Omic Data

Dylan Sun[1], Dr. Xinghua Lu, MD, PhD[2]
[1]Shady Side Academy, Pittsburgh, PA; [2]University of Pittsburgh Hillman Cancer Center Academy, Pittsburgh, PA

Abstract

In this project, a spatial transcriptomics dataset of serous tubal intraepithelial carcinoma was analyzed for gene expression differences between cancerous and adjacent non-cancerous epithelial cells. Gene expression was also analyzed between stroma surrounding tumors and adjacent normal stroma. Genes that significantly differed in expression underwent enrichment analysis to identify changes in biological processes.

Introduction

Ovarian cancer is difficult to detect and highly fatal. Its development is a progressive process, starting with a mutation in the *TP53* gene, followed by serous tubal intraepithelial carcinoma (STIC), and finally metastatic high-grade serous carcinoma (HGSC). A better understanding of the disease mechanisms at different stages will provide insights into the diagnosis and treatment of the disease. Digital spatial profiling (DSP) is a spatial transcriptomics methodology that studies intact tissue for gene expression. This technique gives not only gene expression data, but also spatial information. DSP data and gene enrichment analysis can be combined to identify changes in biological processes between cancerous and noncancerous tissue.

Methods

Data was collected from tissue samples of patients with serous tubal intraepithelial cancer. Tissue samples were stained, ROIs were selected and analyzed using the GeoMx Digital Spatial Profiler.[1] Samples of STIC and adjacent stromal and epithelial tissue were identified, and significant changes in gene expression between types identified using t-test. Significant genes were then run through the PANTHER enrichment test[2] to find a list of biological processes changed.

Results

Out of 18815 genes tested, 42 were expressed differently between cancerous and non-cancerous epithelial cells. Distinct differences in processes include in regulation of rho-dependent protein serine/threonine kinase activity, regulation of apoptotic processes, and mesenchyme migration. Out of the same total, 63 were expressed differently between cancerous and non-cancerous stromal cells. Distinct differences in processes included

Discussion

In this study, we have identified a set of differentially expressed genes between cancerous tissue and adjacent normal tissue. Genes involved in mesenchymal development were enriched in cancerous tissue. This indicates that early development of ovarian cancer involves undifferentiation of cells. Future research could include repeating this experiment with a larger sample size. Including genomic data could shed light on disease mechanisms.

References

1. Hernandez, S., Lazcano, R., Serrano, A., Powell, S., Kostousov, L., Mehta, J., ... & Solis, L. M. (2022). Challenges and opportunities for immunoprofiling using a spatial high-plex technology: the NanoString GeoMx® digital spatial profiler. Frontiers in Oncology, 12, 890410.
2. Thomas, P. D., Ebert, D., Muruganujan, A., Mushayahama, T., Albou, L. P., & Mi, H. (2022). PANTHER: Making genome-scale phylogenetics accessible to all. Protein Science, 31(1), 8-22.

Title: Neuronal PD-L1 expression modulates baseline tissue immunity

Scholar: Aarav Surapaneni
High School: Moon Area High School, Pittsburgh, PA
PI: Dr. Nicole Scheff, Ph.D
Mentor: Dr. Lisa McIlvried Ph.D
Site: Cancer Biology

Introduction: Immunoreceptor proteins PD-1 (program death one) and PD-L1 (program death ligand one) are "immune checkpoint" proteins that control excessive inflammation. In cancer, tumor cells release PD-L1, which inhibits cytotoxic T cell function via PD-1 activation. Meerschaert et al (2022) found that peripheral "pain-sensing" (i.e. nociceptive) neurons, a key component of the tumor microenvironment, also express PD-L1. We aim to understand the impact of nociceptive PD-L1 expression on baseline (no disease) tissue immunity. We hypothesized that loss of PD-L1 expression in "pain-sensing" sensory neurons will dysregulate baseline immunity.

Methods: To determine the impact of nociceptive PD-L1 expression on immunity, we quantified immune cell subpopulations using flow cytometry in cervical lymph nodes, spleen, tongue, pancreas, and skin using three different mice phenotypes: (1) TRPV1crePDL1$^{fl/fl}$, a conditional knockout mouse that lacks PD-L1 in all nociceptive neurons, (2) PD-L1$^{fl/fl}$ mouse that has the flox gene only without activation, and (3) wildtype mice with no genetic mutation. PCR and immunohistochemistry were used to confirm genetic mutations.

Results: Lymphatic tissues (spleen, lymph node) and pancreas from TRPV1crePDL1$^{fl/fl}$ contained substantially less CD3$^+$ T lymphocytes (i.e. CD4$^+$ T helper and CD8$^+$ cytotoxic T cells) compared to PDL1$^{fl/fl}$ and wildtype mice; we found ~20% less in CD3$^+$ cells in spleen, ~40% less CD3$^+$ cells in lymph node and ~55% less CD3$^+$ T cells in pancreas tissue. While there was no change in baseline immunity in the tongue muscle, we found ~300% increase in CD3$^+$ T lymphocytes in the skin tissue from TRPV1crePDL1$^{fl/fl}$ compared to controls. There were no substantial differences in non-T cell immune subtypes between phenotypes across tissues.

Conclusions: The data suggests that PD-L1 checkpoint expression on nociceptive neurons can regulate the presence of CD3$^+$ T cells in lymphatic, visceral, and somatic tissues. Future studies will determine the impact of neuronal PD-L1 on anti-tumor immunity in tumor-bearing mice.

Determining Protein Levels of Key Factors Involved in Macrophage Metabolism

Scholar: Jermaine Taylor

School: Shady Side Academy, Pittsburgh, PA
Lab: Rachel Gottschalk Lab
Mentors: Rachel Gottschalk and Morgan Jackson-Strong
Site: Immunology

Background: Macrophages are phagocytic cells found in every organ that specialize in tissue repair, homeostasis, and development and the ingestion of bacterial cells and debris. The function of tissue-specific macrophages are dependent on specific stimuli, such as cytokines and growth factors in their microenvironment. These specific signals dictate their gene expression and their behavior. Alveolar macrophages have a critical role of breaking down surfactant in the lungs to assist in gas exchange. The goal of these experiments is to determine how various signals regulate macrophage gene expression and function.

Methods: To investigate the role of GATA2 in alveolar macrophages, we used two different techniques to measure protein expression. To explore the role of GATA2, we used the Bronchoalveolar Lavage method to harvest the alveolar macrophages to then be plated and stained via IF staining to detect our (antibody). The purpose of this preliminary experiment is to ensure that GATA2 isn't expressed in knockout mice. After this experiment, we culture bone marrow derived macrophages by extracting monocytes from mice femurs. Next, we rinse the bones to obtain our monocytes. The monocytes are then stimulated with M-CSF to differentiate them, and then GM-CSF to make our macrophages to behave specifically like alveolar macrophages. We take the samples and use the lysates from the cells to quantify the proteins that were previously in the cell via electrophoresis.

Results: Our images from the Western show that when our lysates were stimulated with GM-CSF, there was an increase in P-GATA2(Ser401), total GATA2, and in PPAR gamma. On the contrary, we see a decrease in P-GATA2(Ser192) when stimulated with GM-CSF.

Conclusion: From our Western Blot experiment we can conclude that the proteins: P-GATA2(Ser401), total GATA2, and in PPAR gamma, are more reliant on the GM-CSF signal to be expressed than P-GATA2(Ser192).

Intra-Amniotic Injections in Congenital Diaphragmatic Hernia

Michael Ulis

Penn State University, State College, PA

Church Lab at Rangos Research Center

Joseph T. Church, MD

Surgery Site

Background: Congenital diaphragmatic hernia (CDH) is an opening in the diaphragm during fetal development that allows organs within the abdomen to migrate into the chest cavity leading to a combination of pulmonary hypoplasia and pulmonary hypertension. The current mortality is 29%, there are no prenatal therapies that consistently address both pulmonary hypoplasia and pulmonary hypertension. Fetal endoscopic tracheal occlusion has shown promise as prenatal therapy but is invasive and often causes premature delivery. We hypothesized that intra-amniotic injection of either sildenafil or rosiglitazone late in gestation would reduce pulmonary hypertension in a rodent model of CDH. We also hypothesized the injection of the combination of both drugs would produce a synergistic effect.

Methods: Nitrofen was given to pregnant rats at E9.5 to produce CDH. Non-nitrofen-fed rats served as controls. All rats then underwent intra-amniotic injection of PBS, sildenafil, rosiglitazone, or both on gestational day E19.5 (Term=21-22 Days). On day E21.5, fetuses were harvested and weighed. Lungs were then harvested after removal of the fetal heart, weighed, and placed in 4% paraformaldehyde for fixation. The extracted lungs were then cryoprotected in 30% sucrose overnight and embedded in Tissue-Tek O.C.T. Sections (5μm) were cut by cryo-stat and mounted. The slides then underwent immunofluorescence staining with Ki67 and Smooth Muscle Actin to assess for smooth muscle cell proliferation. Ki67 and DAPI stained cells were counted and the percentage double positive for Ki-67 and alpha-SMA calculated to determine the degree of proliferation.

Results: In pups with CDH, sildenafil, rosiglitazone, and sildenafil+rosiglitazone all resulted in lower percent of Ki67 to DAPI than the vehicle control (4.22±4.27 vs. 4.19±3.5 vs. 2.61±3.39 vs. 7.40±1.73 respectively; $p<0.05$). The combination produced the lowest rate of proliferation.

Conclusion: We concluded that an intra-amniotic injection of sildenafil, rosiglitazone or both decreases arterial wall cell proliferation thereby reducing pulmonary hypertension in the rat CDH model.

Future Directions: We will continue to look at Ki67 immunofluorescence staining, and we will begin to look at PECAM staining with the goal of beginning statistical analysis on it soon.

Evaluating anti-tumor potency of Tumor Infiltrating Lymphocytes using ELISA

Scholar: Terrell Wafford

High School: Westinghouse High School, Homewood, PA

Lab: Dr. Udai S. Kammula, MD

Mentor: Dr. Udai S. Kammula, Chetana Bhaskarla, PhD

Site: Surgery/CoSBBI

Background

Adoptive T-cell Therapy (ACT) utilizing autologous Tumor Infiltrating Lymphocytes (TIL) represents a personalized cancer immunotherapy. TIL cultures are generated in the laboratory from a patient's surgically resected tumor and tested for anti-tumor reactivity by coculture with autologous tumor. TIL are capable of targeting private and public mutations resulting from tumor somatic mutations. Anti-tumor reactivity can be measured by release of Interferon (IFN)-gamma and upregulation of 4-1BB by flow cytometry. After careful assessment, tumor reactive TIL are infused into the patient, where they can mediate tumor destruction. Not all TIL have anti-tumor reactivity and thus, screening reactivity is clinically important. In this project, we are evaluating the anti-tumor activity of TIL through release of IFN-gamma using ELISA.

Methods

TIL were generated from a surgically resected pancreatic cancer metastasis harboring mutations in *ATM* and *ARID1A* genes, which are involved in the DNA damage pathway. These TIL were found to have anti-tumor reactivity. Whole genome sequencing was performed to identify the somatic mutations expressed by the cancer.

Results

High throughput antigen screening identified mutated ATM and ARID1A as the immunologic targets for the TIL. TIL reactivity against mutated ATM and ARID1A was evaluated by measurement of IFN-gamma using sandwich ELISA. ELISA for IFN-gamma release demonstrated that this TIL released higher IFN-gamma when cocultured in presence of mutated ATM and ARID1A as compared to wild type.

Discussion

Adoptive T-cell Therapy (ACT) utilizing autologous Tumor Infiltrating Lymphocytes (TIL) represents personalized cancer immunotherapy. Here, we show the potency of tumor reactive TIL by measuring the release of IFN-gamma in presence of the antigen.

A Cytonuclear Translocation Reporter System Using Split-GFP

Lauren Weaver
Mentors: Bo Lv, PhD & Jay Tan, PhD
Aging Institute, Technology Drive (TDX) Site
University of Pittsburgh School of Medicine (Pittsburgh, PA)

Introduction: In response to various cellular stresses, transcription factor EB (TFEB) is activated to upregulate lysosomal, mitochondrial, and autophagy-related genes. However, the underlying mechanisms of TFEB activation have been controversial. Existing protein translocation reporter systems, such as TransitID and protease-based reporters, suffer from limitations in terms of time, accuracy, and broad application. To detect TFEB activators in unbiased, large-scale screens, a cytonuclear TFEB translocation reporter system would be valuable. To address these shortcomings, we aimed to develop a cytonuclear translocation reporter for TFEB using the split-GFP technique.

Methods: Recombinant DNAs encoding TFEB fused to different split GFP fragments were cloned with the In-Fusion cloning method. Lentiviruses were packaged with psPAX2, pMD2.G, and pCDH-Puro backbone using Lipofectamin 2000 in HEK 293T cells. Puromycin-selected cells were treated Apilimod, CCCP, Chloroquine, EBSS, LLOMe, ML-SA1, Nigericin, Rapamycin, or Torin1, then analyzed by immunoblotting or live-cell imaging to track TFEB nuclear translocation.

Results: TFEB activation was observed in response to Torin1, Nigericin, Apilimod, CCCP, Chloroquine, EBSS, LLOMe, ML-SA1, and Rapamycin. Among these chemicals, Torin1 and Nigericin exhibited the most potent effects, with Torin1 selected for further experiments. The TFEB-$GFP_{11\ x7}$-mCherry fusion protein demonstrated superior performance when combined with NLS-GFP_{1-10}, compared to GFP_{1-10} -NLS or NLS-GFP_{1-10} -NLS. However, no significant difference was observed in the overall fluorescent intensities across all three combinations before and after TFEB activation. To reduce the basal GFP signal, TFEB-$GFP_{11\ x1/2/3}$-mCherry combined with NLS-GFP_{1-10} was tested, and TFEB-$GFP_{11\ x1}$-mCherry showed the lowest background.

Conclusion: The split-GFP system displays rapid spontaneous complementation between TFEB-GFP_{11} and GFP_{1-10}, rendering it unsuitable for direct use as a cytonuclear translocation reporter. To overcome this limitation, alternative strategies should be investigated to develop a reliable and precise reporter system for tracking TFEB cytonuclear translocation. Inducible expression of GFP_{1-10} by a TFEB-binding promoter may prove to be a successful approach, which should be further explored.

TPI DF Abstract

Jada Weikel Mentors: Dr. Andreas Vogt, Laura Vollmer

Introduction and Rationale

TPI DF (Triosephosphate Isomerase Deficiency) is a pediatric metabolic disease that is diagnosed within patients as early as six months old, and that in the most severe cases results in death before age 5. Symptoms include anemia, increased susceptibility to infection, neurological dysfunction, and progressive neuromuscular degeneration. There is no current cure or treatment for TPI DF. The root cause for TPI DF is a mutation in the TPI protein that results in lower stability and reduced expression in the cell. Work at the Drug Discovery Institute (DDI) in the Vogt lab alongside with the Palladino lab had identified hits from a high-content, high-throughput compound library screen that increased mutant TPI in HeLa cells genetically modified to express GFP-tagged mutant TPI and a reactive oxygen biosensor (HyPerRed), and which confirmed in dose-response with low toxicity. The top hits in the screen shared a hydrazone moiety. Hydrazones are frowned upon within drug discovery because they can hydrolyze into aldehydes and hydrazines, fragments that make up a hydrazone.

Hypothesis

Aldehydes in particular are reactive chemicals that can bind to proteins within a cell, making them potentially toxic and harmful. Because of their chemical reactivity, aldehydes are also commonly used as building blocks for synthesis. There are several sources of evidence that aldehydes are toxic to humans, for example commonly used chemicals like formaldehyde and acetaldehyde have harmful properties including respiratory and skin irritation, headaches, and cancer.

Hypothesis: Aldehydes and possibly hydrazides that result from hydrolysis of our library hits will show cellular toxicity in our model system.

The **objective** of our research is to test activity and toxicity with the parent compounds and their fragments in the HeLa TPI-GFP-HyperRed cell line.

Results and Conclusion

We completed three independent experiments in which we included two hydrazones and their corresponding fragments. We analyzed compounds for activity and toxicity in ten-point, two-fold dose-response using the HeLa TPI-GFP-HyperRed cell line. Activity was measured by levels of cellular GFP. Toxicity was measured by the activity of the HyPerRed ROS biosensor, and by staining nuclei with a DNA binding dye (Hoechst 33342). We quantified nuclei size, DNA staining intensity, and shrinkage. These parameters provided a profile readout on activity and toxicity. We found that our parent hydrazones showed activity in the low micromolar range and little cellular toxicity. One aldehyde showed increased ROS production and apoptosis, although at concentrations that were 20 times the EC50 for the parent compound's TPI-GFP. We conclude that hydrolysis of our hydrazones – if it occurs – could be an obstacle to further developing these compounds in patient cells and animal models.

Title: Danger of Artificial Sweeteners combined with Tumor Cells
Scholar: Camilla Zarour
High School/City/State: Taylor Allderdice Pittsburgh, PA
PI of Lab: Abby Overacre
Mentors: Abby Overacre, Jess Jana, Kristin Morder
Site: ICI (Immunotherapy)

Background: The use of NNS(Non nutritional sweeteners) are on a rise: In a survey given in 2009 and 2011, 25.1% of children and 41.4% of adults in the US reported consuming NNS. The problem is that they don't know a lot of the effects it has on tumor growth. In addition we have found that Sucralose (Splenda) increases the expansion rate of tumor cells (Fig 1, Fig 2). Therefore, we wanted to compare this in different tumor types across a number of NNS, beyond just sucralose.

Methods: B16 and MC38 cell lines were thawed and added to separate medias supplemented with artificial sweeteners including: Sucralose (Positive Control), Sucrose, Saccharin, Aspartame, Erythritol, or None (Negative Control). We split cells every 2-3 days and split them all once one condition was confluent.We also always reseeded at 300k no matter the cell count. During the multiple experiments, viability, total cells, and live cells were taken into consideration. We will be using an eSight for MC38 expressing OVA to measure how the cells die overtime as well.

Results: We found in B16 melanoma cell lines cultured in the presence of sucralose grow much faster, but other sweeteners have a stronger impact in the second and third passages (Fig 3, Fig 4). Aspartame and Saccharin are examples of them. Also, in the first B16 experiment Aspartame has a large count of total cells and it corresponds to its high viability, showing the danger of its growth. For MC38 at first split, None and Sucrose had the highest cell number count in comparison to artificial sweetener grown cells, but later on in the second and third passages, the artificial sweetener grown cells increase their growth rate. In the end, the cell count for None and Sucrose is lower than all the artificial sweetener groups.

Discussion: This study suggests that artificial sweeteners support increased tumor cell growth and are shown to be a disadvantage to protecting yourself from cancer. Things to note are that in B16 Experiment 1 (Fig 3), the cells grow faster as we passage them and this might be because they were all growing so slowly to start. We saw many trends that had certain artificial sweeteners grow the cells later on in the passages and less towards the beginning where the negative control was higher. Aspartame has been growing faster than many of the other sweeteners as well.

References

Abby Overacre, Kirstin Morder, Jess Jana

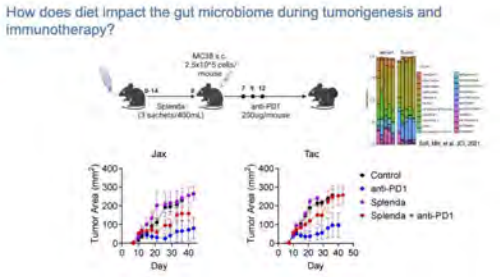

(Fig 1)

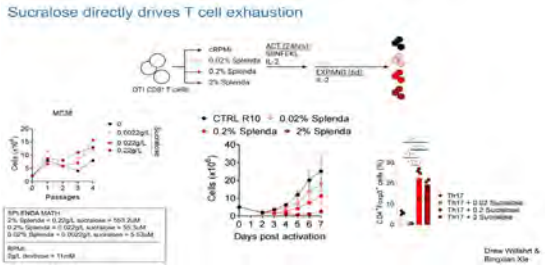

(Fig 2)

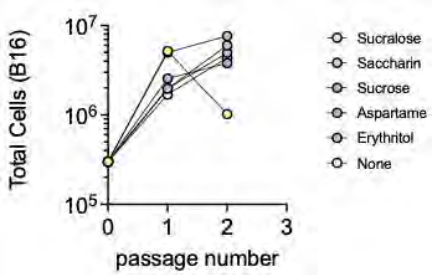

(Fig 3) B16 Experiment 1 Live Cells

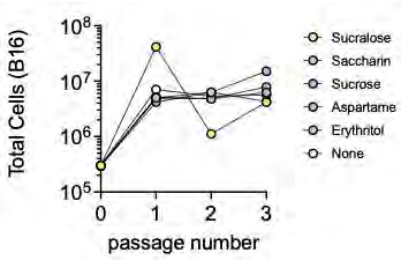

(Fig 4) B16 Experiment 2 Live Cells